Winter 2019

Assessment of the Localized Flow and Tidal Energy Conversion System at an Estuarine Bridge

Kaelin Chancey
University of New Hampshire, Durham

ASSESSMENT OF THE LOCALIZED FLOW AND TIDAL ENERGY CONVERSION SYSTEM AT AN ESTUARINE BRIDGE

BY

KAELIN CHANCEY

BS, Mechanical Engineering, University of New Hampshire, 2017

THESIS

Submitted to the University of New Hampshire
in Partial Fulfillment of
the Requirements for the Degree of

Master of Science

in

Mechanical Engineering

December 2019

This thesis has been examined and approved in partial fulfillment of the requirements for the degree of Master of Science in Mechanical Engineering by:

Thesis Director, Martin Wosnik,
Associate Professor of Mechanical Engineering

Erin Bell,
Associate Professor of Civil and Environmental Engineering

Thomas Lippmann,
Associate Professor of Earth Sciences

on 6/6/2019.

Original approval signatures are on file with the University of New Hampshire Graduate School.

ACKNOWLEDGMENTS

I would like to thank the National Science Foundation, United States Department of Energy, New Hampshire Department of Transportation, and United States Federal Highway Administration for supporting this project. I would also like to thank the rest of the Living Bridge Project team, especially the main members of the tidal energy team; Ian Gagnon, Jon Hunt, and my advisor Martin Wosnik. Many other undergraduate and graduate students have also added to this work and I am thankful for their contributions.

TABLE OF CONTENTS

LIST OF TABLES

LIST OF FIGURES

Figure **Page**

ABSTRACT

Assessment of the localized flow and tidal energy conversion system at an estuarine bridge

by
Kaelin Chancey
University of New Hampshire, December, 2019

As part of the Living Bridge Project, a cross-flow tidal turbine and estuarine instrumentation have been deployed in the Piscataqua River at the Memorial Bridge connecting Portsmouth, New Hampshire and Kittery, Maine. At the turbine location, flow measurements were taken and are compared to a previous, nearby tidal energy resource assessment. A higher mean kinetic power density was observed for the most recent acoustic Doppler current profiler (ADCP) survey conducted. Acoustic Doppler velocimeter (ADV) data was collected in order to study the spatial distribution of the currents around the turbine. Differences along the turbine deployment platform were determined to be caused by structural interactions with the bridge. Off-grid testing of the turbine produced a power curve that was used to calculate updated predictions of energy production. Compared to the initial design calculations, lower energy production can be expected based on the as-built system. The operation and maintenance procedures for the turbine deployment system are discussed. Valuable information has been gained about the turbine system, instrument integration and installation, and environmental factors. With additional testing of the turbine and instrument systems, the tidal energy conversion system at the Memorial Bridge in Portsmouth, NH will continue to produce local renewable energy and enhance public awareness of ocean renewable energy technology.

CHAPTER 1

INTRODUCTION

1.1 The Living Bridge Project

The Living Bridge Project [1] transforms the Memorial Bridge in Portsmouth, NH into a self-diagnosing, self-reporting, smart bridge. The project demonstrates that user-centered infrastructure combined with emerging renewable energy systems can lead to a more resilient, sustainable community. The structural health monitoring and environmental sensors installed on the bridge and in the river below are powered by a locally available renewable resource, tidal energy. Figure 1.1 is a picture of the Memorial Bridge showing the main aspects of the Living Bridge Project.

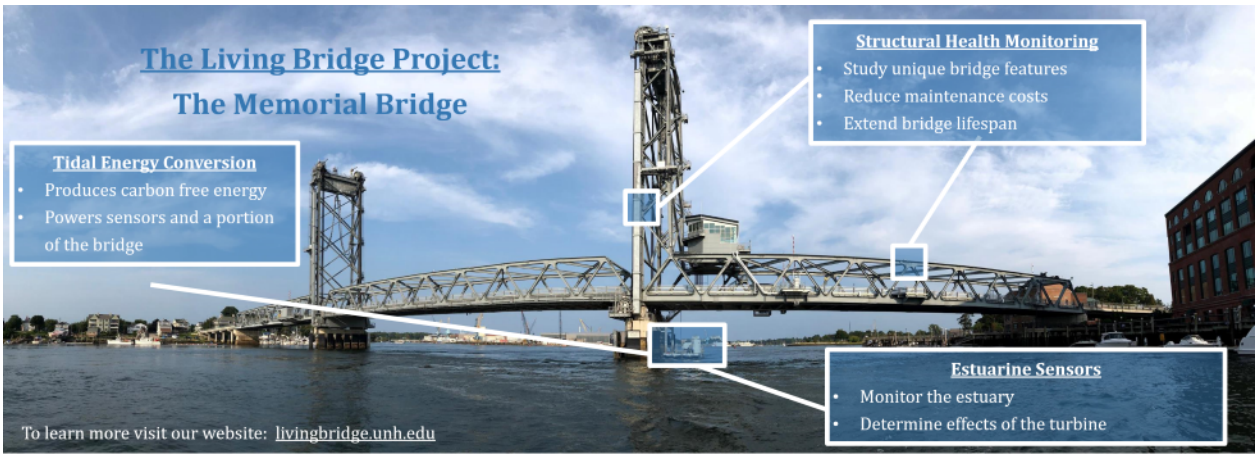

Figure 1.1: Diagram of the Living Bridge project located at the Memorial Bridge

The bridge is outfitted with structural health monitoring sensors to reduce maintenance, study the structural components, and extend the life of the bridge. The bridge features unique, gusset-less truss connections which are studied by civil engineers through data collected from strain gauges and accelerometers and modeling. Below the bridge, a tidal energy conversion system harnesses

the power of the currents to produce electricity. The tidal energy system also serves as a platform for deploying estuarine instrumentation. The project focuses on engaging and educating the public about both bridge innovation and renewable energy technologies. The many researchers in civil engineering, mechanical engineering, and computer science at UNH work with partner companies to enhance knowledge on both sides. As part of this research, Maryam Mashayekhizadeh has produced multiscale finite element models of the Memorial Bridge [23], Ian Gagnon designed and fabricated the turbine deployment platform [9], and Eric Doherty designed the baseline instrumentation integration system [7].

1.2 Tidal Energy Conversion System Overview

The tidal energy conversion system consists of a turbine deployment platform (TDP), turbine, and power electronics [9]. The floating turbine deployment platform pictured in Figure 1.2 is capable of deploying turbines with up to a $9m^2$ cross-sectional area rotor.

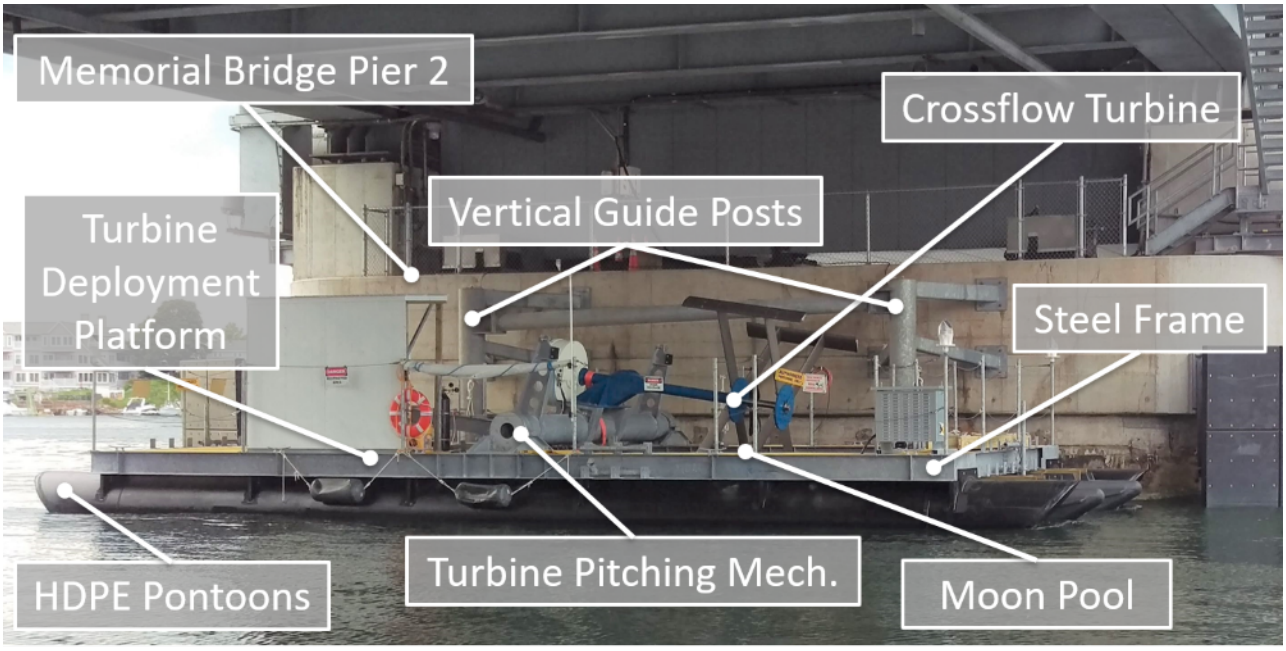

Figure 1.2: Diagram of the Tidal Deployment Platform at the Memorial Bridge

The galvanized steel frame floats on high density polyethylene (HDPE) pontoons. The platform is attached to the bridge by two vertical guide posts. UNH has partnered with New Energy

Corporation, who has provided their Envirogen 025 turbine for this project. This project is the first installation of this turbine in a tidal environment. It was previously only deployed at riverine sites. The vertical axis crossflow turbine uses a 4 bladed 3.2m diameter and 1.7m tall rotor. The system includes a direct drive permanent magnet generator located above the waterline. The power electronics are housed on the TDP and are connected to the bridge grid via a droop cable. The system can operate on or off the grid with net-metered and load bank configurations.

1.3 Instrumentation System Overview

The instrumentation system for the Living Bridge Project aims to gain information about the structural health of the bridge, estuarian health, current speeds and characteristics, environmental conditions, and loads on the turbine deployment platform.

The original instrumentation purchased for the Living Bridge Project tidal energy conversion system, referred to as the baseline instrumentation, includes the two LinkQuest FlowQuest 1000 ADCP's, the Valeport Midas CTD+, the two Luxus underwater cameras, and wildlife deterrent light bars developed by Lite Enterprises. The baseline instrumentation is provided power on the platform and the data is cabled to a server and database on the bridge.

The turbine deployment platform has several locations to mount instrumentation on a universal instrument mounting system. The locations of the baseline instrumentation and other possible mounting locations are indicated in Figure 1.3.

Additional instrumentation has also been added to the system for more temporary measurement campaigns. A mobile data acquisition system was designed in order to collect data from these additional instruments and from the baseline instrumentation if the system is not connected to the bridge.

1.4 Tidal Energy at Bridges

The motivation for including a tidal energy conversion system in the smart infrastructure focused Living Bridge Project as seen in Figure 1.4 was the idea that estuarine bridges are well positioned to capture tidal energy.

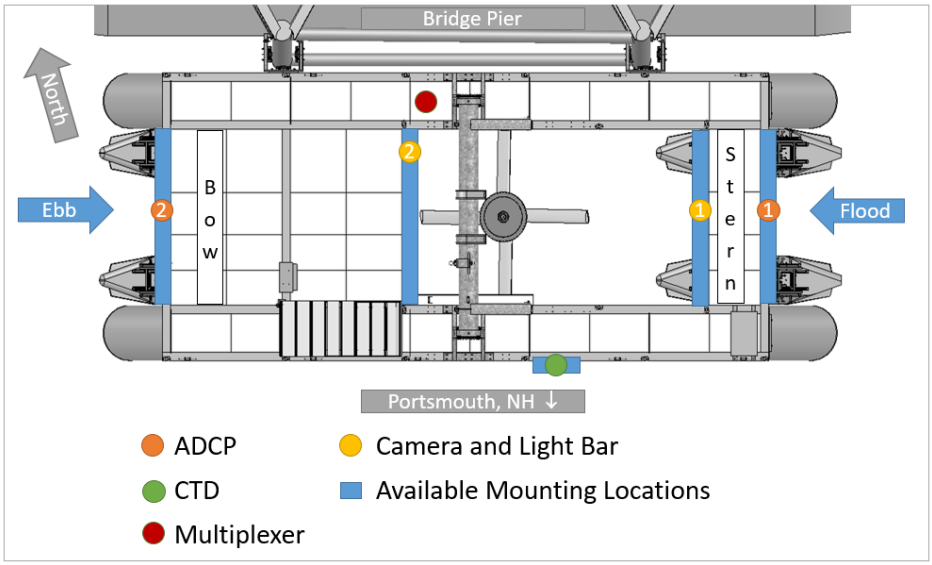

Figure 1.3: Baseline instrumentation mounting locations on the turbine deployment platform

Figure 1.4: Tidal energy conversion system at the Memorial Bridge

The main advantages of positioning tidal energy conversion systems at bridges are listed below: [9]

1. Constrictions where bridges are built offer faster currents. Bridges are often built where the spanning distance is minimized, the flow is constricted, and the current speeds are the fastest.
2. Existing support structures provide mooring locations.
3. Permitting can be reduced by combining systems with the existing bridge structure.
4. Bridges offer a location for routing power and data cables to the grid and local servers.
5. Public exposure to tidal energy can be increased by accessible locations such as the Memorial Bridge in Portsmouth, NH.

The Living Bridge Project has taken the first step towards investigating the possibilities of tidal energy at bridges by acting as a test site for tidal turbines. The tidal energy conversion system at the Memorial Bridge is the first of it's kind to be deployed at a bridge. The Living Bridge deployment leverages the bridge location by including a mooring capable of supporting the deployment platform year-round and providing a connection for power and data for instruments on the platform. UNH had previously deployed tidal turbines in the Muskeget Chanel in Massachusetts and farther up the Piscataqua River at the General Sullivan Bridge [31]. These deployments were from a floating platform similar to that used for the Living Bridge project but were short deployments, less than one day. Tidal turbines have also been tested with short deployments from a floating platform in the Strangford Lough in the United Kingdom ([17], [18]). Longer deployments of a bottom deployed turbine have occurred in the Kvichak River in Alaska with accompanying flow measurements [13]. The Living Bridge tidal site provides a location to test systems for longer periods of time, from several months up to a year.

The Living Bridge site also provides the opportunity to study the flow characteristics surrounding the turbine relatively easily because it is deployed from the surface. Tidal flow measurements

taken at other deployment sites are focused on the tidal resource assessment ([30],[14]), and characterizing the turbulence at the site ([24],[12],[38]). The resource assessment is used for turbine selection and sizing, energy production predictions, and determining the design loads for the deployment structure [16]. Analogously to wind turbines, the tidal flow turbulence characteristics, such as the size and occurrence of coherent structures, can influence the loading on the tidal turbine [21].

A resource assessment was completed prior to the fabrication and installation of the tidal energy conversion system [10]. With the installation of the system at the Memorial Bridge it provided the opportunity to take further flow measurements at the site to compare to the original resource assessment and characterize the turbulence at the site. The characteristics of the flow directly next to a structure, such as the Memorial Bridge pier, have not been studied in the context of tidal energy. The flow measurements for the Living Bridge tidal energy conversion system will provide insight into the effects of the bridge structure and help to inform future tidal energy installations near bridges or other structures.

1.5 Thesis Outline

This thesis will focus on the work following the fabrication of the tidal energy conversion system. The main goals during this period were to gain additional information about the flow conditions at the site, test the turbine system and quantify it's performance, develop and implement the instrumentation systems, and to keep the system maintained and operating while learning more about the components involved. This thesis touches on these main goals as outlined below:

1. Introduction

2. Characteristics of the Localized Flow at the Tidal Energy Conversion System Deployment Site

    - Acoustic Doppler current profiler (ADCP) measurements will be compared to the initial tidal current resource assessment

- Acoustic Doppler velocimeter (ADV) measurements will expand upon the knowledge of the currents around the turbine deployment platform

3. Tidal Energy Conversion System Testing

    - An as-built power curve produced from off-grid turbine testing will be presented along with energy production predictions

4. Instrumentation Systems

    - The instrumentation systems will be described, including instrument integration and mounting solutions

5. Operation and Maintenance of the Tidal Energy Conversion System

    - Turbine operation and seasonal hazards will be discussed

6. Conclusions and Future Work

CHAPTER 2

CHARACTERISTICS OF THE LOCALIZED FLOW AT THE TIDAL ENERGY CONVERSION SYSTEM DEPLOYMENT LOCATION

Previous acoustic Doppler current profiler (ADCP) surveys were used to conduct an initial tidal current resource assessment of the Piscataqua River at the Memorial Bridge [10]. The installation of the turbine deployment platform allowed flow measurements to be taken at the turbine location. An ADCP survey over the summer of 2017 is used to compare local measurements to the initial resource assessment. An acoustic Doppler velocimeter (ADV) measurement campaign provides even more information about the spatial distribution of the currents around the turbine.

2.1 Acoustic Doppler Current Profiler (ADCP) Measurements

2.1.1 ADCP Operating Principles

Acoustic Doppler Current Profilers (ADCP's) are used to measure current velocity throughout the water column. Active acoustic transducers are used in instruments such as ADCP's to determine fluid velocities by measuring the Doppler shift of acoustic signals scattered by particles passively advected with the flow. This measurement technique assumes that small particles in the fluid follow the flow. The Doppler effect is the frequency shift that occurs when a wave hits an object moving at a relative velocity to the source and bounces back. As shown in Figure 2.1, a sound pulse is transmitted, reflected by scatterers in the fluid, and then reflected back to the transducer at a different, shifted frequency.

This frequency shift between the transmitted and reflected sound pulse is composed of two Doppler shifts as indicated in Figure 2.1. The sound frequency is affected as the original signal, F_s, impacts the scatters and again when that signal impacts the transducer for the second time.

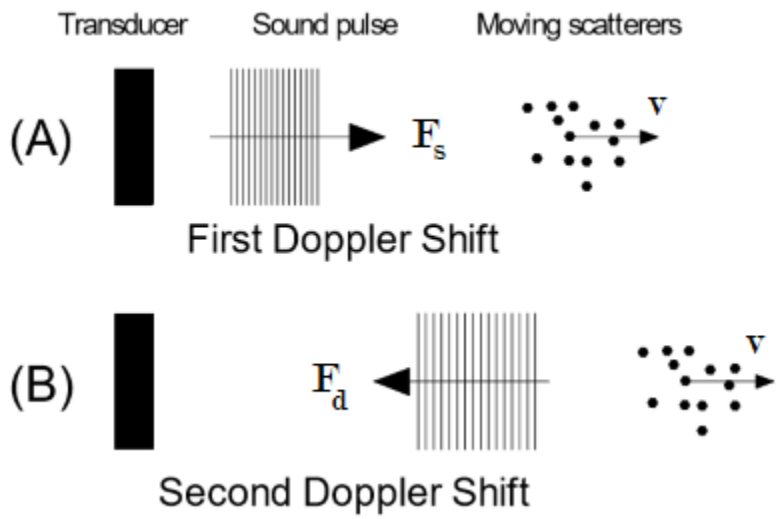

Figure 2.1: Diagram depicting the transmission and receiving of signals from acoustic current measurement transducers and the Doppler shift of that signal [36]

Velocities are often not aligned with the acoustic source direction, resulting in an angle, A, between the source and the scatterer velocity, v, as seen in Figure 2.2.

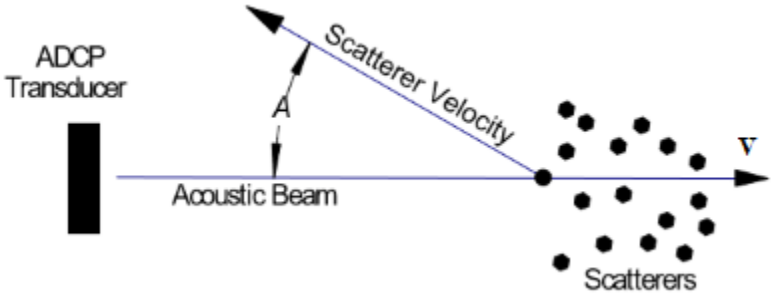

Figure 2.2: Diagram depicting the difference in direction between the acoustic pulse and the particle velocity. [36]

The two Doppler shifts and difference in direction of the particle velocity are both captured in the Doppler equation below to compute the frequency shift, F_d,

$$F_d = 2F_s\frac{v}{c}cos(A) \tag{2.1}$$

Where F_s is the source frequency, v is the relative velocity between the source and the receiver, c is the speed of sound, and A is the scattering angle. The resulting frequency shift can be used to determine the flow velocity along the direction of the acoustic pulse.

Broadband acoustic devices such as most ADCP's use a band of frequencies for the source instead of one frequency, F_s. This makes it difficult to measure differences in frequency needed to utilize the Doppler effect using Equation 2.1. Instead, a time delay technique is used. If two distinct acoustic pulses are scattered by a stationary particle, as seen in part (A) of Figure 2.3, then the acoustic response has the same time between pulses. If the particle is moving then that same acoustic pulse will cause a delay in the response as seen in part (B). This same illustration applies to signals of any shape, with any frequency content. Parts (C) and (D) in Figure 2.3 demonstrate the same time delay effect for a sinusoidal signal.

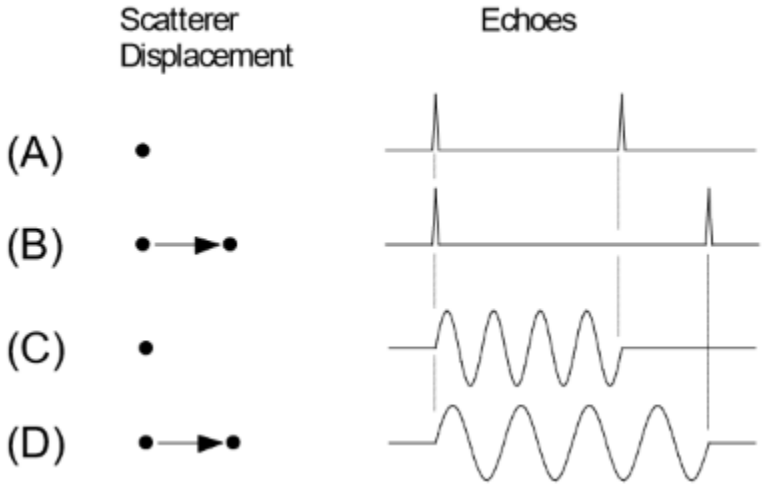

Figure 2.3: Diagram of how moving particles create a time delay in the sound pulse received by the transducer [36]

This time delay technique is used with more complicated broadband signals to determine the Doppler shift and the velocity of the particles in the flow. The time delay is usually measured as a phase shift between the transmitted and received broadband signal. The Doppler shift and time delay strategies to determine the current velocity were demonstrated here for one transducer. A single transducer can only resolve velocities in the along-beam direction. ADCP's can have

3,4, or 5 transducers, but presently the most common configuration is with 4 acoustic beams. The transducers are angled away from the vertical so that three components of velocity can be resolved. By combining different beam directions, the components of the velocity in three directions can be resolved. ADCP's create a current profile throughout the water column by range gating the acoustic pulses received by the transducer. Range gating uses time intervals to "gate" velocities into depth bins. The speed of sound, c, relates a time interval, Δt, to the depth range, R, by

$$R = c\Delta t \tag{2.2}$$

To determine the sound speed of the water ADCP's are often equipped with a temperature sensor, as sound speed in water is dependent on temperature. In addition to temperature sensors ADCP's also include a compass and tilt sensor. These sensors make it so that velocities can be assigned the correct location and direction. Compasses are used to convert the ADCP beam velocities into the Earth-North-Up reference frame. This is very important because often ADCP's are deployed without any reference direction (such as being dropped on the sea floor). The tilt sensor is used to correct velocities into the right depth bins even when the ADCP is not upright. This is important for bottom deployments on un-even sea-beds and on floating platforms with pitch and roll motion. The pitch and roll angle of the instrument are used to map the range gated cells to the correct depth bin as seen in Figure 2.4.

The errors in ADCP data must be kept below a certain level to obtain meaningful data over the profiling range. The random errors, ϵ, are calculated by,

$$\epsilon \propto \frac{1}{N^{1/2}\Delta z f_{sonar}} \tag{2.3}$$

Where N is the number of pings in an ensemble, Δz is the bin size, and f_{sonar} is the frequency of the sonar. There are a minimum number of pings, bin size, and frequencies that must be used in order to obtain low error data over the intended depth range.

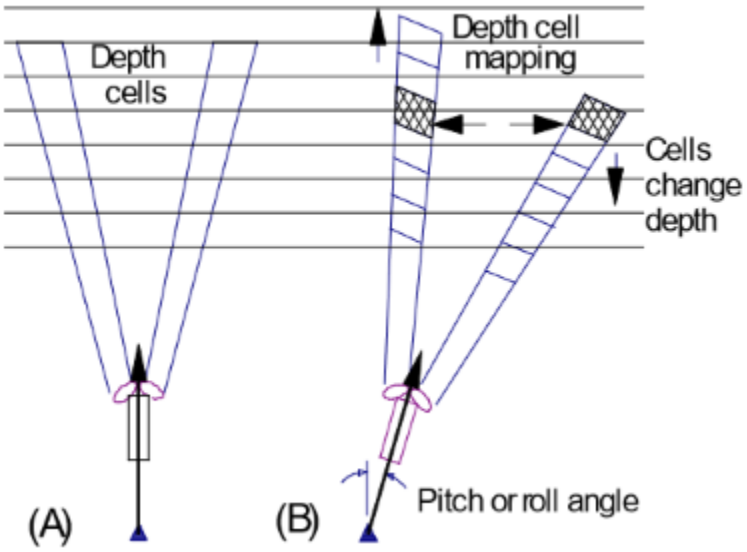

Figure 2.4: Diagram of how tilt angles effect the depth of bins and how tilt sensors are used to correct that [36]

2.1.2 Review of Previous Resource Assessment

One of the initial steps in the process of deploying a tidal energy conversion system is the tidal energy resource assessment. The current speeds and their distribution at the intended deployment site are important to determine the size of the turbine, the loads on the deployment structure, and the predicted energy production. A resource assessment was conducted prior to the design and fabrication of the turbine deployment platform [10]. The resource assessment followed the International Electrotechnical Commission (IEC) technical specification for a tidal current stationary survey in IEC TS 62600-201 [16] as closely as possible.

Resource characterization metrics were used to quantify the results of the resource assessment [30]. To characterize the amount of power available in the flow the mean kinetic power density is used as defined by,

$$\overline{K} = \overline{\frac{1}{2}\rho|U^3|} \tag{2.4}$$

which is a function of the current speed, U, and water density, ρ. This parameter remains general by only depending on the flow characteristics, not the device size, so it can easily be used for comparing different sites. The difference in the power available from the ebb and flood tides is quantified by the mean kinetic power asymmetry,

$$\Phi = \frac{\overline{K_{ebb}}}{\overline{K_{flood}}} \tag{2.5}$$

The tidal dependence of the flow is further quantified by the ebb/flood directional asymmetry,

$$\overline{\Theta_{flood}} - \overline{\Theta_{ebb}} - 180^{\circ} \tag{2.6}$$

which is a function of the mean ebb and flood current directions.

The resource assessment was based on two bottom mounted ADCP deployments. The first ADCP survey (referred to as K-07) was conducted over the summer of 2007 as part of a larger NOAA/NOS survey of the currents throughout the Great Bay Estuary [20]. This survey served as the initial feasibility assessment, determining that the Piscataqua River below the Memorial Bridge had enough current resource to support a tidal energy conversion system. The second ADCP survey (referred to as HG-14) was conducted in 2013 and 2014 with the goal of characterizing the currents at the Memorial Bridge near pier $\#2$ for tidal energy deployments [15]. These deployments were located approximately 64m apart as indicated in Figure 2.5. The final location of the turbine deployment platform is marked by the letter C.

The K-07 survey was conducted over a 3 month period near the center of the shipping channel at an approximate depth of 20.5 m. The HG-14 survey was closer to the location of the tidal energy conversion system at an approximate depth of 16 m. The HG-14 deployment location was chosen as the closest location to the Portsmouth side of bridge pier $\#2$ that was possible with a ship deployment of a bottom-mounted ADCP. The full survey was over a 4 month period but there was a construction barge over the ADCP for part of the deployment, resulting in 2 months of usable data. Due to the location and duration of these surveys, the original resource assessment would be classified as a feasibility study according to IEC TS 62600-201 [16]. A feasibility study should

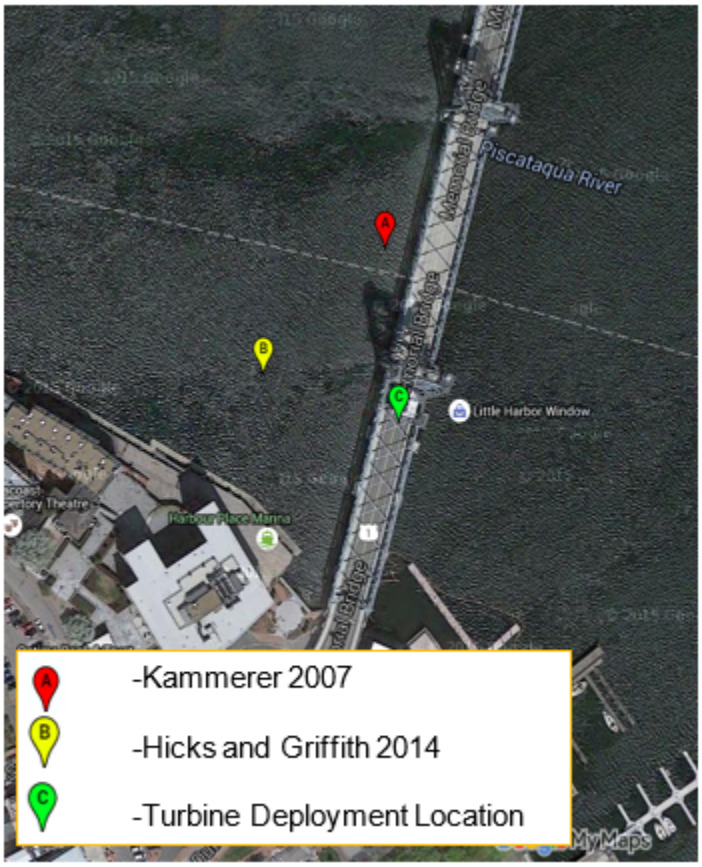

Figure 2.5: Locations of ADCP deployments at the Memorial Bridge [9]

be used to determine the location of the turbine deployment but not for accurately determining the annual energy production expected at the site.

To not exclude tidal elevation interference the range of the HG-14 ADCP was limited to 50 0.25 m bins. The top bin located at approximately 12.1 m above the river bed was used for the resource assessment. The resource assessment used the 1 m bin from K-07 that corresponded to a depth of approximately 4 m below the surface. Based on battery and storage limitations, the K-07 ADCP recorded 6 minute ensembles and the HG-14 ADCP recorded 15 minute ensembles. The parameters used in these two surveys are summarized in Table 2.1.

	K-07	HG-14
Latitude [°N]	43.0795	43.0791
Longitude [°W]	70.75283	70.7534
Orientation	Upward Facing	Upward Facing
Approximate Deployment Depth [m]	20.5	16
Record Dates	6/21/07 - 9/24/07	12/19/13 - 2/16/14
Instrument Model	RDI Workhorse Sentinel	RDI Workhorse Sentinel
Frequency [kHz]	600	1200
Beam Angle [°]	20	20
Ping Interval [s]	2	2
Ensemble Interval [min]	6	15
Number of Pings per Ensemble	180	450
Cell Size [m]	1	0.25
Blanking Distance [m]	0.88	0.8
Number of Bins	30	50
Velocity Accuracy	0.3 %	0.3 %
Compass Accuracy	$\pm$ 2 °	$\pm$ 2 °

Table 2.1: Parameters for the Previous K-07 [20] and HG-14 [15] ADCP Surveys [35]

The current speed and direction for the resource assessment are shown in the polar plots in Figure 2.6. The flood tide is represented by directions greater than 180 °, while the ebb tide is represented by the directions less than 180 °. In general, the K-07 survey shows more symmetry between the magnitude of the ebb and flood tides. The HG-14 survey shows a stronger ebb tide and weaker flood tide than the K-07 survey. These differences can be attributed to the difference in cross-river location of the deployments.

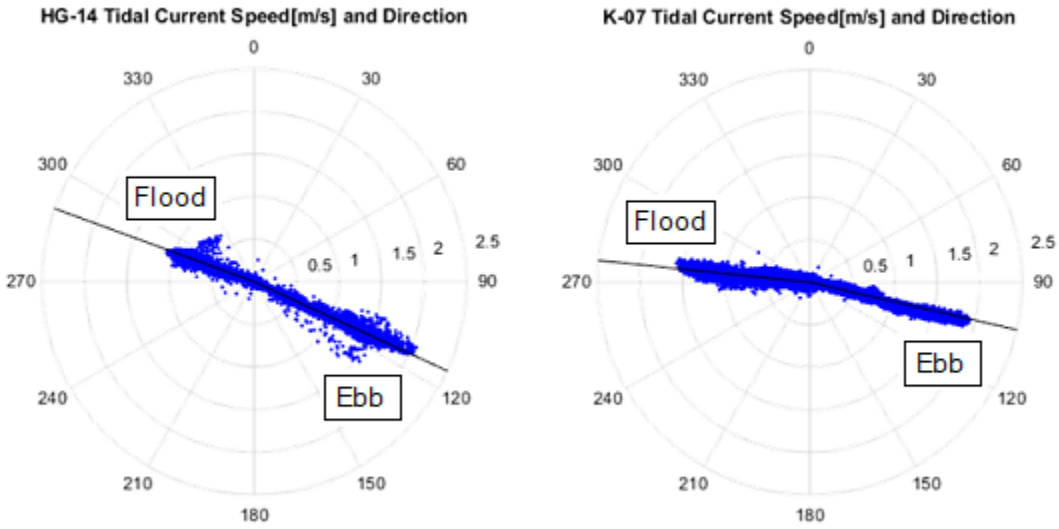

Figure 2.6: Polar plots of the current speed and direction from the K-07 and HG-14 ADCP surveys [9]

The results of the previous resource assessment from the two different ADCP surveys are shown in Table 2.2. [9] The different results from the ADCP surveys are due to the difference in location and the ensemble interval. The location of the deployment is very important, as the currents vary across the river according to the local bathymetry. Data at or very close (<10 m) to the turbine deployment location will provide the most accurate results for power prediction. The HG-14 survey location is closer to the turbine deployment location in the along-river direction, while the K-07 survey location is closer to the center of the river. It is expected that the currents measured at the HG-14 location would be a better representation of the currents at the turbine location, but data closer to the turbine deployment location was desirable in order to confirm this prediction.

ADCP ensemble averaging removes current fluctuations with timescales less than the ensemble time. It is predicted that the tidal current may be changing speed faster than the 6 min and 15 min ensemble times used in the K-07 and HG-14 surveys. To confirm this, current data with higher temporal resolution is required.

	K-07	HG-14
Mean Kinetic Power Density $[kW/m^2]$	0.766 $\pm$ 0.00689	0.668 $\pm$ 0.00601
Mean Kinetic Power Asymmetry	1.72 $\pm$ 0 *	5.39 $\pm$ 0 *
Maximum Current $[m/s]$	1.93 $\pm$ 0.0058	2.06 $\pm$ 0.006
Ebb/Flood Directional Asymmetry [°]	-7.04 $\pm$ 2	-5.04 $\pm$ 2

Table 2.2: Resource characterization metrics from the initial tidal energy resource assessment (* within instrument's velocity resolution) [9]

2.1.3 Living Bridge 2017 ADCP Deployment

The goal of the ADCP deployment at the Living Bridge site was to obtain a long-term data set of current velocities before and during the turbine deployment to compute expected power production. The ADCP's are mounted at the bow and stern of the platform along the center line, approximately two turbine diameters on either side of the turbine. The ADCP's are used to measure the inflow to the turbine from the ebb and flood tides as seen in Figure 2.7.

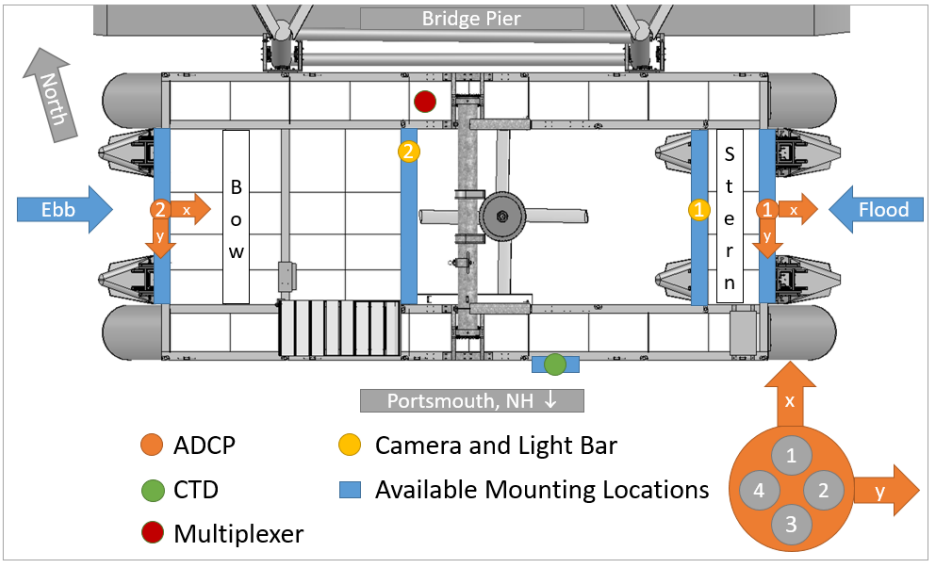

Figure 2.7: Location and orientation of ADCP's on the turbine deployment platform

The ADCP's are also used to produce as-built power curves for the turbine, showing the relationship between the current speed and the power output. The ADCP's are part of the baseline

instrumentation that is connected to grid power and a server database, so power and battery usage are not an important issue.

The ADCP's chosen for this project are LinkQuest FlowQuest 1000's which are four beam 1000 kHz devices. These devices use the FlowQuest software, but terminal communication is usually required to start a deployment as described in Appendix B.

The ADCP's were deployed and recording data continuously in the summer and fall of 2017. Due to the weather, electrical routing changes, and software issues, this is the longest set of continuous data that is available to date from these instruments. The deployment over this time frame will be referred to as the LB-17 ADCP survey. The parameters used for the LB-17 survey are listed in Table 2.3.

	LB-17
Latitude [°N]	43.0790
Longitude [°W]	70.7528
Orientation	Downward Facing
Approximate Deployment Depth [m]	0.3
Record Dates	6/22/17 - 11/7/17
Instrument Model	LinkQuest FlowQuest
Frequency [kHz]	1000
Beam Angle [°]	22
Ping Interval [s]	2
Ensemble Interval [min]	2
Number of Pings per Ensemble	60
Cell Size [m]	0.25
Blanking Distance [m]	0.4
Number of Bins	92
Velocity Accuracy	0.25 % $\pm$ 0.2 mm/s
Compass Accuaracy	$\pm$ 2 °

Table 2.3: Parameters for the Living Bridge 2017 ADCP Survey

The record length of the LB-17 survey satisfies the 90 day requirement specified in IEC TS 62600-201 for a stage two, or layout design study [16]. These measurements were also taken at the turbine location so they can be used for accurate predictions of the annual energy production. Recommendations about the possible effects of seasonality on the currents are not provided in the

IEC standard. Differences between the winter-spring currents captured in the HG-14 survey and the summer-fall measurements of the K-07 and LB-17 surveys may exist, but they are expected to be small.

These ADCP's will be able to measure throughout the water column and water velocities higher than those expected at the site. The depth at the deployment site is approximately 20 m (tidally varying) and the maximum current measured during HG-14 was 2.06 m/s. The smallest bin sizes, highest ping rates, and shortest ensemble times were chosen so that as much data as possible was collected in this area of interest.

The downfall of decreasing the ADCP ensemble interval is an increase in the random error. The estimated random error in the ADCP measurements is proportional to the number of pings in an ensemble as was seen in Equation 2.3. By reducing the ensemble interval to 2 minutes for the LB-17 survey from the 15 minute ensemble used in the HG-14 survey, the random errors are 2.3 times greater. This error is still expected to be small (within the instrument accuracy), but a quantitative measure cannot be determined because the variation of the pings within each ensemble is not available for LinkQuest FlowQuest ADCP's.

The region of interest is the deployment depth of the turbine, which is around 0.25 m to 2 m below the surface. The ADCP's are mounted approximately 0.3 m below the surface, combined with the blanking distance the first bin would not start until 0.7 m below the surface. This depth would miss the current at the top 0.2 m of the turbine rotor, but 6 depth bins would still be recorded over the area of the turbine. The middle of the third bin is approximately 1.3 m below the surface, close to the mid-turbine depth of 1.4 m. The third bin of the bow and stern ADCP's was used as the representative bin for estimating power production.

The spatial resolution of ADCP measurements decreases with distance away from the instrument because the beams are expanding and the distance between the beams is larger farther away from the instrument. The basic assumption is that the flow is uniform over that distance and if that is not shown in the velocities then they are discarded. Since the bottom mounted ADCP's used in the previous resource assessment used bins near the surface, the spatial resolution is lower than for

the surface mounted ADCP's used in the LB-17 survey. The distance between opposite beams in the bin used for analysis was on the order of 10 m for the HG-14 and K-07 surveys and 1 m for the LB-17 survey. The shorter distance between beams for the LB-17 survey allows smaller scale motions to be captured than was possible with the previous surveys.

Although multiple compass calibrations were conducted following the procedure in Appendix in A, the compass direction was still influenced by the magnetic interference caused by the metal at the site. As an example of this, the mounting orientation of ADCP 2 was changed mid-deployment due to damage to the pressure sensor. If the compass was working correctly then the change in orientation would not effect the compass direction readings. Figure 2.8 shows that the flow direction of ADCP 2 changed by around 40 °due to the change in the ADCP mounting orientation.

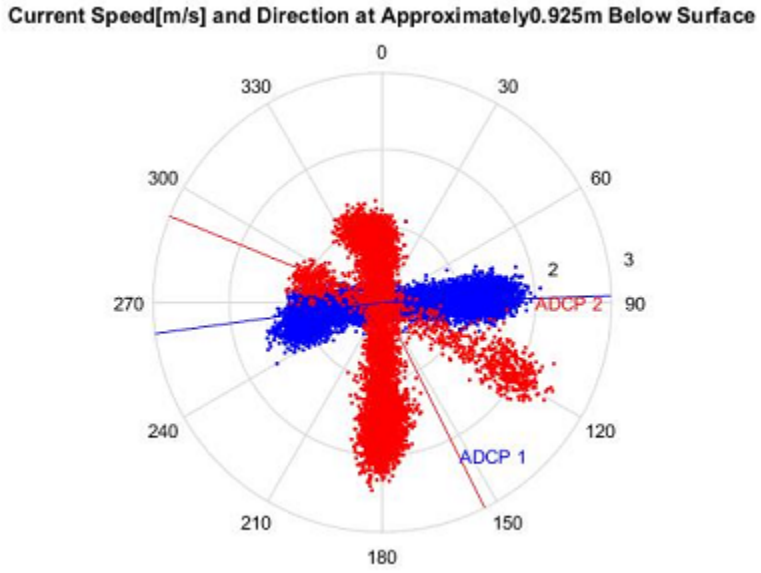

Figure 2.8: Polar plot of ADCP data in East, North, Up coordinates produced using the internal compass, demonstrating compass errors. The compass output changed after an orientation change of ADCP 2 (rotation)

The ADCP compass direction and the resulting velocity values in the east, north, up (ENU) coordinate system should not be used when deploying ADCP's on the turbine deployment platform. The presence of steel interference cannot be avoided on the platform and any data using the compass input would provide meaningless flow directions.

To overcome the compass errors the instrument coordinate system velocity, instead of the velocity in ENU coordinates, was used from the ADCP's. The instrument coordinate system is defined by the orientation of the instrument. In the case of this deployment the orientation is constant on the platform and is assumed to be the same as the angle of the bridge pier, which is 105.05 °relative to north. All of the ADCP data was corrected with this value so that zero degrees represents north. The assumption that the ADCP orientation is the same as the bridge pier could result in errors in the current direction. The ADCP alignment within the instrument is assumed to be within $\pm$ 2 °. The platform can rotate by approximately 2.5 cm (1 in) over 7.3 m (255 in) in the pile guides connecting to the vertical guide posts. This misalignment of the platform results in a $\pm$ 0.0035 °error in the ADCP direction. In total, the ADCP direction accuracy is estimated to be $\pm$ 2.0035 °, which is comparable to the $\pm$ 2 °accuracy of the compass direction.

Polar plots showing the current speed and direction from the two ADCP's used in the LB-17 survey are seen in Figure 2.9.

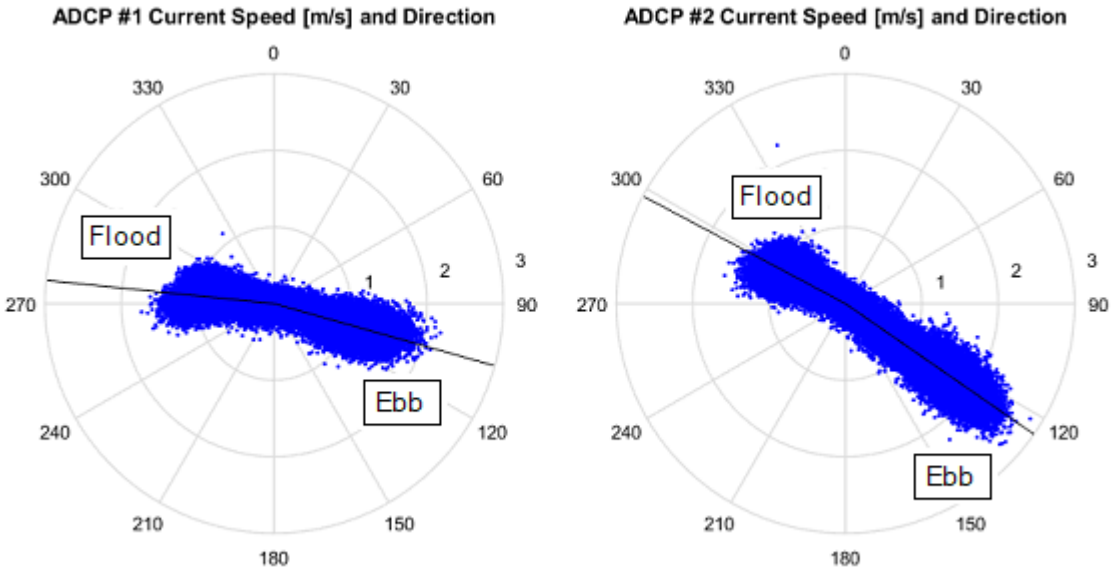

Figure 2.9: Polar plots showing the current speed and direction from ADCP's 1 and 2 in the bin 1.4m below the surface (flood tide is > 180 °, ebb tide is < 180 °)

ADCP 2 shows a stronger ebb tide as seen in Figure 2.10 of current magnitude measured using ADCP 1 and 2 during a representative day. The current magnitude is the amplitude of the

current velocity x-direction and y-direction vectors. There is also a direction associated with the magnitude to fully describe the horizontally velocity vectors. The ebb tide is represented as a negative magnitude and the flood tide is represented as a positive magnitude. This sign convention follows that used by the National Oceanic and Atmospheric Administration (NOAA). [25] During data processing, the positive and negative signs were assigned based on the assumption that the flood tide has a direction greater than 180 °, and the ebb tide has a direction less than 180 °.

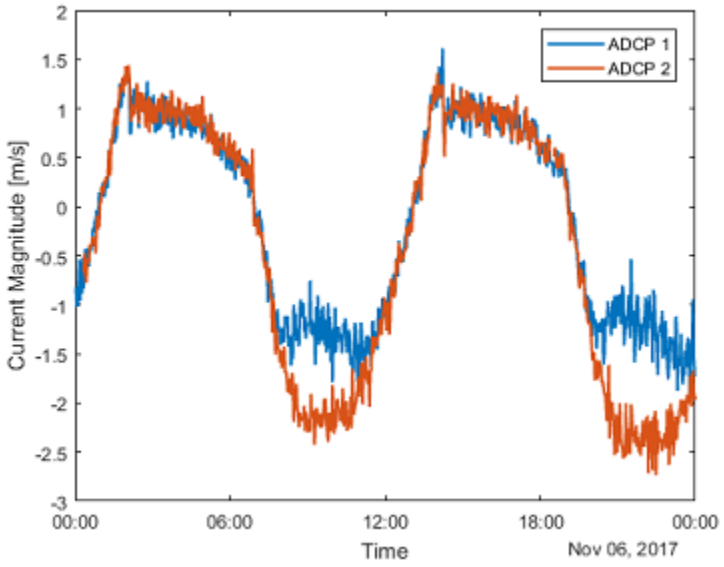

Figure 2.10: Current magnitude from a representative day measured using ADCP 1 and 2 in the bin 1.4m below the surface (flood tide is positive, ebb tide is negative)

Differences in the magnitude and direction from the two ADCP's can be attributed to their location on the turbine deployment platform. ADCP 1 is located at the stern of the platform as seen in Figure 2.7, so the ebb tide appears to be slower during parts of the tidal cycle due to interactions with the platform and bridge pier. The direction is also different between the two devices because of the influence of the bridge pier. Due to these differences, a combination of the data from both devices is used for the analysis. Since the turbine inflow is the most important for power production estimates, data for the flood tide is from ADCP 1 and data for the ebb tide is from ADCP 2. The combined current speed and direction can be seen in Figure 2.11.

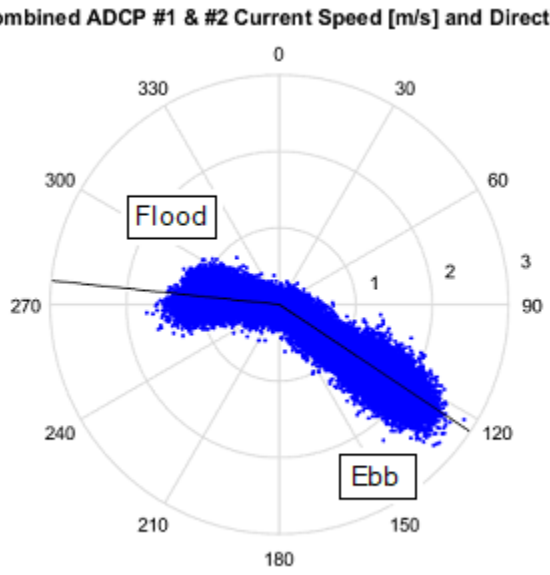

Figure 2.11: Polar plot showing the combined current speed and direction from ADCP's 1 and 2 in the bin 1.4m below the surface

In both data sets there is a shift in the flood tide direction and magnitude near the beginning of the more steady portion of the tide. This can be seen as a drop in magnitude in Figure 2.10 and an asymmetry in the flood tide leg in Figures 2.9 and 2.11. This can be attributed to structure interactions or a change in direction of the flood current in the main channel away from the deployment location.

	LB-17 (2 min ensemble interval)
Mean Kinetic Power Density $[kW/m^2]$	1.110 ± 0.00831
Mean Kinetic Power Asymmetry	6.77 ± 0 *
Maximum Current $[m/s]$	2.85 ± 0.0071
Ebb/Flood Directional Asymmetry [°]	-27.6 $\pm$ 2

Table 2.4: Resource characterization metrics from the LB-17 survey, using the combined current data from ADCP's 1 and 2 (* within the accuracy of the measurements)

Compared to the resource assessment completed with the K-07 and HG-14 surveys, the ADCP measurements taken on the turbine deployment platform indicate a more powerful and asymmetric flow as seen in Table 2.4. The mean kinetic power density calculated using the LB-17 survey is 45% greater than the K-07 survey and 66% greater than the HG-14 survey. The stronger ebb tide

results in an increased mean kinetic power asymmetry similar to that seen from the HG-14 survey. The measurements taken farther toward the New Hampshire side of the river demonstrate a faster ebb tide with a greater maximum current value.

The ensemble interval also influences the resource characteristic metrics. According to IEC TS 62600-201 [16], ensemble intervals ranging from 2 minutes to 10 minutes are appropriate for tidal energy resource assessments. Ensemble intervals below 2 minutes can be influenced by turbulent fluctuations and ensemble intervals greater than 10 minutes do not capture all of the tidal current variations of interest.

Although the 15 minute interval does not meet these specifications, to demonstrate the affect of the ensemble interval the LB-17 data was averaged to convert the 2 min ensemble interval to 16 minutes. The biggest difference seen in the polar plot in Figure 2.12, is the decrease in the spread of the currents due to the averaging. The longer ensemble polar plots look more like the HG-14 and K-07 plots seen in Figure 2.6, but with greater asymmetry and a faster maximum current.

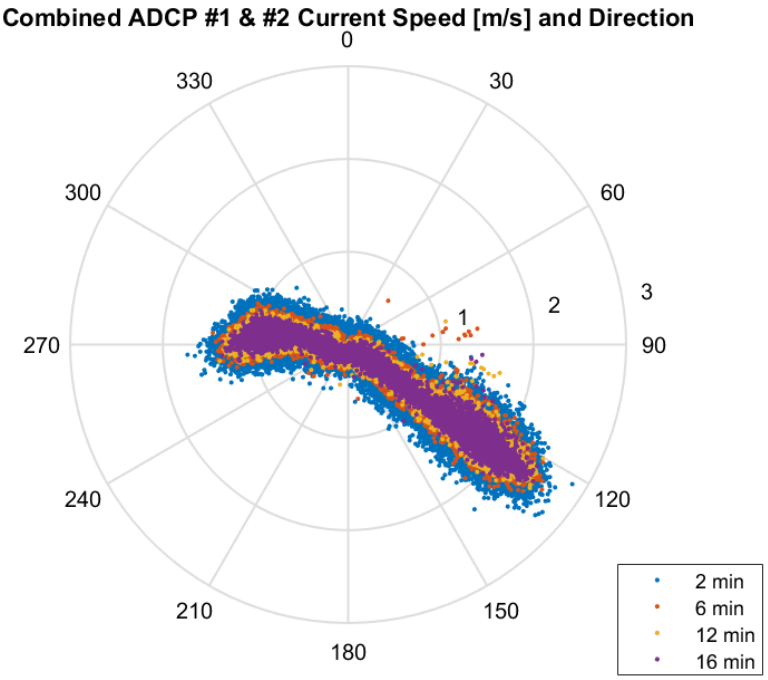

Figure 2.12: Polar plot showing the combined current speed and direction from ADCP's 1 and 2 in the bin 1.4 m below the surface using a 16 min ensemble interval

The resource characteristic metrics were also calculated for the different ensemble intervals for the LB-17 survey, as seen in Table 2.5.

LB-17				
Ensemble Interval [min]	2	6	12	16
Mean Kinetic Power Density [kW/m^2]	1.110 $\pm$ 0.00831	1.090 $\pm$ 0.00817	1.085 $\pm$ 0.00813	1.081 $\pm$ 0.00810
Mean Kinetic Power Asymmetry	6.77 $\pm$ 0 *	6.91 $\pm$ 0 *	6.94 $\pm$ 0 *	6.96 $\pm$ 0 *
Maximum Current [m/s]	2.85 $\pm$ 0.0071	2.61 $\pm$ 0.0065	2.50 $\pm$ 0.0062	2.48 $\pm$ 0.0062
Ebb/Flood Directional Asymmetry [°]	-27.6 $\pm$ 2	-30.9 $\pm$ 2	-32.1 $\pm$ 2	-33.0 $\pm$ 2

Table 2.5: Resource characterization metrics from the LB-17 survey, using the combined current data from ADCP's 1 and 2 using 2 min, 6 min, 12 min, and 16 min ensemble intervals (* within the accuracy of the measurements)

A decrease in the mean kinetic power density and maximum current is seen with longer ensemble intervals. The biggest change is seen with the 16 minute interval. Compared to the original LB-17 survey, the 16 minute ensembled data shows a 2.6$\%$ decreased in mean kinetic power density and a 13$\%$ decrease in the maximum current as a result of the averaging. The ensemble averaging has a greater effect on the maximum current, which would effect the current loads used to design a turbine and deployment system. The LB-17 survey still showed a 62$\%$ greater mean kinetic power density and a 20$\%$ faster maximum current speed than the HG-14 survey, even with the 16 minute ensemble interval that is comparable to the 15 minute interval used for the HG-14 survey. The faster currents from the Living Bridge survey can be attributed to the location difference between the three surveys. The maximum current speed is used for determining the design loads for drag on the support structure. The 2.06 m/s maximum current speed from the HG-14 survey was used for the design of the turbine deployment platform. The measurements from the LB-17 survey indicate that this value was lower than currents at the installation site at the platform. This suggests that measurements at the turbine location and with a short ensemble interval should be used when determining the current design loads.

2.2 Acoustic Doppler Velocimeter (ADV) Measurements

2.2.1 ADV Operating Principles

Acoustic Doppler velocimeters (ADV's) can measure water velocity at higher temporal and spatial resolution than ADCP's. The instrument consists of one acoustic transmitter and several pronged receivers as seen in Figure 2.13.

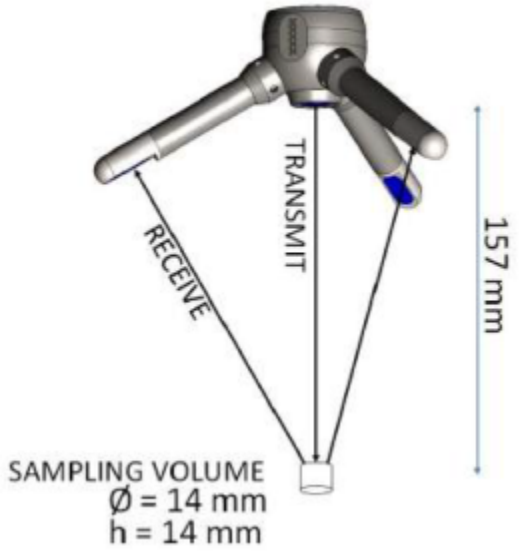

Figure 2.13: Diagram of the Nortek Vector ADV showing the transmit and receive beams, which intersect to form the measurement volume [28]

ADV's use the same principle as ADCP's to measure the water velocity by measuring the Doppler shift of acoustic pulses scattered by particles following the flow. A broadband acoustic pulse is transmitted and the time shift is determined by measuring the phase lag relative to the received acoustic pulse using the Doppler effect (discussed in Section 2.1.1). The sampling volume of the measurement is located at the intersection between these acoustic beams. The along beam velocity can then be transformed into the coordinate system of the instrument by knowing the placement of the prongs. ADV's are also equipped with sensors to measure heading, pitch, and roll which can be used to convert to an earth (east, north, up) or some other coordinate system.

To convert between the along beam velocity and the XYZ coordinate velocity the transformation matrix is used. [32]

One source of error in the measurement of velocity using pulse coherent acoustic instruments such as an ADV is refered to as phase wrapping. Phase wrapping results from the ambiguous determination of the Doppler phase shift. Based on the velocity range set in the instrument software by the user, the expected phase shift range is scaled. If the instrument reads a higher velocity, and higher phase, than the range, the phase will "wrap" around to the other end of the range. This wrapping then affects the velocity as well, resulting in non-physical velocity values. To avoid phase wrapping an adequate velocity range should be selected. However, a velocity range that is too high will result in more noisy data. Prior infromation about the flow conditions can be used to determine a good velocity range. [32]

Nortek Vector ADV's were selected for this project, as they are designed to be deployed in a field environment. These instruments consist of a three-pronged probe and a housing that encases the instrument electronics. The Vector is available with a fixed stem or a cable connecting the probe to the housing. For this project the cabled version was chosen to allow for different mounting configurations. The relevant parameters for the ADV experiments discussed here are found in 2.6.

Approximate Deployment Depth	1.4 m (55 in)
Deployment Dates	4/22/19 - 4/26/19
Instrument Model	Nortek Vector
Frequency [MHz]	6
Sampling Rate (Output) [Hz]	64
Internal Sampling Rate [Hz]	250
Measurement Volume [cm^3]	2.65 (1.5 cm diameter and height)
Velocity Range	$\pm$ 4.00 m/s
Velocity Accuracy	$\pm$ 0.5 % of measured value $\pm$ 1 mm/s

Table 2.6: Parameters for the ADV Measurement Campaign [27]

To capture the fast time scales of turbulent motions, the highest sampling rate of 64 Hz is used. The velocity range is set to 4 m/s based on the previous ADCP measurements where the fastest velocities measured were under 3 m/s. The small ADV measurement volume will provide much

more fine scale velocity measurements than the ADCP's. The depth of the instrument corresponds to the mid-turbine depth and is comparable to the ADCP bin at 1.4 m below the surface.

2.2.2 ADV Experiment Motivation

The ADCP measurements at the Living Bridge site showed a strong dependence on deployment location and on ensemble time. To better characterize the flow at the site, ADV's were used to take measurements with higher temporal and spatial resolution. Changes in flow characteristics around the turbine are of interest because they could affect the power output. It was also important to investigate the effects of the bridge pier and turbine deployment platform on the local flow conditions.

The ADCP measurements at the bow and stern of the platform showed a lower ebb tide current speed at the stern. ADV measurements were taken at different locations on the platform in order to better define structural interactions that may have caused this discrepancy between the two ADCP's.

There was also a dip in the flood tide magnitude observed in the ADCP data from both the bow and stern. This could either be caused by structural interactions or a change in the mean flood tide direction. The ADV measurements on the turbine deployment platform provided more data in order to determine which was the likely cause of the dip in magnitude.

The length scales of structures in the flow can be influenced by the local bathymetry, topography, and structures in the flow. These length scales are of interest power production and flow interactions with the turbine.

2.2.3 ADV Experimental Set Up

Several different ADV measurement campaigns were attempted with varying success. Major issues that were encountered included mount vibration interference, long set up time, and debris damaging instruments. Mounting and equipment problems and solutions will be discussed in Chapter 5. Previous experiments provided insight that helped to inform the design of the final experiment campaign that was conducted from 4/22/19 to 4/26/19.

In previous experiments using both ADV's, the data sets were not synchronized and therefore could not be used for temporal comparison. The wiring harnesses in the instrument housing were changed to allow the two devices to be synchronized. Wires were also added to extend the synchronization leads of the instrument cables. Extra rounding wires were also soldered onto the cable as seen in Figure 2.14.

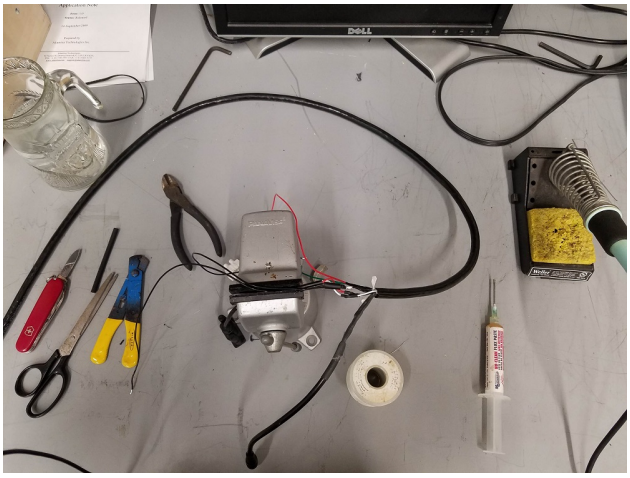

Figure 2.14: Extra grounding and synchronization wires being soldered onto an ADV cable

The set up of the ADV's including the synchronization wiring is shown in Figure 2.15. A picture of the set up installed on the turbine deployment platform is provided as Figure 2.16.

The fixed ADV is wired to act as the master, so that it provides the "sync out" signal to "sync in" channel of the moving ADV acting as the slave. To maintain the synchronization over the deployment the ADV's were configured to "start on sync" and "sample on sync". The "sync out" signal includes pulses at the completion of the sampling interval, the "sync in" device will then begin the next sample at the conclusion of the pulse, as shown in Figure 2.17.

The synchronization signal ensures that the instruments are sampling at the same time. This synchronization is reflected in the data internally logged by the ADV's but is not when recording to an external disk. For this reason, the ADV data was collected using the internal data logger. To provide a back up set of data that could be monitored, the ADV's also recorded to a laptop.

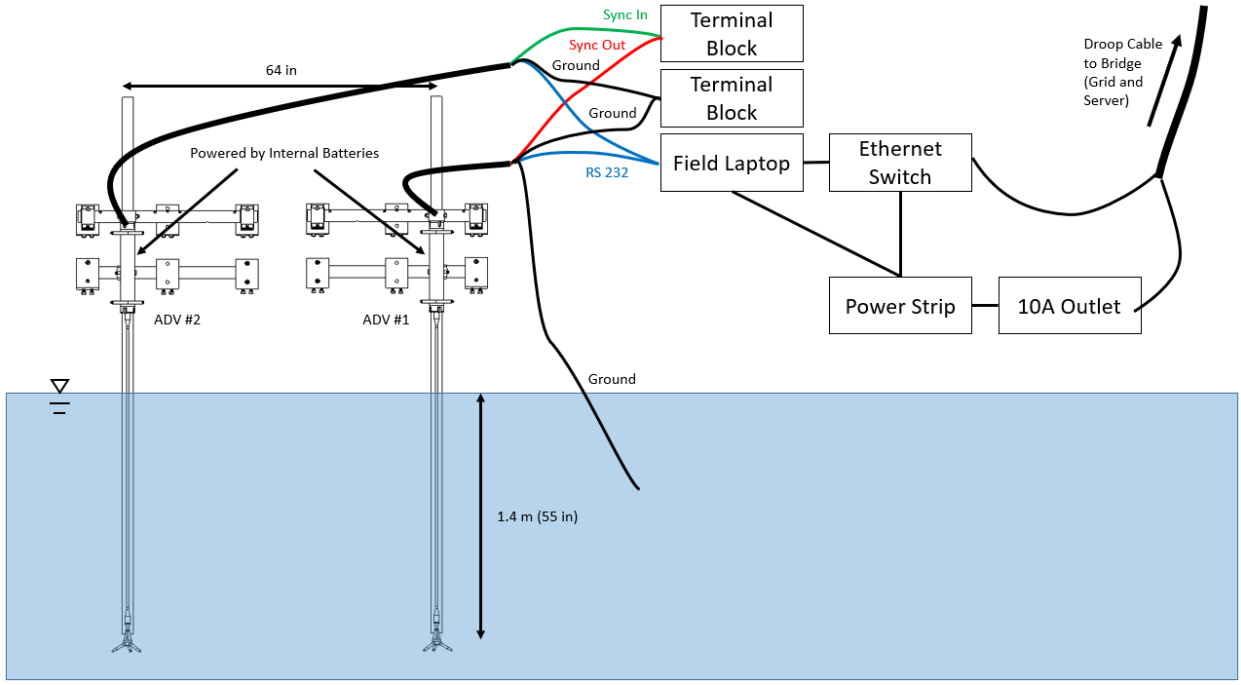

Figure 2.15: Diagram of the experimental set up for the ADV measurement campaign (wiring colors are system accurate)

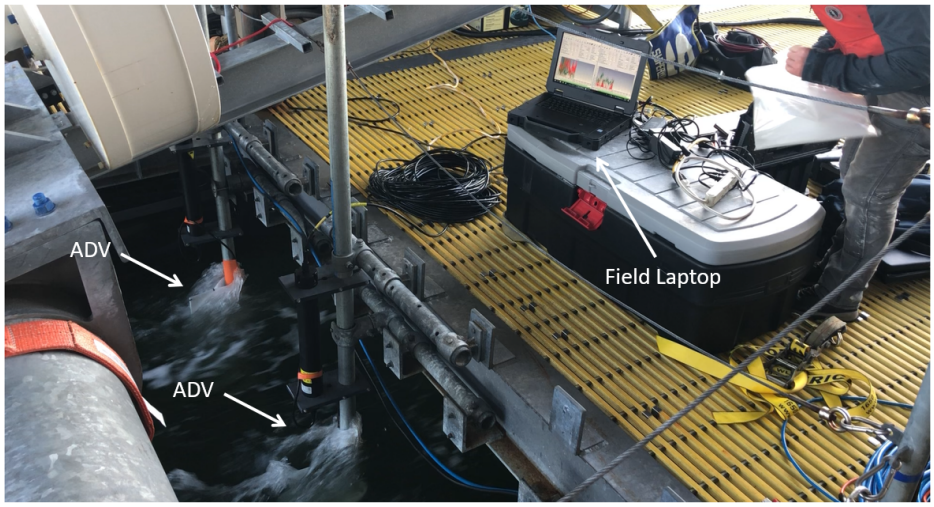

Figure 2.16: Picture of the experimental set up taken during a previous measurement campaign on 2/4/19

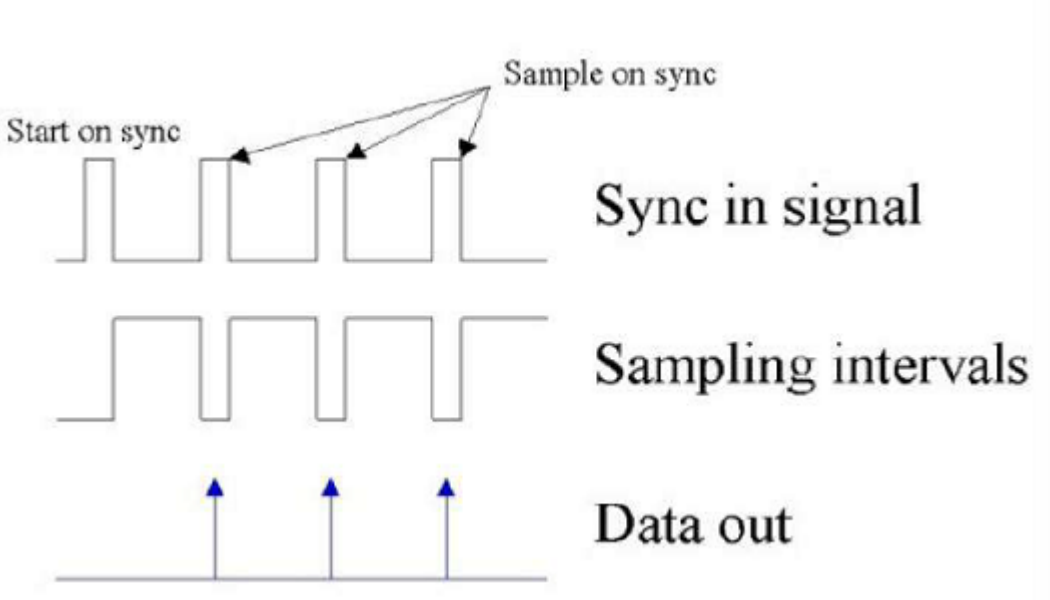

Figure 2.17: Diagram showing the sync pulses and sampling intervals for two Nortek Vector ADV's [28]

The synchronization utilizes the same channels as would be used for additional sensors, such as the inertial measurement unit (IMU) installed inside the Nortek Vector housing. The experiments with synchronization therefore were not able to have the IMU enabled, which may induce pitch, roll, and heading errors. The ADCP's used in the LB-17 survey measured pitch and roll at 1 minute increments, the maximum varition over this time period for was 4 °for pitch and 6 °for roll. Based on the dimensions of the platform and assuming that the angle change occurred over 1 minute, errors of 0.014 m/s from pitch and 0.011 m/s from roll were calculated. In total this would result in a maximum error of $\pm$ 0.025 m/s caused by pitch and roll motion interference in the ADV data.

Most of these previous experiments included data sets that only captured part of a tidal cycle, such as the peak ebb tide. It was difficult to determine differences between tidal variation and other factors with these short data sets. Planning deployments around the tidal cycle also introduces scheduling and logistics issues. It was decided that the best approach for determining the tidal and spatial dependence of the currents was to keep the ADV's stationary for at least one full tidal cycle. To investigate the spatial variation one of the ADV's would be periodically moved to different locations. This move would occur once a day so that one to two full tidal cycles could be

obtained. The other ADV would remain fixed in the same location so that an even longer data set could be obtained and it could be used as a reference for the other ADV measurements.

The choice of locations for the moving ADV were informed by previous flow measurements. Differences were observed between current measurements taken at the bow and stern of the platform (such as from the LB-17 ADCP survey shown in 2.9 and 2.10). These differences could be attributed to the bridge and platform structures. To investigate these differences in more detail, measurements were taken along the centerline of the platform. Differences in the flow characterizations across the inflow of the turbine location were also of interest, so measurements along the bow edge of the moon pool were also taken. Since there were concerns about influence of the bridge pier structure on the flow, the stationary ADV location was chosen to be on the left-most side of the moon pool. The chosen locations and deployment dates for the ADV experiment are shown in Figure 2.18.

An ADV was always installed as the fixed reference at the left location. For most of the deployment the instrument referred to as ADV 2 was installed at the left location, but for 4/23-4/24 it was easier and saved time to move it to the middle location and have ADV 1 installed at the left location. The ADV's can be seen installed in Figure 2.19 in the middle, left, and bow locations.

The current magnitude during the deployment can be seen in the ADCP data provided in Figure 2.20. The periods of time when the moving ADV was at the different locations are indicated on the plot.

In addition to spatial differences, it was also of interest to compare measurements from an ADV and an ADCP. For one day the moving ADV was installed 32 in from the ADCP at the bow of the platform. This distance was determined to be far enough away to avoid interference between the two devices, even though they have different operating frequencies.

The moon pool measurement locations also provide measurements to look at the length scales of the flow. The two different moon pool distances between the ADV's of 1.32 m (52 in) and 0.17 m (6.75 in) provide information about the length scales relative to the rotor radius 1.6 m (63.0 in)

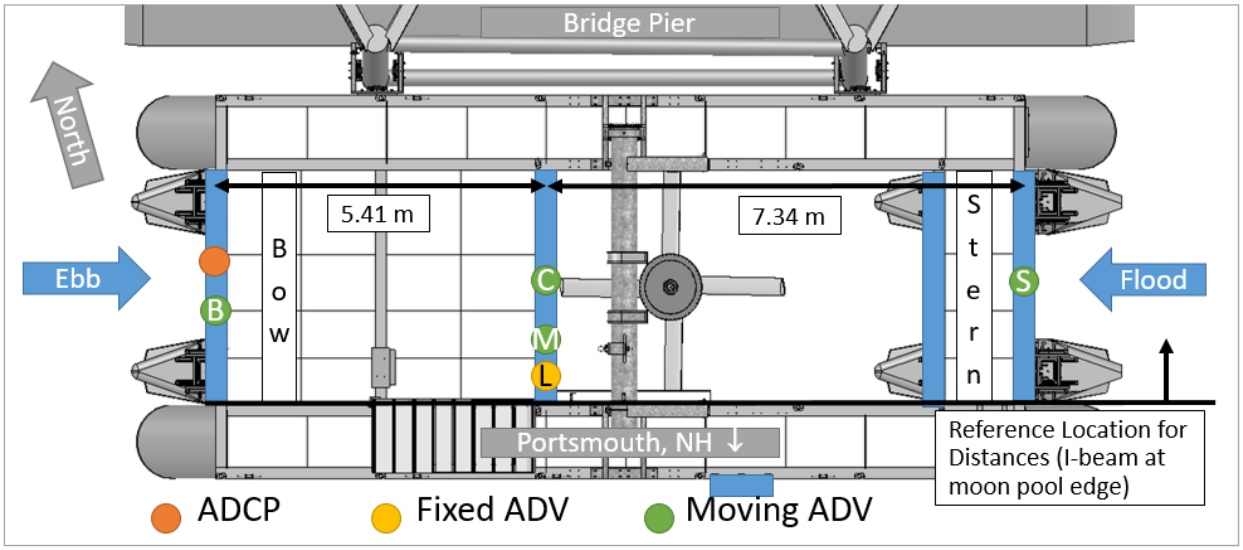

Location	Dates	Distance	Instrument
Left (L)	4/22-4/23	0.40 m (15.75 in)	ADV 2
Left (L)	4/23-4/24	0.38 m (15 in)	ADV 1
Left (L)	4/24-4/26	0.40 m (15.75 in)	ADV 2
Center (C)	4/22-4/23	1.72 m (67.75 in)	ADV 1
Middle (M)	4/23-4/24	0.55 m (21.75 in)	ADV 2
Stern (S)	4/24-4/25	1.71 m (67.5 in)	ADV 1
Bow (B)	4/25-4/26	1.27 m (50 in)	ADV 1
Bow	4/22-4/26	2.10 m (82.5 in)	ADCP 2

Figure 2.18: Locations and times of the ADV deployments on the turbine deployment platform

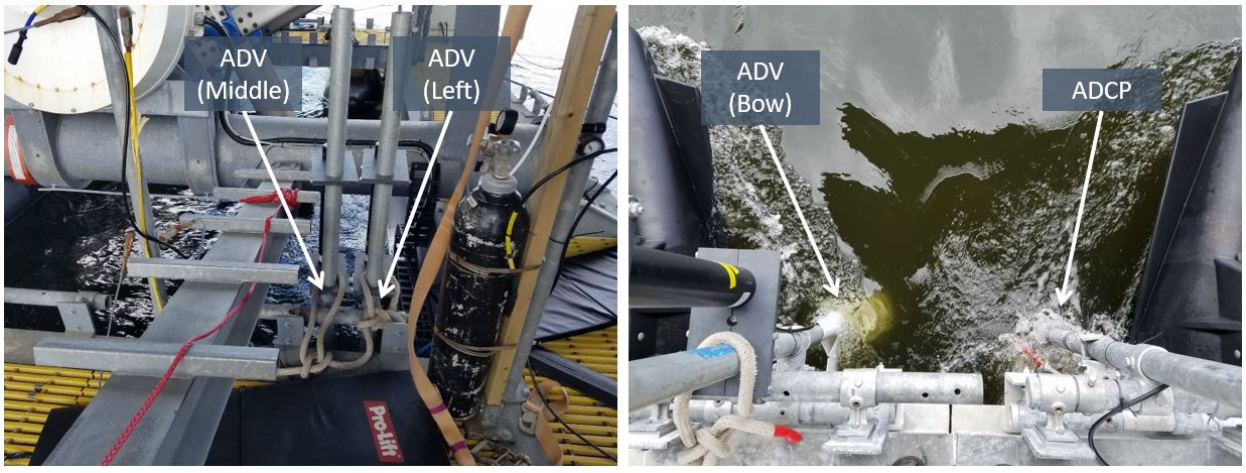

Figure 2.19: ADV's installed in the middle and left positions in the moon pool (left), ADV and ADCP installed at the bow (right)

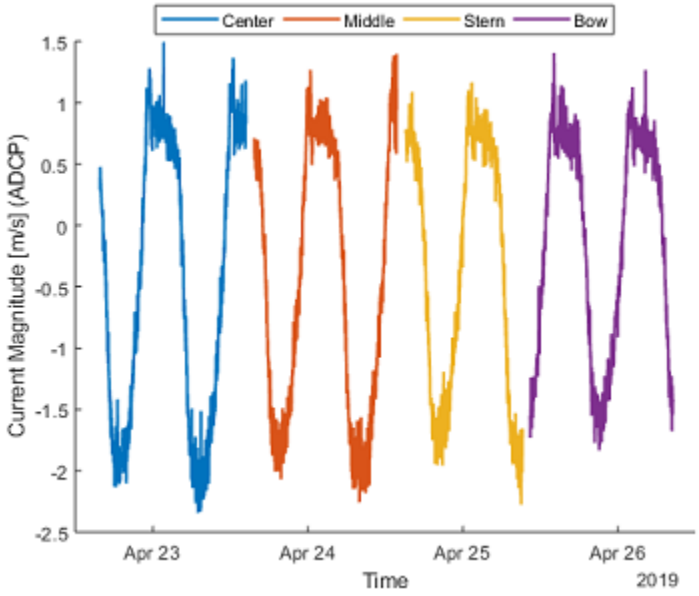

Figure 2.20: Current magnitude measured by the ADCP during the week of 4/22/19 - 4/26/19, indicating the location of the moving ADV during the deployment

and turbine blade chord 0.25 m (9.84 in). Specific ADV distances were restricted by the instrument mounting system, so the exact turbine lengths could not be achieved.

2.2.4 ADV Data Processing Techniques

To process the ADV data collected during the 4/22/19-4/26/19 measurement campaign, the data was broken up into ebb and tide events and filtered. The processes used to isolate sections of the tide with a relatively constant flow and filter those sections are described below. There was electrical interference that caused noise in the data that needed to be filtered out before analysis. The tide events were isolated from the raw ADV data so that the filtering could be applied to sections with an approximately constant mean. This was done so that it was not necessary to remove the tidal trend through regression or by computing the moving average.

2.2.4.1 Ebb and Flood Tide Event Separation

The portion of the tidal cycle that is of interest is when the current speed remains approximately constant and the flow can be considered somewhat stationary in the mean. The period of time from

4/25-4/26 when the ADV and ADCP were both positioned at the bow of the platform will be used to demonstrate the method for separating the ebb and flood tide events. The ADCP data is used to separate the tide events because it represents an averaged version of the flow measured by the ADV's. The dates and times that define the tidal cycles are then used to isolate the ebb and flood events in the ADV data. The filtering techniques used require a section of data with an approximately constant mean, so the separation of tide events is completed with the raw ADV data sets.

Before isolating the ebb and flood tide events the signed ADCP data is computed, where negative represents the ebb direction and positive represents the flood direction. The positive and negative signs were assigned based on the assumption that the flood tide is has a direction greater than 180 °, and the ebb tide has a direction less than 180 °. The magnitude and direction indicating the separate tides are shown in Figure 2.21. The colors shown in all of the following figures do not necessarily have the same meaning from one figure to another.

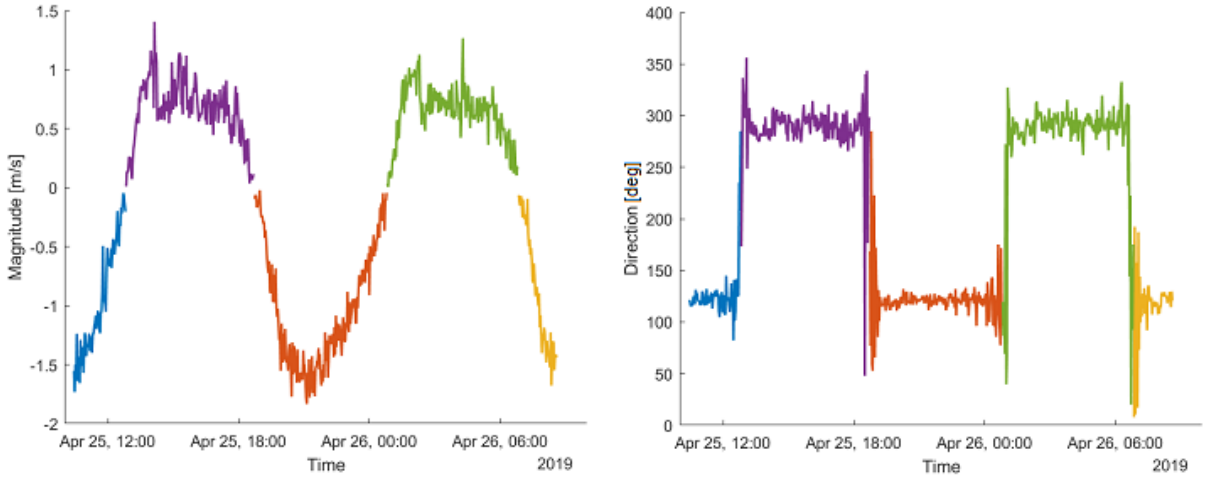

Figure 2.21: Current magnitude and direction from the ADCP measured while ADV 1 was at the bow location (4/25 - 4/26)

To focus on the sections when the mean current is approximately constant, a combination of a magnitude threshold and an auto-correlation check is applied to each of the flood and ebb tides of the ADCP data. To compensate for the changing tidal current magnitude over the spring-neap

(monthly) cycle, the threshold value is determined relative to the maximum current magnitude of the individual tide. This magnitude threshold does not represent a physical velocity at which an ebb or flood tide occurs, but defines a process for isolating the tide events. The magnitude cut-off, C_{mag}, is subtracted from the maximum unsigned ADCP magnitude for that tide, $U_{ADCP,Tide}$, to produce a threshold value specifically for that tide, $U_{Threshold,Tide}$.

$$U_{Threshold,Tide} = max(U_{ADCP,Tide}) - C_{mag} \tag{2.7}$$

For the ebb tide, C_{mag} was varied from 1.5 m/s to 0.1 m/s to determine which value would produce a stationary section of current data. Figure 2.22 shows the portions of the ebb tide from the ADV positioned at the bow on 4/25-4/26 that were produced using these varying magnitude cut-off values.

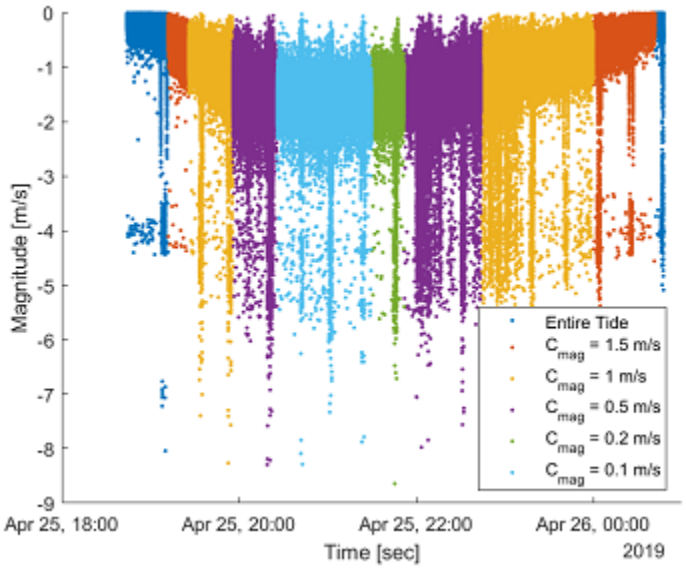

Figure 2.22: Current magnitude during an ebb tide from ADV 1 at the bow location (4/25 - 4/26), showing the change in record length using different magnitude cut-off values

To quantify the stationarity of the ebb and flood tide events, the auto-correlation is computed. The auto-correlation is the average of the multiplication between the random variable (such as velocity $u(t)$) and that random variable lagged by time, τ,

$$R_{yy}(t,\tau) = \langle u(t)u(t+\tau)\rangle \tag{2.8}$$

The auto-correlation is normalized by the auto-correlation at a time lag of $\tau = 0$ to create the auto-correlation coefficient,

$$\rho_{yy}(\tau) = \frac{\langle u(t)u(t+\tau)\rangle}{\langle u(t)^2\rangle} \tag{2.9}$$

If a random process is stationary then the auto-correlation will go to zero and stay at zero as the lags become longer. [11]

The auto-correlation coefficient of the current magnitude sections pictured in Figure 2.22 are shown in Figure 2.23. The auto-correlation approaches zero as the ebb tide section gets smaller due to the tighter magnitude cut-off value.

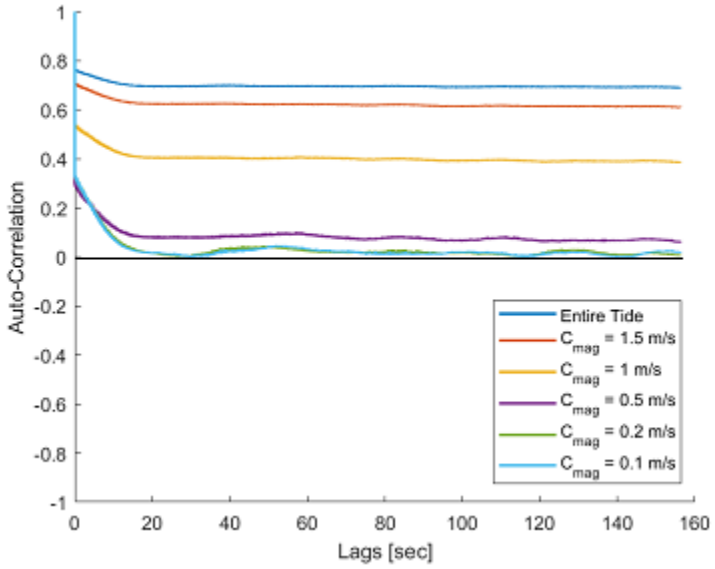

Figure 2.23: Auto-correlation coefficient of current magnitude during an ebb tide from ADV 1 at the bow location (4/25 - 4/26), showing the change in convergence using different magnitude cut-off values

The goal of the ebb and flood separation is to end up with the longest possible section of stationary data. As shown in Figure 2.23, both the 0.2 m/s and 0.1 m/s auto-correlations approach

zero and can be considered stationary. The longer length of the 0.2 m/s ebb tide section, leads to the conclusion that the 0.2 m/s magnitude cut-off should be used for the ebb tide data sets.

The same process was used to select a magnitude cut-off of 0.5 m/s for the flood tide sections. The magnitude of the flood tide from the ADV at the bow location with the different magnitude cut-offs is shown in Figure 2.24.

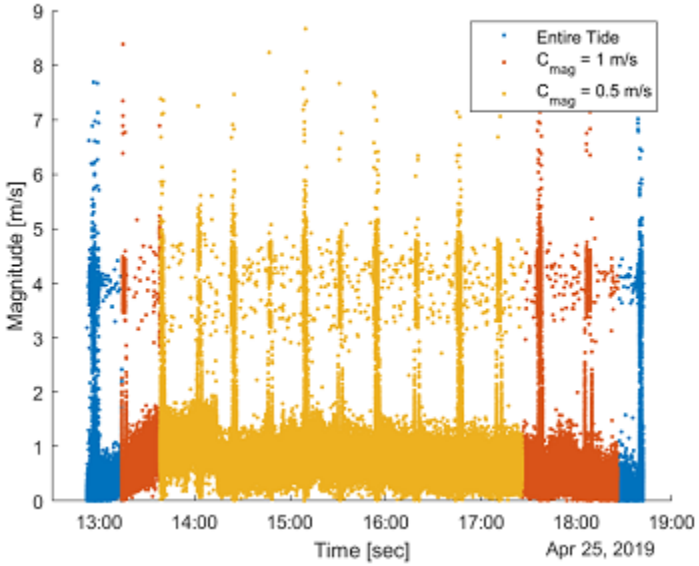

Figure 2.24: Current magnitude during a flood tide from ADV 1 at the bow location (4/25 - 4/26), showing the change in record length using different magnitude cut-off values

The dip in the current magnitude during the flood tide can be attributed to a change in flow direction of approximately 20 °as shown in Figure 2.25 of the raw ADV data from the stern location.

The drop in current magnitude and direction change occurs in all of the ADV data sets that were collected and the ADCP data collected during the LB-17 survey. This suggests that the current changes course in the river at a certain stage early on in the flood tide.

The change in direction during the flood tide causes the flood tide magnitude sections shown in 2.24 to not be stationary. The auto-correlation coefficient stays high and does not converge on zero, as shown in Figure 2.26.

To account for the change in direction, a direction threshold is also required for the flood tide data sets. Direction cut-off values of 290 °, 300 °, and 310 °based on the consistent behavior seen

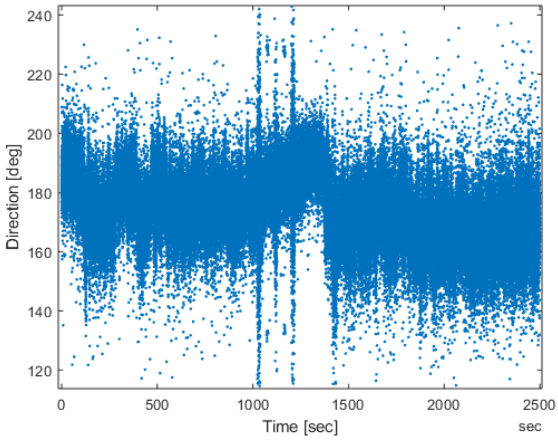

Figure 2.25: Direction during a flood tide from the ADV at the stern location, showing the change in direction associated with the drop in current magnitude

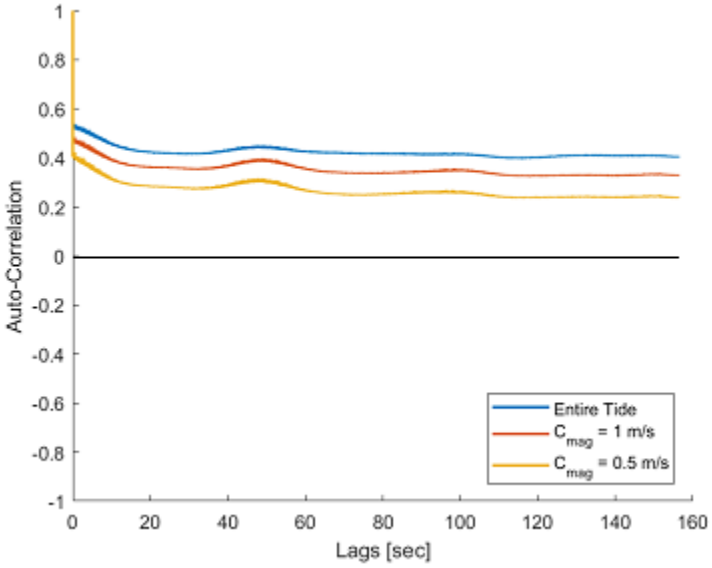

Figure 2.26: Auto-correlation coefficient of current magnitude during an flood tide from ADV 1 at the bow location (4/25 - 4/26), showing the change in convergence using different magnitude cut-off values

during the flood tides. Figure 2.27 shows the ADV magnitude sections created by the direction threshold values.

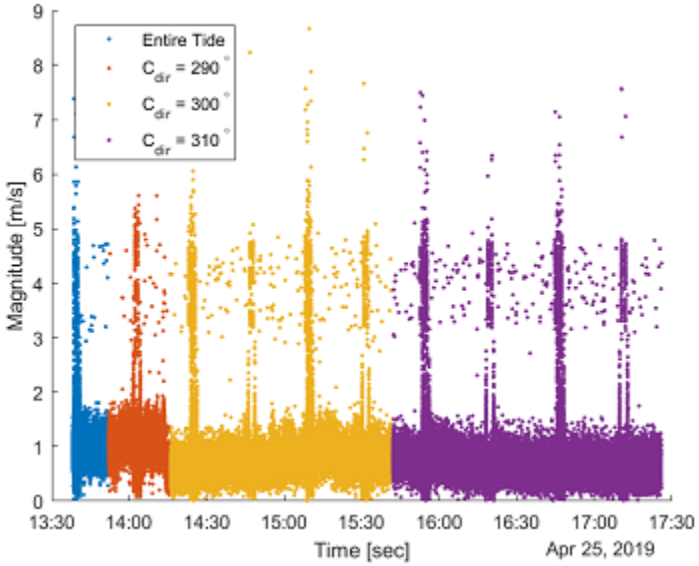

Figure 2.27: Current magnitude during a flood tide from ADV 1 at the bow location (4/25 - 4/26), showing the change in record length using different direction cut-off values

The sections that do not include the magnitude drop (300 °and 310 °), show a better auto-correlation in Figure 2.28, indicating that it is effecting the stationarity of the time series.

The flood data auto-correlation does not reach zero, but the filtering of the data will remove noise that keeps the data correlated with itself.

2.2.4.2 ADV Data Filtering

The ADV data collected using the two Nortek Vectors contained interference that caused events of large velocity spikes. These events occur at around 20 minute intervals as shown in the ebb tide event in Figure 2.29.

The interference events consist of 4-5 bands of velocity spikes that are evenly spaced in 20-40 second increments as shown in Figure 2.30.

To further investigate these events, the quality parameters outputted by the instrument were inspected. The quality parameters include amplitude, signal to noise ratio (SNR), and correlation.

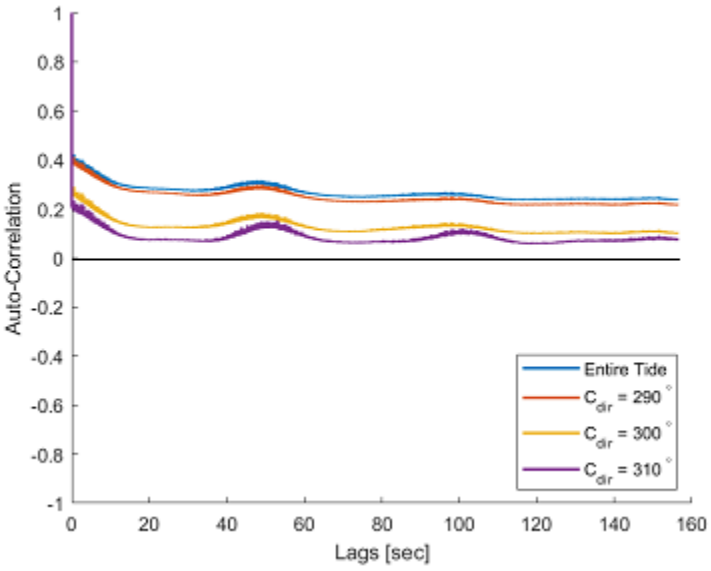

Figure 2.28: Auto-correlation coefficient of current magnitude during a flood tide from ADV 1 at the bow location (4/25 - 4/26), showing the change in convergence using different direction cut-off values

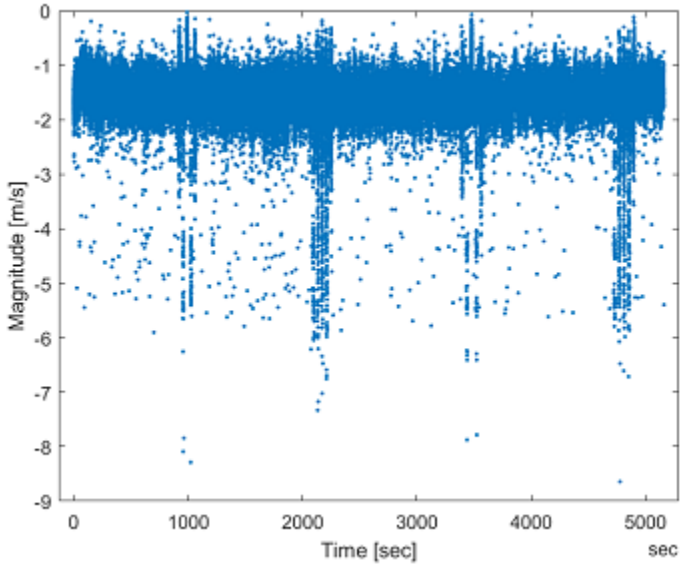

Figure 2.29: Segment of the raw ADV current magnitude during an ebb tide

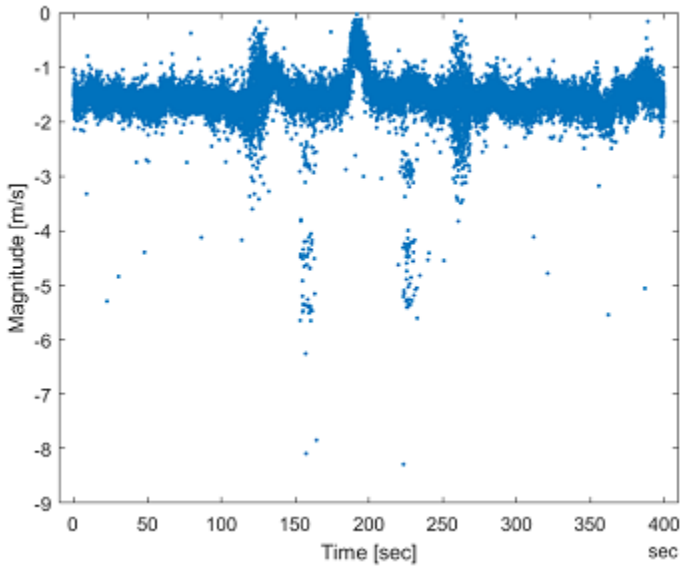

Figure 2.30: Segment of the raw ADV current magnitude during an ebb tide, showing an interference event

Amplitude is a representation of the signal strength that is a funcion of the amount of particles in the water. [28] Amplitude is provided as the raw signal amplitude in counts, which is a dimensionless unit. The SNR is also a representation of the signal strength and is provided in dB as defined by,

$$SNR = 20log_{10}\frac{Amplitude_{signal}}{Amplitude_{noise}} \tag{2.10}$$

The correlation is a measure of the similariy between two pulse echoes recieved along each beam. A high correlation indicates that the instrument measured the phase shift correctly for those two pulses. Data with low correlation should be discarded, as it is probably not measuring velocity correctly. [32] The quality parameters are given in beam coordinates, with small differences seen between beams. Figure 2.31 shows the quality parameters for beam 1 during the ebb tide interference event pictured in Figure 2.30.

The peaks in amplitude and SNR occur approximately centered around the velocity event. The dips in correlation correspond to the four main velocity magnitude bands. This behavior is consistent for other interference events in all of the data sets collected on the turbine deployment platform for the ADV measurement campaign. These type of events were also seen in data collected in the

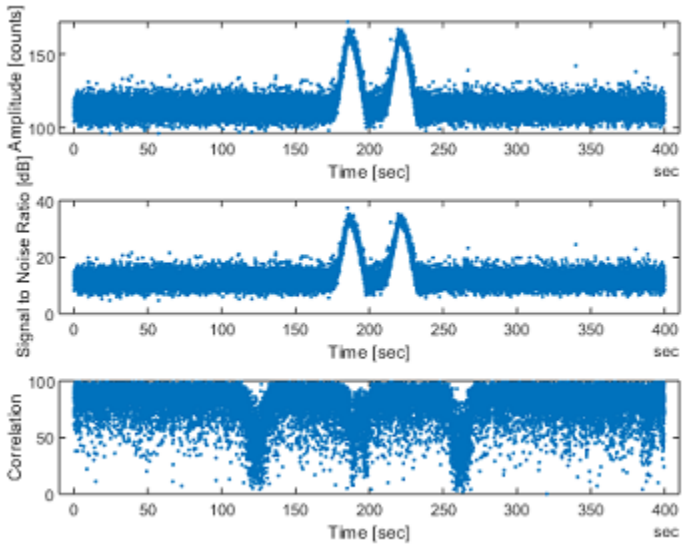

Figure 2.31: Quality parameters for beam 1 during the ebb tide interference event shown in Figure 2.30

UNH Tow and Wave Tank using the same instruments. Figure 2.32 shows one data set, featuring similar interference events.

The velocity bands have been discussed with representatives from Nortek. They have determined that the issue is likely electrical interference. An upgrade to the hardware that would include an additional filter board would be required to avoid this interference in future measurements.

The correlation dips seem to correspond to the bands of velocity more than increases in signal strength, so the correlation will be the focus of the filtering. To show the relationship between the correlation and the current magnitude, a scatter plot with the interference event shown in Figure 2.30 and a segment of data without any obvious interference events is provided as Figure 2.33.

The main lobe of the non-event data is shorter and less spread out than the event main lobe, indicating that the significant portion of the data can be isolated by removing low correlation values and magnitude variations far from the mean.

The threshold for the correlation was determined by the number of standard deviations away from the mean of the correlation along each beam. The standard deviation threshold serves as a way to isolate the significant portion of the data and discard the data points that are likely due to

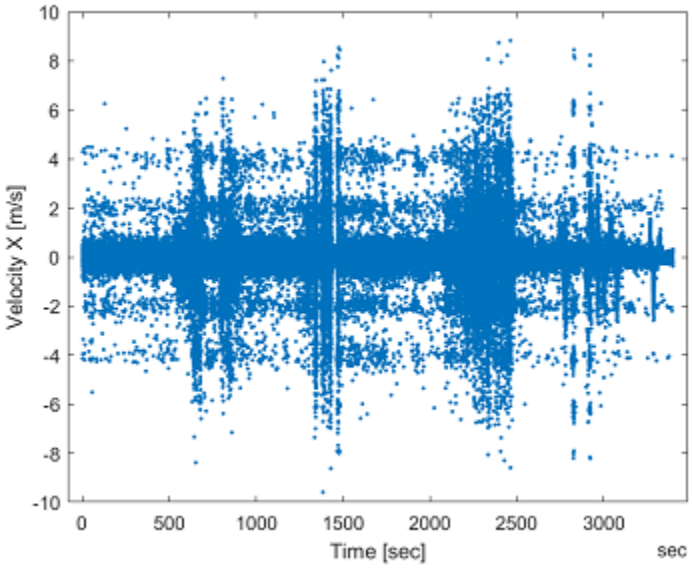

Figure 2.32: Velocity measured in the UNH Tow and Wave Tank using one of the Nortek Vectors

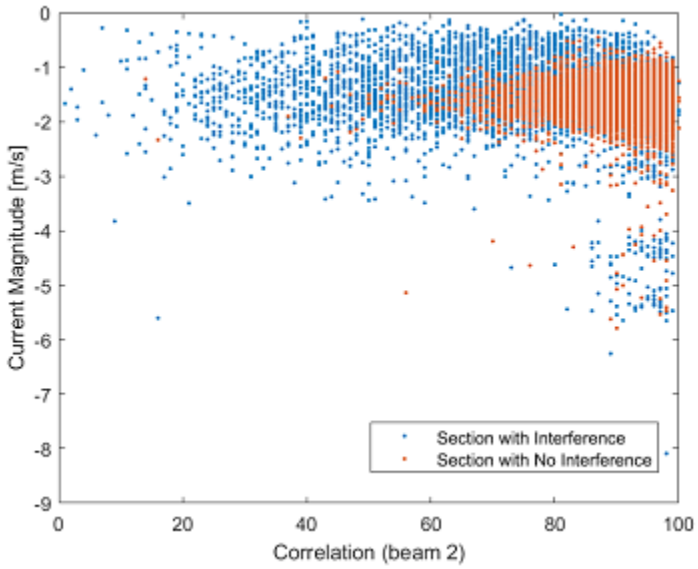

Figure 2.33: Scatter plot showing the correlation and current magnitude for an ebb tide interference event compared to a section of ebb tide data with no interference

the interference events. The correlation filter is applied first so that the main bands of velocity are removed before applying a velocity filter. The number of standard deviations away from the mean of the correlation of beam 3 was varied from 1 to 6 to investigate the effect on the current magnitude. For each threshold the filter was passed by 10 times in order to ensure that it reached it final level for that filter. The plots in Figure 2.34 shows that the velocity bands are not removed unless a filter of three standard deviations or stricter is used.

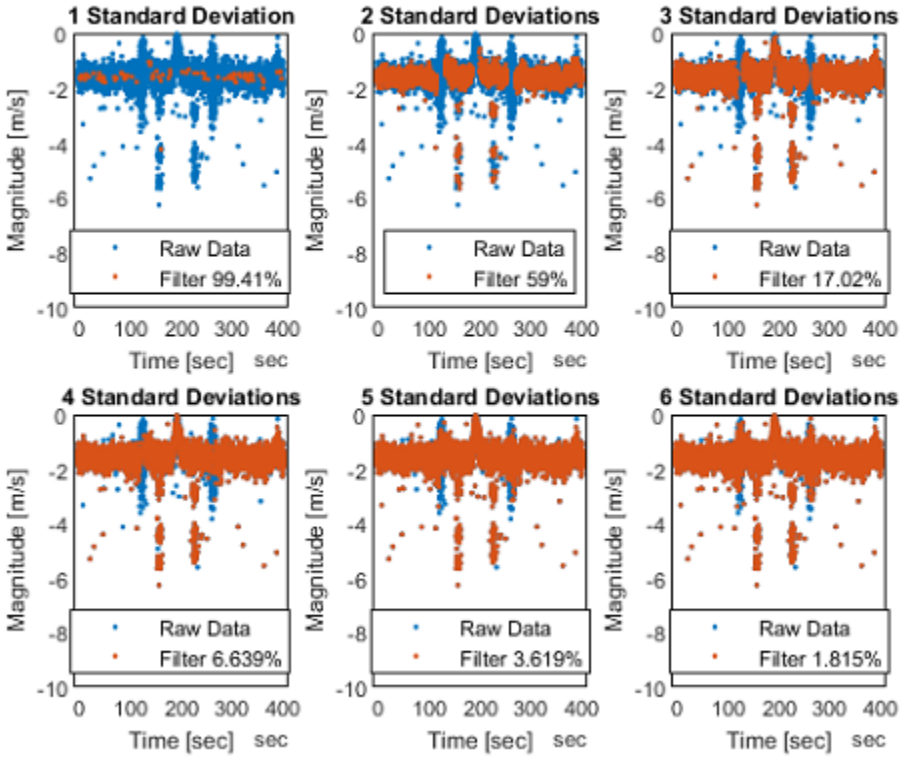

Figure 2.34: Correlation filter threshold varied from 1 to 6 standard deviations away from the mean, showing the effect on the interference section of the ebb tide

The percent filtered listed on the plots shows that filters of 1 and 2 standard deviations remove a significant portion of the data. Due to this, 3 standard deviations away from the mean is used for the correlation filter. The correlation filter applied to the entire ebb tide event shown in Figure 2.29, removes 17.02 % of the raw data as seen in Figure 2.35.

To filter out velocity excursions not removed by the correlation filter, a moving standard deviation filter was applied on the velocity. The standard deviation of the current magnitude was

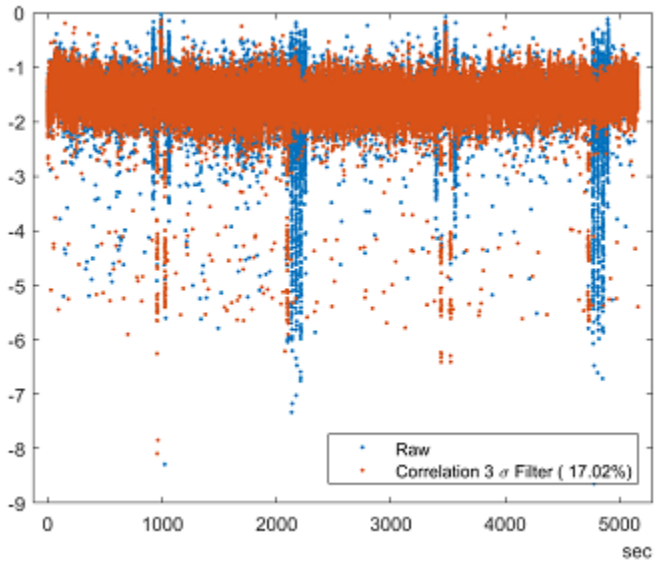

Figure 2.35: Segment of the ADV current magnitude during an ebb tide, showing the effect of the correlation filter

computed over a specified window, centered at each point. Points where the standard deviation value was above a certain value were then removed. The window size and the standard deviation threshold were varied in order to minimize the effect of the filter on the overall standard deviation of the current magnitude. Figure 2.36 shows the effect of the moving standard deviation threshold on the standard deviation of the current magnitude section. The window length is varied from 0.03 to 2 seconds, this range was chosen so that only small amounts of data were removed in high standard deviation areas.

The standard deviation of the current magnitude begins to flatten out and then remain constant for the 0.25 and 0.5 second windows. This behavior is desired as it indicates that the filter threshold no longer has a major effect on the statistics of the data. The 0.25 second window was chosen so that minimal data was removed. The threshold was chosen to be 0.3 based on where the curve in Figure 2.36 begins to flatten out. The moving standard deviation filter with these parameters is applied to the data already filtered for low correlation. The final filtering on the ebb tide bow event removes an additional 2.042 $\%$ of the overall raw data in the ebb tide segment as can be seen in Figure 2.37.

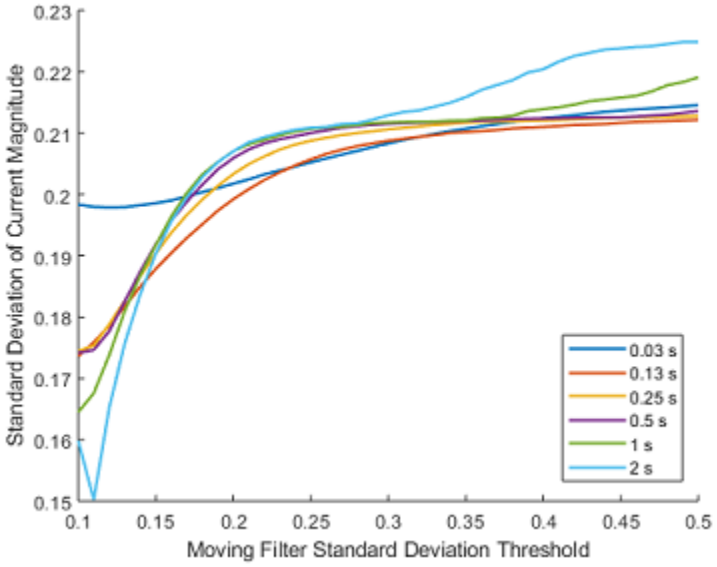

Figure 2.36: Effect of the moving standard deviation threshold and window length on the standard deviation of the overall ebb tide current magnitude

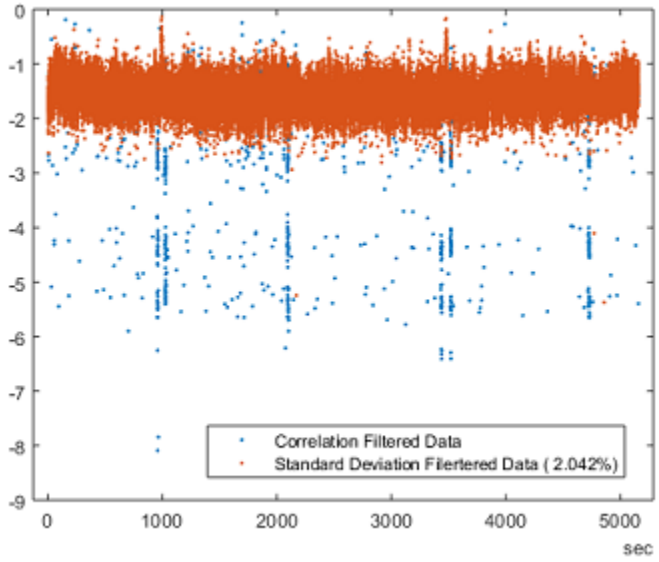

Figure 2.37: Segment of the ADV current magnitude during an ebb tide, showing the effect of the moving standard deviation filter

For the analysis, the data points removed by the filtering were replaced with the last good magnitude value.

2.2.5 ADV Experimental Results

One representative flood and ebb event from each location was chosen for analysis. The current magnitude measured using the fixed ADV at the left location was also separated into these tide events. The data sets were aligned so that a comparison could be made between the measurements at each location and the fixed location. The ADCP data was also aligned with the ADV data set collected at the bow to make co-located comparisons between the two instruments.

2.2.5.1 Ebb and Flood Tide Event Analysis

Each of the representative tidal events were analyzed independently to look at the statistics, time and length scales, and frequency content of each data section. The representative tidal events are shown in Figure 2.38.

Tidal events when the instrument was changed, leaving a gap in the data, were not chosen to be representative events. It was important to choose the events so that they were consistent with either the stronger or weaker tide in the semi-diurnal cycle. Since, all of the data gaps occurred during the stronger tide events, the weaker flood and ebb tide events were chosen for analysis.

The mean and turbulence intensity are used to describe the overall properties of the tide events. The turbulence intensity is a non-dimensional measure of how much turbulence is in the flow. The turbulence intensity is calculated as the standard deviation of the current magnitude divided by the mean. [11]

$$TI = \frac{\sigma_u}{\langle u \rangle} \tag{2.11}$$

The dominant time and length scales of the flow will indicate which structures might have an influence on the tidal energy conversion system output during different tidal conditions. An important representation of the time scales in the flow is the integral time scale, which is defined by the integral of the auto-correlation coefficient [11].

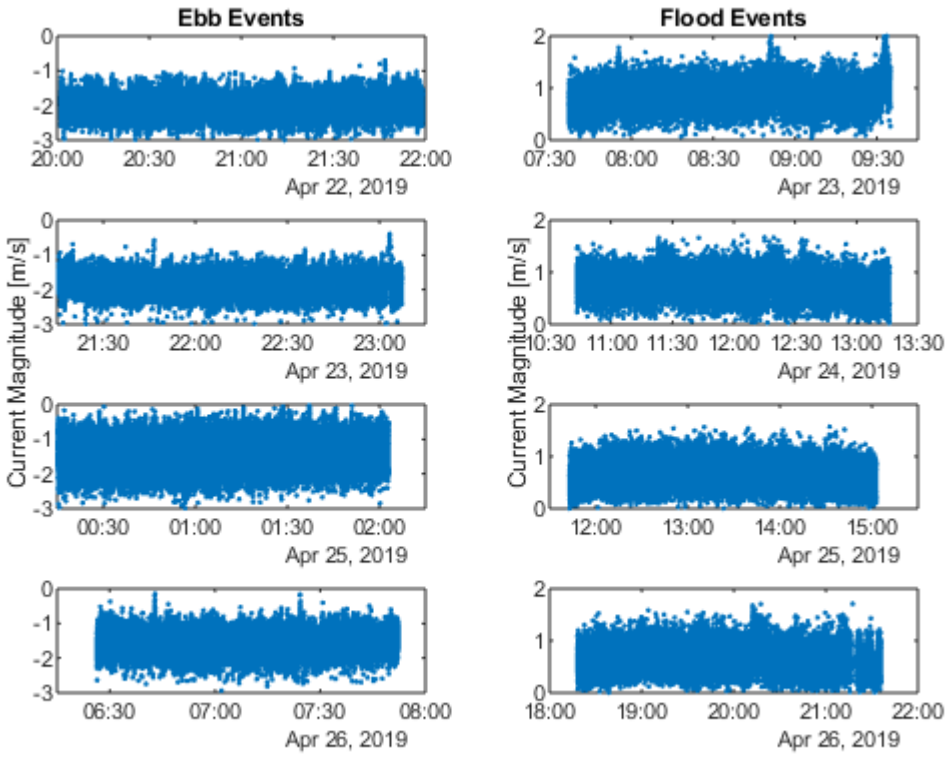

Figure 2.38: Current magnitude from the moving ADV for the representative tidal events

$$T_{int} = \int_0^\infty \rho(\tau) d\tau \tag{2.12}$$

To calculate an approximate length scale from the integral time scale, Taylor's frozen field hypothesis is used. [33] The integral time scale is multiplied by the current magnitude mean of the event,

$$L_{int} = T_{int} \langle u \rangle \tag{2.13}$$

Spectral analysis is used to investigate the dominant frequencies of the flow. The Fourier transform forms the basis of the sample power spectral density used for spectral analysis. [5] The discrete Fourier transform is defined as,

$$\widehat{G_j} = \frac{1}{N} \sum_{n=0}^{N-1} g_n e^{-i2\pi jn/N} \tag{2.14}$$

where $N =$ record length, $g_n =$ time series, Δ = sampling interval (sec), and the frequency as a function of j is,

$$f_j = \frac{j}{N\Delta} \tag{2.15}$$

The fast Fourier transform (FFT) is used to numerically compute the discrete Fourier transform. The FFT output is defined as,

$$\widehat{X_j} = \sum_{n=0}^{N-1} g_n e^{-i2\pi jn/N} \tag{2.16}$$

This definition does not include the $1/N$ factor found in the discrete Fourier transform so,

$$\widehat{G_j} = \frac{1}{N} \widehat{X_j} \tag{2.17}$$

The sample power spectral density is defined as,

$$\widehat{S}_j = N\Delta\widehat{G_j}\widehat{G_j}^* \tag{2.18}$$

Where the $*$ indicates the complex conjugate. If g_n is real, then the two-sided power spectral density, $\hat{S}_j$, is symmetric about $f = 0$. Due to this symmetry, the one-sided spectral density for $0 > f > \frac{1}{2\Delta}$ is defined as,

$$\tilde{S}_j = 2N\Delta\widehat{G_j}\widehat{G_j}^* \tag{2.19}$$

Where the area under $\tilde{S}_j$ is equal to the variance of the time series,

$$\sigma^2_{g_n} = \sum_{j=0}^{N/2-1} \tilde{S}_j \Delta f \tag{2.20}$$

where Δf is the frequency bandwidth.

In order to better examine the power in low frequencies, the pre-multiplied spectrum is computed,

$$(\tilde{S}_j)_{Pre-Multiplied} = f * \tilde{S}_j \tag{2.21}$$

The pre-multiplied spectra is generally used because the area under the curve is representative of the amount of energy in a specific frequency band. [29] When the pre-multiplied spectra is plotted with a logarithmic frequency axis is equal to the area under the spectra on a linear scale,

$$\int \tilde{S}_j f d(log(f)) = \int \tilde{S}_j df \tag{2.22}$$

The pre-multiplied spectra technique is typically used to extract expected power law behavior in the turbulence, such as with wall-bounded flows. [22] The pre-multiplied spectra can also be used to isolate the large scale (low frequency) motions since the energy in turbulent flows tends to become independent of frequency as the frequency approaches zero. [19] Here, the pre-multiplied spectra is used so that the large-scale motions of the flow that relate to the scales of the river can be investigated.

In order to avoid any leakage due to low-frequency contamination from the tidal cycle, pre-whitening and post-coloring was used to process the spectral density. Pre-whitening removes the red trend (high low frequency energy) in the spectra by applying a first difference filter to the time series. The first difference filter takes each data point at time and subtracts the previous point,

$$y_t = x_t - x_{t-\Delta} \tag{2.23}$$

The sample spectral density is then computed with y_t. Post-coloring puts the low frequency back into the spectra by dividing the spectrum by the filter gain factor,

$$G(f) = 4sin^2(\pi f \Delta) \tag{2.24}$$

So that the final spectrum is computed by,

$$\tilde{S}(f) = \frac{\tilde{S}_y(f)}{4sin^2(\pi f \Delta)} \tag{2.25}$$

The pre-whitening and post-coloring reduces energy leakage from low frequencies to higher frequencies by removing the low frequency energy during the computation of the spectrum.

To smooth the spectrum and reduce the confidence intervals, band and ensemble averaging were used. The time series was broken up into 5 ensembles before computing the spectrum. The spectra were averaged to produce one spectrum that was broken up into bands of 5 frequencies and averaged. The final spectrum had 50 degrees of freedom.

There is noise in the ADV data inherent in taking Doppler measurements. The Doppler noise level can be determined from the spectrum. The section of the spectrum where it begins to flatten out and become white noise is the noise floor.

Since the area under the spectrum is the variance, the variance of the noise can be calculated by,

$$\sigma_N^2 = \sum_{j=0}^{N/2-1} \tilde{S}_{j\,N} \Delta f \tag{2.26}$$

The noise floor is assumed to be white noise, and constant over all frequencies. The area that represents the variance of the noise is defined as the region below the noise floor, $\tilde{S}_N$, over the frequency range, $0 > f > \frac{1}{2\Delta}$,

$$\sigma_N^2 = \tilde{S}_N \frac{1}{2\Delta} \tag{2.27}$$

The standard deviation can be calculated by taking the square root of the variance. So, the standard deviation of the noise can be calculated by,

$$\sigma_N = \sqrt{\tilde{S}_N \frac{1}{2\Delta}} \tag{2.28}$$

The noise floor is calculated here by averaging the last 1000 points in the spectrum. The noise floor can be seen as the blue line in the spectrum of the ebb tide taken at the stern of the platform in Figure 2.39.

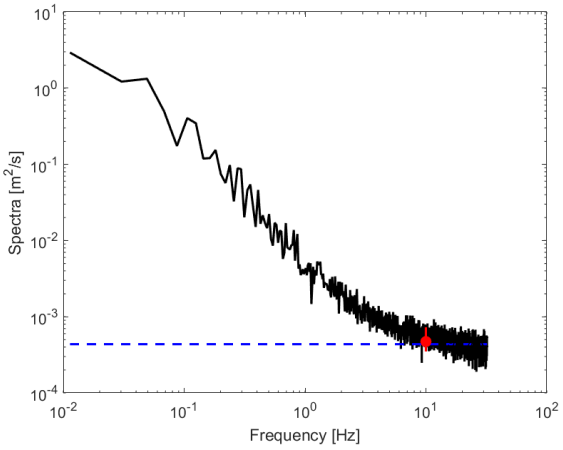

Figure 2.39: Spectral density of the current magnitude measured with the ADV at the stern during an ebb tide where the blue line indicates the noise floor and the red line indicates the 95% confidence interval

The flow characteristic most influenced by the noise level is the turbulence intensity, which directly depends on the standard deviation. To correct for this, Equation 2.29 is modified to,

$$TI_{corrected} = \frac{\sqrt{\sigma_u^2 - \sigma_N^2}}{\langle u \rangle} \tag{2.29}$$

The mean, corrected turbulence intensity, integral time and length scales, and spectral peaks were determined for each of the representative tide events and are displayed in Table 2.7.

Date and Tide Direction	ADV Location	Event Length [hr]	Mean [m/s]	Turbulence Intensity	T_{int} [s]	L_{int} [m]	Spectral Peak [Hz]
4/22 Ebb	Center	1.96	2.03	0.126	11.4	23.2	0.0480
4/22 Ebb	Left	1.96	1.99	0.140	16.6	33.0	0.0374
4/23 Flood	Center	1.97	0.858	0.180	55.9	48.0	0.341
4/23 Flood	Left	1.97	0.849	0.178	34.5	29.3	0.267
4/23 Ebb	Middle	1.87	1.84	0.116	10.8	19.8	0.0097
4/23 Ebb	Left	1.87	1.75	0.109	11.0	19.3	0.0246
4/24 Flood	Middle	2.55	0.783	0.209	33.2	26.0	0.0344
4/24 Flood	Left	2.55	0.748	0.159	69.4	52.0	0.427
4/24 Ebb	Stern	1.80	1.43	0.220	18.4	26.2	0.0332
4/24 Ebb	Left	1.80	1.67	0.149	52.2	87.0	0.0216
4/25 Flood	Stern	3.33	0.657	0.281	47.4	31.2	0.221
4/25 Flood	Left	3.33	0.663	0.181	94.8	62.9	0.0179
4/25 Ebb	Bow	1.43	1.57	0.161	13.8	21.7	0.0562
4/25 Ebb	Left	1.43	1.43	0.172	10.2	14.6	0.0223
4/26 Flood	Bow	3.30	0.661	0.241	58.5	38.7	0.134
4/26 Flood	Left	3.30	0.619	0.193	96.4	59.6	0.371

Table 2.7: Mean, turbulence intensity, integral time and length scale, and spectral peak for each of the representative tide cycles

The trends in the calculated values for the fixed ADV (left location) shown in Table 2.7 are shown in Figure 2.40.

During the week of the deployment the tidal cycle going from a spring to a neap tide, resulting in a day-to-day decrease in the mean current speed. The turbulence intensity increases due to both the decrease in mean and increase in standard deviation. This implies that there is some spring/ neap cycle dependence of the turbulence intensity. The turbulence intensity is also higher for the flood tide sections because of the lower current speed observed and possibly due to the presence of upstream obstacles. The integral time and length scale show more mixed results in terms of the spring/ neap cycle. It can be observed that the integral time scale is longer for the flood tide, than

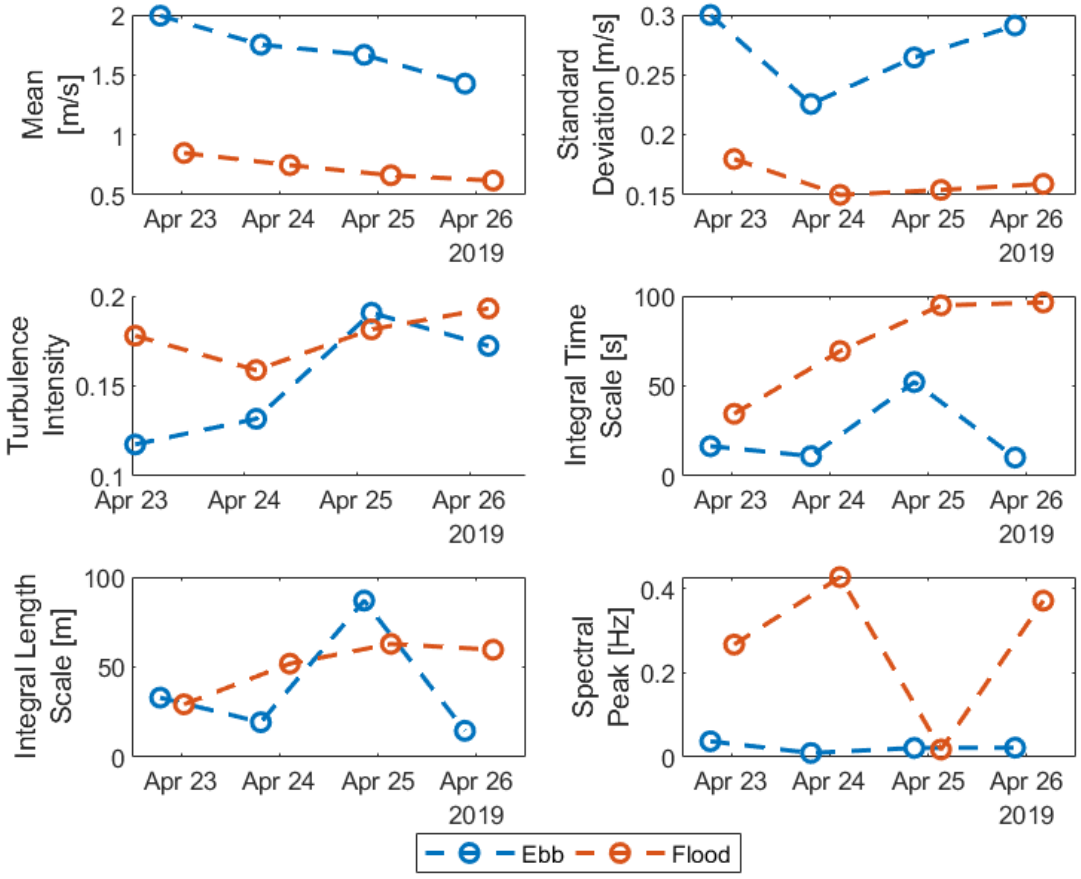

Figure 2.40: Mean, turbulence intensity, integral time and length scale, and spectral peak for each of the representative tide cycles from the stationary ADV (left location)

ebb tide. This can be seen by looking at the examples of the auto-correlations shown in Figure 2.41.

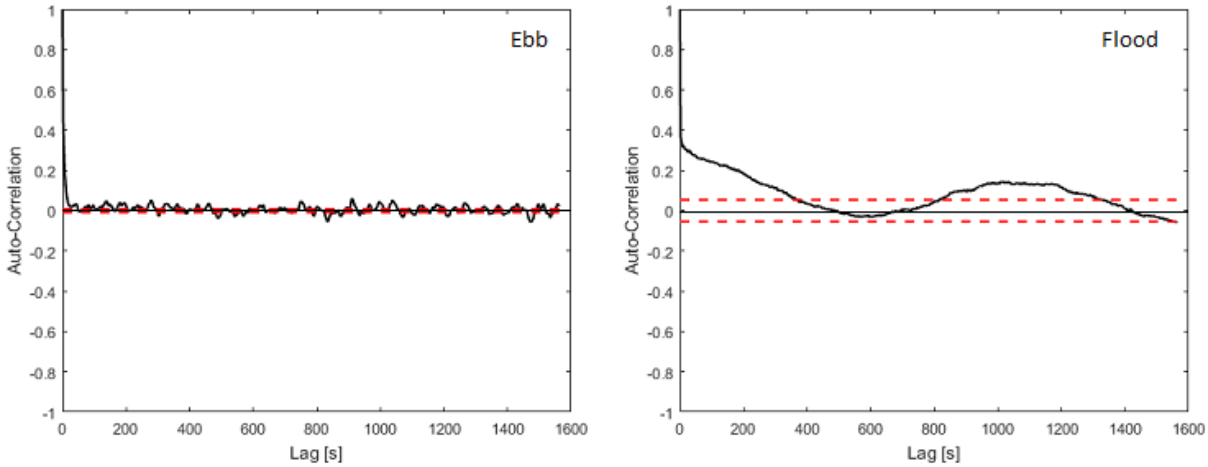

Figure 2.41: Examples of the auto-correlation coefficient from the fixed ADV (left location) for ebb and flood tide events (red lines indicate the 95% confidence interval)

The flood tide auto-correlation has a slower roll off, resulting in a higher integral time scale when integrated. Differences in the time scales of the ebb and flood tides could be caused by differences in the bathymetry and topography up and down stream of the bridge. The characteristics of the river channel influence the size of eddies that can form and remain intact. The size of these eddies is reflected by the integral length scale, which is generally larger for the flood tide direction.

The range of integral time and length scales is consistent with the scales of the tidal estuary and physical obstacles that may be affecting these results. For example, the average of the integral length scale from the fixed ADV is 38.5 m for the ebb tide and 50.9 m for the flood tide. These values are both less than the distance between the bridge piers (approximately 90 m) and the width of the river at the deployment location (approximately 275 m).

Flow structures with different length scales can effect the turbine in different ways. This concept has been outlined in wind energy [6] can also be applied to tidal energy. Small structures, less than the blade chord length (0.25 m), effect the lift and drag on the blades, which can impact the overall power output. Medium structures, between the length of the blade chord and diameter of

the rotor (3.2 m), can introduce intermittent loading on the structure. Large structures, larger than the rotor diameter, appear as "gusts" that effect the power output over time and the total amount of energy produced.

The estuary sized length scales seen in the flow, will appear as gusts to the turbine. This gusting will result in periods of higher and lower power output corresponding to the time scales of the flow. The instantaneous power of the turbine will fluctuate with the gusts and the cut-in speed might be effected if periods of higher flow speed are not sustained for a long enough period.

Low frequency energy is dominant for both the ebb and flood tides, with frequencies of approximately 0.03 Hz seen for most of the ebb tide sections. The amplitude of the low frequency energy is also higher for the ebb tide as seen in Figure 2.42.

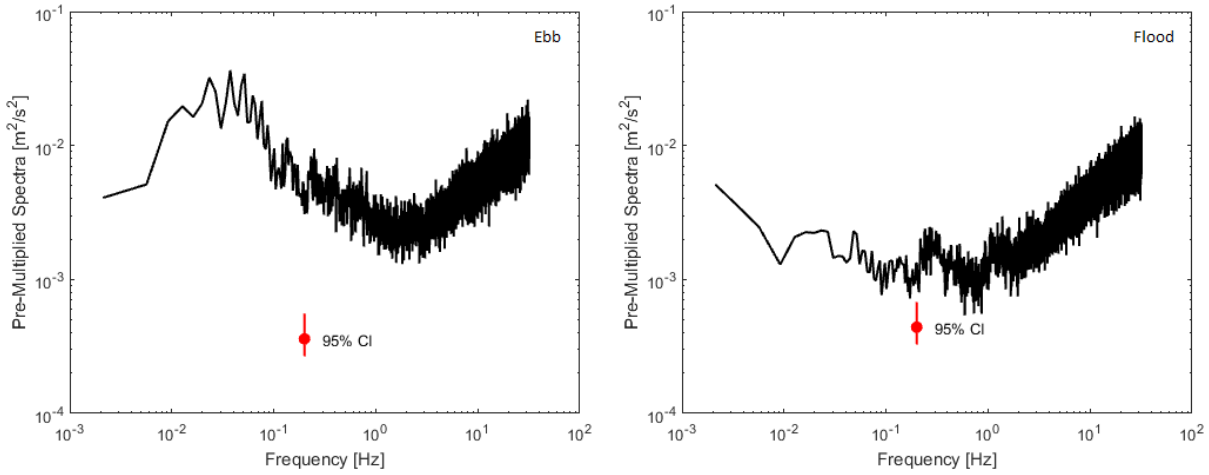

Figure 2.42: Examples of the pre-multiplied spectral density from the stationary ADV (left location) for an ebb and flood tide events (red lines indicate the 95% confidence interval)

2.2.5.2 Comparison Between Moving and Fixed ADV Data Sets

To investigate the spatial variations of the current more closely each of the moving ADV data sets was compared to the synchronized data from the fixed ADV. The differences in the mean current can be seen in Figure 2.43 for the ebb tide events and Figure 2.44 for the flood tide events.

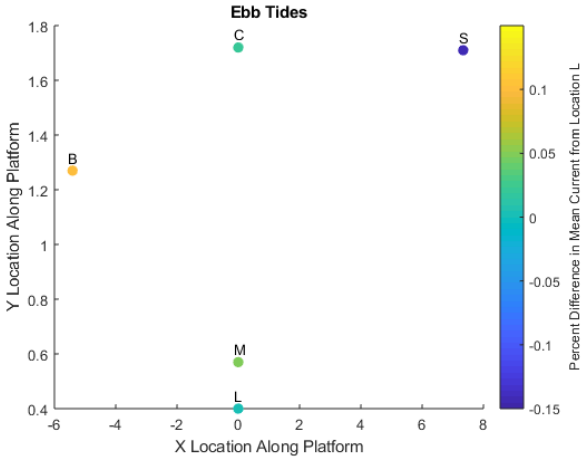

Figure 2.43: Mean current differences between the moving and fixed ADV's for the ebb tide events, the percent difference is calculated with the fixed ADV at the left location as the reference

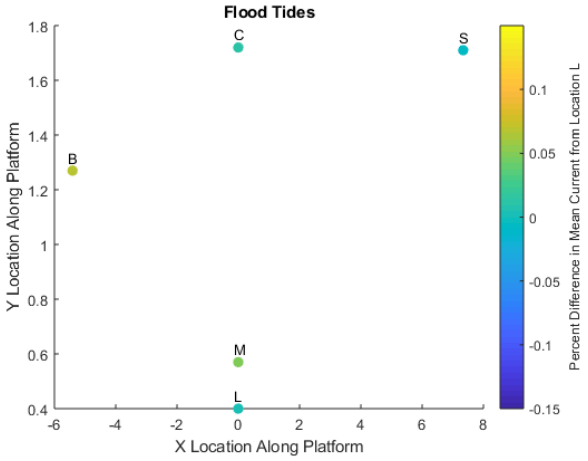

Figure 2.44: Mean current differences between the moving and fixed ADV's for the flood tide events, the percent difference is calculated with the fixed ADV at the left location as the reference

On the ebb tide, a larger magnitude is seen at the bow and a smaller magnitude is seen at the stern. This indicates that structural interactions influence the flow as it moves under the turbine deployment platform.

The same colorbar is used for both figures, showing that larger differences in the mean are seen for the ebb tide than the flood tide. This is consistent to the ADCP results from the LB-17 survey. The bow and stern ADCP's showed a large discrepancy when measuring the ebb tide but similar results for the flood tide, as shown in Figure 2.10.

To look more closely at the comparison between the fixed and moving ADV data sets the cross-correlation and cross-spectra were computed. The more general form of the auto-correlation is the cross-correlation. Where the auto-correlation represented how correlated the time series was with itself over varying time lags, the cross-correlation represents how one time series is correlated with another over varying time lags. The cross-correlation is defined as,

$$R_{xy}(t,\tau) = \langle u_1(t)u_2(t+\tau)\rangle \tag{2.30}$$

And the cross-correlation coefficient is,

$$\rho_{xy}(\tau) = \frac{\langle u_1(t)u_2(t+\tau)\rangle}{\langle u_1(t)u_2(t)\rangle} \tag{2.31}$$

The peak of the cross-correlation coefficient indicates the time lag between the processes that the two time series represent.

The cross-spectra was also computed to identify the common frequencies in the synchronized data sets. The two-sided cross spectral density is defined by the discrete Fourier transform of the two data sets, $\hat{X}(f)$ and $\hat{Y}(f)$,

$$\widehat{S}_{xy}(f) = N\Delta\widehat{X}^*(f)\widehat{Y}(f) \tag{2.32}$$

This cross-spectra is then used to compute the coherency spectrum, which represents how correlated the frequencies are between the two data sets. The coherency spectrum, $\widehat{\gamma}^2_{xy}(f)$, is usually displayed as it is here in the squared form,

$$\widehat{\gamma}^2_{xy}(f) = \frac{\widehat{S}_{xy}(f)\widehat{S}^*_{xy}(f)}{\widehat{S}_x(f)\widehat{S}_y(f)} \tag{2.33}$$

The peaks of both the cross-correlation and coherency spectrum between the moving and fixed ADV magnitudes are displayed in Table 2.8 for each of the representative tidal events analyzed above.

Date and Tide Direction	Moving ADV Location	Cross-Correlation Peak [s]	Coherency Spectrum Peak [Hz]
4/22 Ebb	Center	0.438	0.0304
4/23 Flood	Center	1.63	0.0021
4/23 Ebb	Middle	-0.078	0.0506
4/24 Flood	Middle	0.125	0.0998
4/24 Ebb	Stern	5.78	0.0718
4/25 Flood	Stern	45.6	no significant peak
4/25 Ebb	Bow	-1.66	0.0174
4/26 Flood	Bow	11.6	0.0328

Table 2.8: Cross-correlation and coherency squared spectra peaks for each set of representative tide cycles

A negative lag is seen between the left and bow locations during the ebb tide while a positive lag is seen between the left and stern locations during the ebb tide. As expected, it follows the direction of the flow along the platform. Interestingly, the same relationship is not seen with the flood tides. A longer lag is seen for the stern and left locations, but it is not different in direction from the bow and stern location lag as would be expected. It should be noted that the flood tide cross-correlation peaks are much less prominent than the for the ebb tide sets. This can be seen in Figure 2.45 where the flood tide cross-correlation coefficient is just barely above the 95% significance level. Much smaller lags are seen with the moon pool measurements at the center and middle locations, which coincides with their perpendicular positioning with respect to the main flow direction.

Peak frequencies in the coherency squared spectrum occur in the range around the 0.03 Hz that was seen dominantly in the ebb tide spectral densities. In order for this frequency to have a high coherency, the signal must also be present in the flood data sets. This indicates that this frequency may be prevalent throughout the river, regardless of the flow direction.

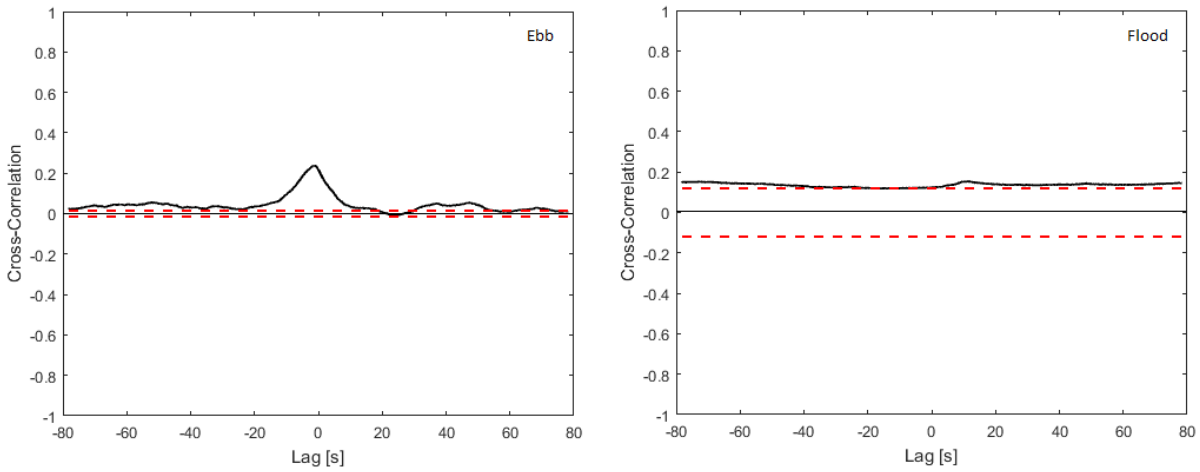

Figure 2.45: The cross-correlation of the fixed ADV at the left and the moving ADV at the bow location for an ebb and flood tide section (red lines indicate the 95% confidence interval)

The spatial correlation is also computed in the cross-stream and streamwise directions. Similarly to the cross-correlation defined above, the spatial cross-correlation varies the separation distance instead of the time lag, τ. The separation distance is a vector, $\overrightarrow{r}$, that is defined along a certain direction. The spatial correlation of the tidal current magnitude, u, is defined as,

$$B(\overrightarrow{r},t) = \langle u(\overrightarrow{x},t)u(\overrightarrow{x}+\overrightarrow{r},t)\rangle \tag{2.34}$$

The correlation is only a function of the separation distance, but there exists a spatial correlation at each time t in the time series. A non-dimensional spatial correlation coefficient can be defined as,

$$b(\overrightarrow{r},t) = \frac{B(\overrightarrow{r},t)}{\langle u(\overrightarrow{x},t)^2\rangle} \tag{2.35}$$

If the correlation is computed over a time period that can assumed to be stationary in the mean, then the coefficient b can be averaged over all time points, t. This results in a spatial correlation coefficient that only depends on the separation distance, $\overrightarrow{r}$.

The cross-stream spatial correlation was computed across the moon pool at the center and middle locations in reference to the fixed ADV at the left location. For this case the separation

vector consists of two distances along the cross-stream direction, 0.17 m and 1.32 m. The spatial correlation coefficient is plotted in Figure 2.46.

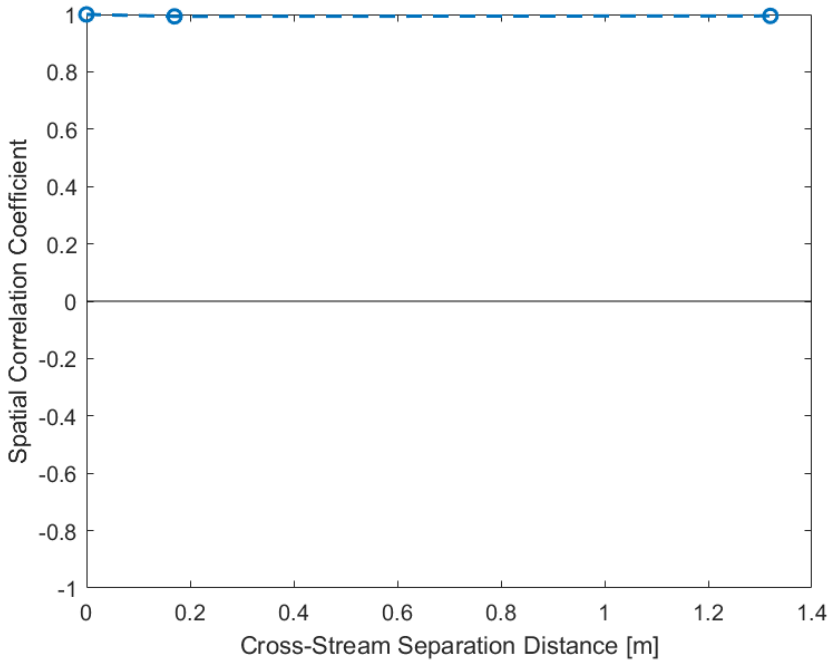

Figure 2.46: The spatial correlation coefficient in the cross-stream direction, using data from the ADV's at the left, middle, and center locations

The streamwise spatial correlation was also computed along the length of the platform at the bow and stern locations in reference to the fixed ADV at the left location. For this case the separation vector consists of two distances along the streamwise direction, 5.41 m and 7.34 m. Since the bow and stern are located on opposite side of the reference location, the bow location is represented as a negative distance. The spatial correlation coefficient is plotted in Figure 2.47.

Both the cross-stream and streamwise spatial correlations remain highly correlated over the separation distances used. This confirms that larger lengths scales on the order of 50 m seen from the auto-correlations are dominant in the flow. These larger structures cause the flow to remain correlated across the dimensions of the turbine deployment platform. The streamwise spatial correlation shows lower coeffient values than those seen for the shorter distances used to

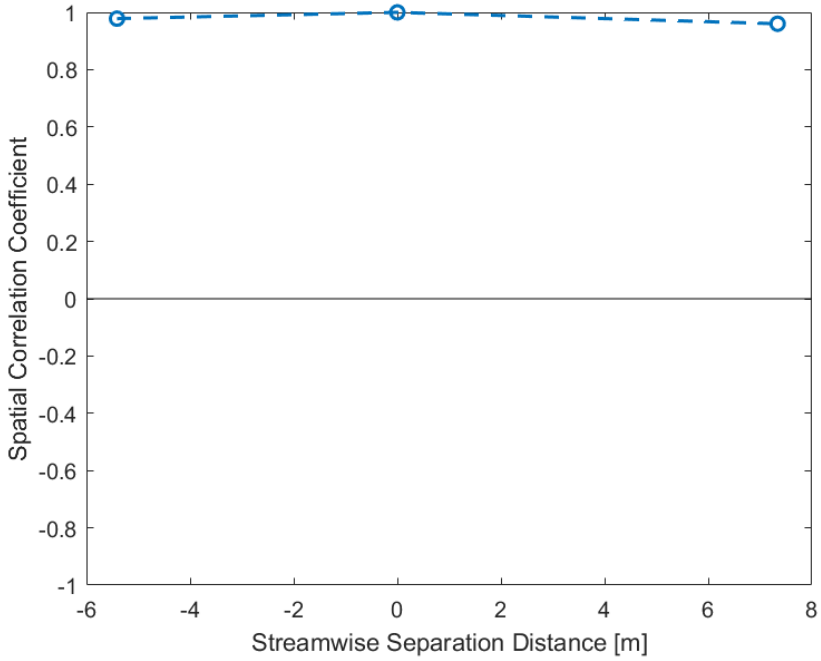

Figure 2.47: The spatial correlation coefficient in the streamwise direction, using data from the ADV's at the bow, left, and stern locations

compute the cross-stream spatial correlation, suggesting that over longer separation distances the flow would eventually become uncorrelated.

CHAPTER 3

TIDAL ENERGY CONVERSION SYSTEM TESTING

3.1 Description of Turbine and Power Electronics

The marine hydrokinetic turbine deployed on the turbine deployment platform was provided by New Energy Corporation out of Calgary, Alberta. The Envirogen 025 turbine is a 4-bladed vertical axis cross-flow turbine with a 3.2 m diameter and 1.7 m height, Figure 3.1. The blades are made from solid aluminum with hydrofoil profiles that have a 0.25 m chord.

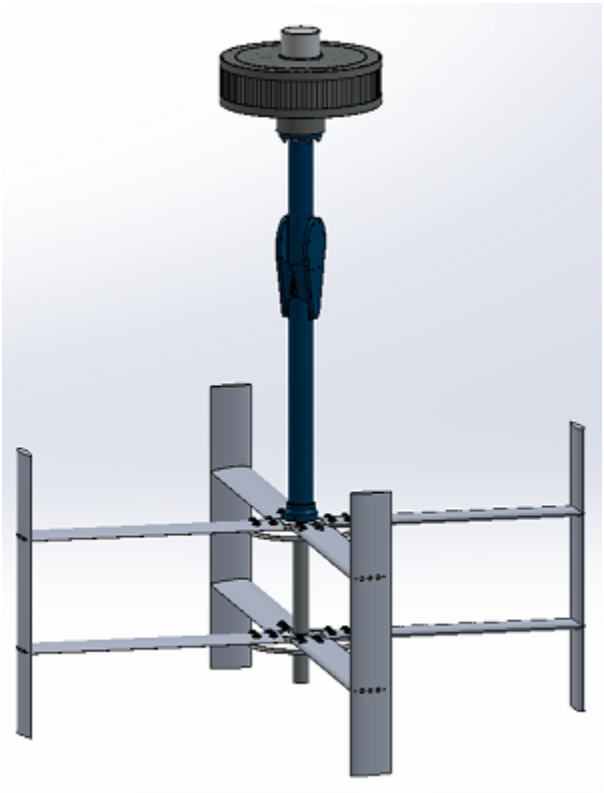

Figure 3.1: 3-D model of the New Energy Corporation Envirogen 025 turbine

The Envirogen 025 rotor dimensions were slightly modified from their original design (3.4 m diameter) to fit into the moon pool size of the turbine deployment platform. This was the first long-term deployment of this turbine in a saltwater environment, so both UNH and New Energy are learning from the deployment.

New Energy Corporation also provided the turbine power electronics as part of their Envirogen 025 system. A diagram of the power electronics can be seen as Figure 3.2.

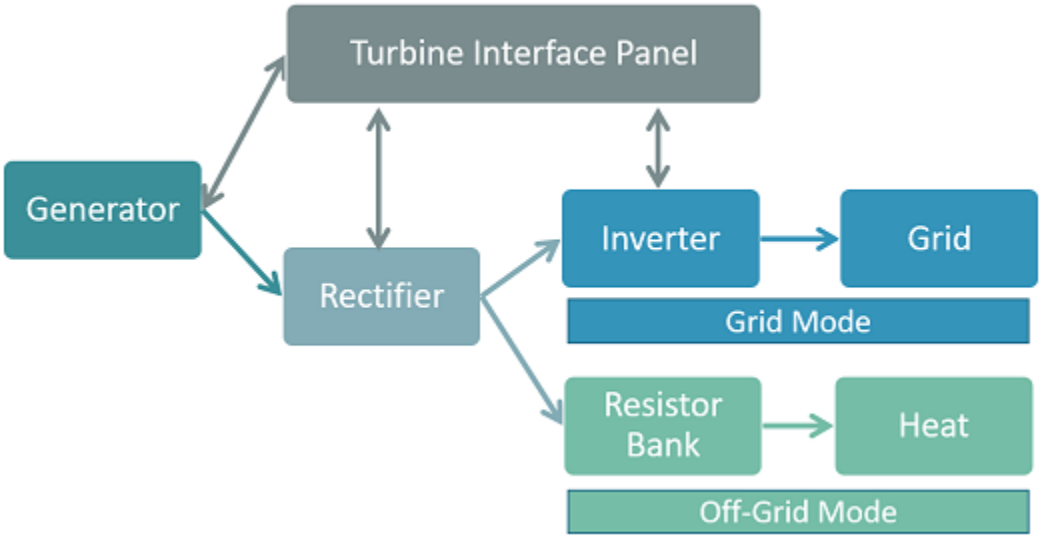

Figure 3.2: Diagram of the power electronics provided by New Energy Corporation

A new direct drive permanent magnetic generator was used for this system so there is no longer a need for a gearbox and associated lubrication fluids. The generator has a maximum capacity of 25 kW and provides tidal current variable, wild AC power. The power is routed to the turbine interface panel (TIP), an electrical panel designed by New Energy that includes control logic, electrical safety systems, and user controls for the system. The wild AC power is routed from the TIP to the Voltsys rectifier for conversion to DC. The rectifier is Voltsys' "Wind Turbine Controller with Dump Load" model. The DC power is then sent to the Ginlong Solis Three Phase 36k inverter (maximum capacity of 36 kW) where it is converted to grid-compliant AC power. The rectifier and inverter communicate via a RS-485 serial connection. This allows the rectifier to collect in-

formation about the inverter power conversion and any errors that the inverter has encountered. If the inverter has an alarm, then the rectifier will automatically display an error and shut the system down.

The rectifier has the capability to log information to either an SD card or a laptop connected with a USB cable. The logging information includes the three phase turbine voltage, turbine frequency, DC power and voltage sent to the inverter, DC voltage send to the dumpload, AC inverter output voltage, and inverter output power. The logging is set up through the Voltsys software.

The power electronics at this stage do not include any power factor correction, which would make the system efficient over a range of current speeds. A capacitor bank or active rectification system could be added in the future to increase the efficiency. The system was tuned to have the maximum efficiency at 2 m/s.

The tidal energy conversion system can operate in two modes, off-grid configuration or grid-connected. The grid connection operates as a net-metered system, where any excess power produced by the system that the bridge doesn't use acts as a negative value on their electricity meter. The off-grid configuration sends the DC power outputted by the rectifier to a dumpload (or load bank) that dissipates it to heat. The dumpload consists of a bank of resistors with a total resistance of 11 Ohms.

3.2 Off-Grid Turbine Test

Current and load bank power data was recorded for a 4 hr and 20 min period during the ramp up of a spring, ebb tide on March 20, 2019. The turbine was set up to run in off-grid mode with the rectifier logging to the field laptop. The currents were recorded with an ADCP mounted at the bow of the turbine deployment platform recording ensembles every 2 minutes in 0.25 m bins. The currents reported here are from the 3rd bin, which is approximately at the mid-turbine depth (1.4 m). Figure 3.3 shows the current speed over time where the flood direction is positive and the ebb direction is negative.

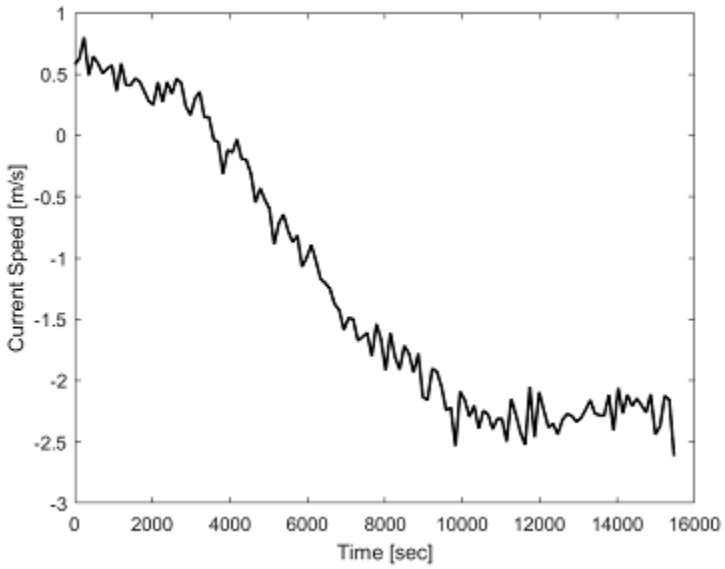

Figure 3.3: Current speed measured with an ADCP during the off-grid test on 3/20/19

The histogram in Figure 3.4 shows the distribution of the currents during the test with 0.15 m/s bins. The currents move quickly from slack to max currents so only a small percentage of the data occurs during the middle section around 1 m/s.

The load bank (also referred to as the dump load) power was recorded with the rectifier logging to the field laptop. The rectifier sends power to the load bank by switching on and off quickly using pulse width modulation (PWM). The PWM is represented as a value from 0-255 where 255 is 100% switched on. The load bank power is determined by,

$$P = \frac{V^2 * PWM}{R * 255} \tag{3.1}$$

Where V is the DC voltage and R is the resistance of the load bank. The resistance of the load bank needs to be inputted into the Voltsys rectifier software (setting Dumpload Ohms) to match the resistance of the physical system so that the dump load power is computed correctly. The dump load resistance is 11 Ohms. The rectifier then provides 1sec, 10sec, and 100sec averages of the power from the dump load, which are shown in Figure 3.5.

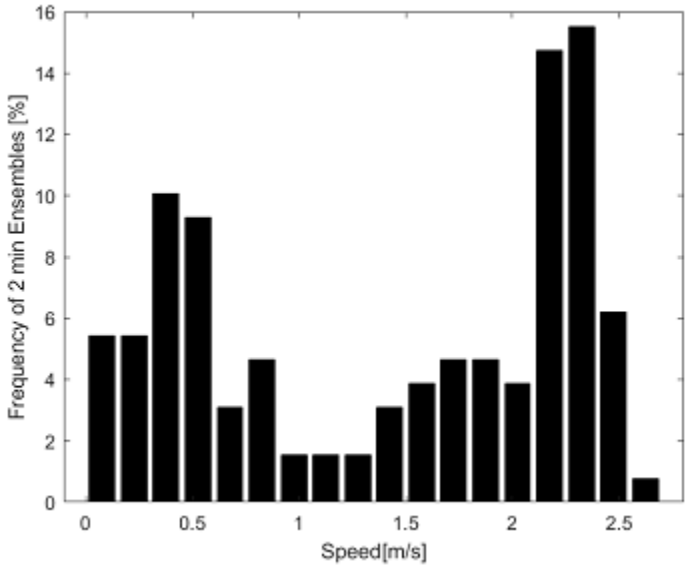

Figure 3.4: Histogram of current speed measured with an ADCP during the off-grid test on 3/20/19

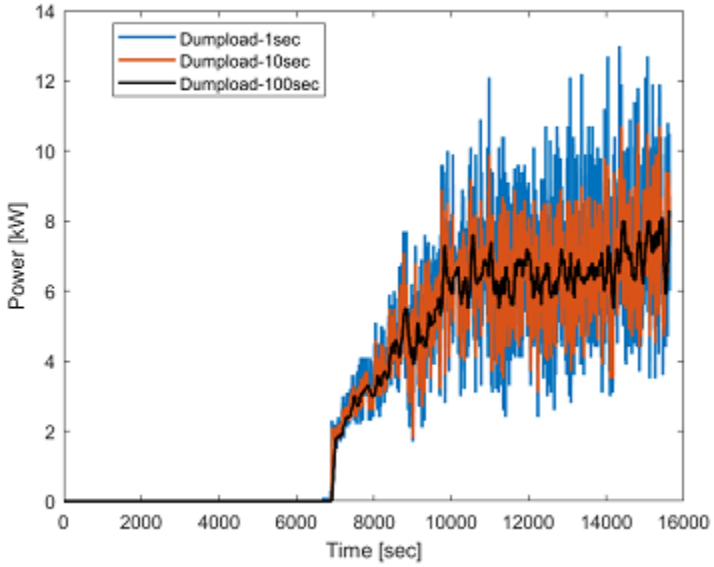

Figure 3.5: Dumpload power showing the differences between the 1sec, 10sec, and 100sec averaged power during the off-grid test on 3/20/19

The rotations per minute (RPM) of the rotor could also be calculated based on the turbine frequency recorded by the rectifier. The turbine frequency is related to the RPM by the number of pole pairs in the generator, $N_{polepairs}$,

$$RPM = \frac{f_{turbine} * 60}{N_{polepairs}} \tag{3.2}$$

Figure 3.6 shows that the RPM ramps up to approximately 30 RPM and remains relatively constant for the rest of the test. The rectifier data was not filtered and includes non-physical values such as the large spikes seen in the figure.

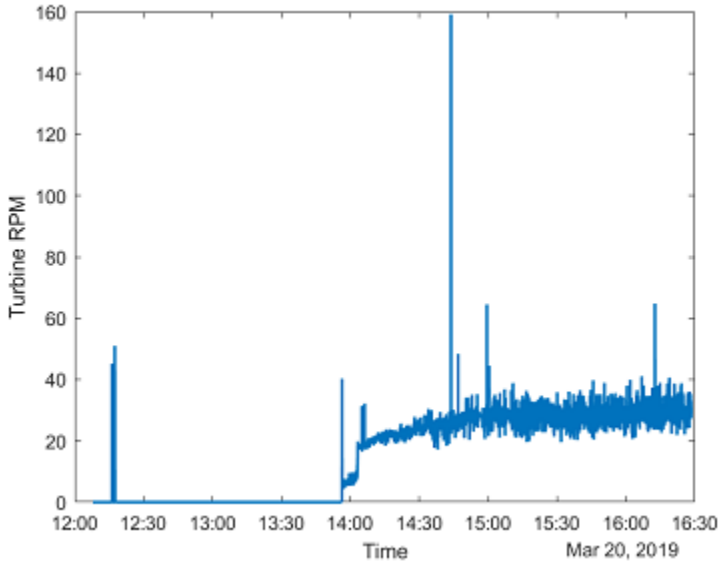

Figure 3.6: Turbine RPM calculated from the turbine frequency recorded by the rectifier during the 3/20/19 off-grid test

The 1sec dumpload power was bin averaged every two minutes to match up with the current data as shown in Figure 3.7.

In Figure 3.8 the currents and the two minute averaged power are shown together over time with the power zero until the current reaches the cut in speed.

The off-grid test data was used to create a power curve by separating the current and power values at each two minute point into 0.15 m/s current bins and then averaging all of the values in

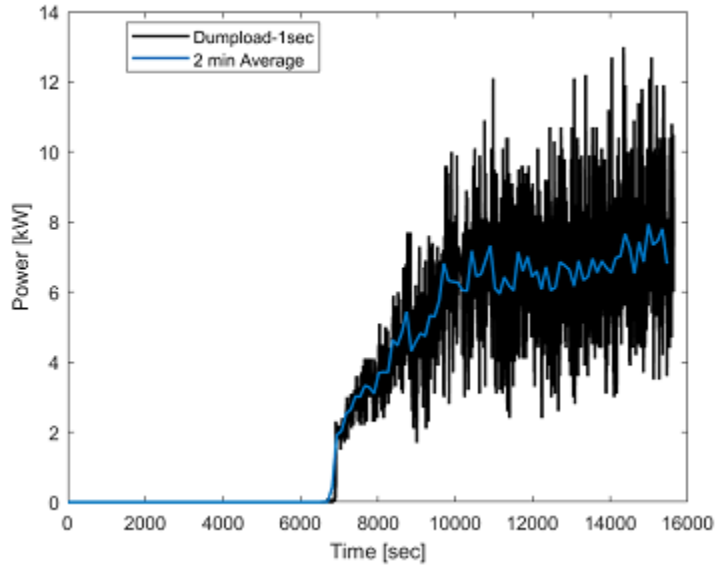

Figure 3.7: 1sec power from the dumpload and the 2 min average during the off-grid test on 3/20/19

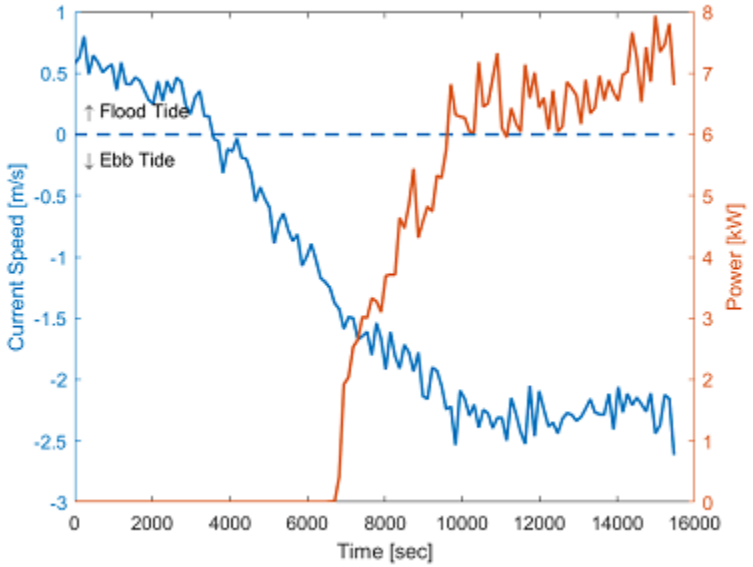

Figure 3.8: Current and 2min averaged power during the off-grid test on 3/20/19

that bin. The power vs. current speed is pictured in Figure 3.9 with the gray points representing each of the data points averaged to form the black curve. The lines in the gray data occur because of the resolution of the power data. The gray data shows that there are gaps along the current axis, which restricts the number of current bins that can be created. The 0.15 m/s bin width was chosen as the smallest bin width without creating gaps in the power curve. These current gaps would be improved by collecting data over multiple tidal cycles.

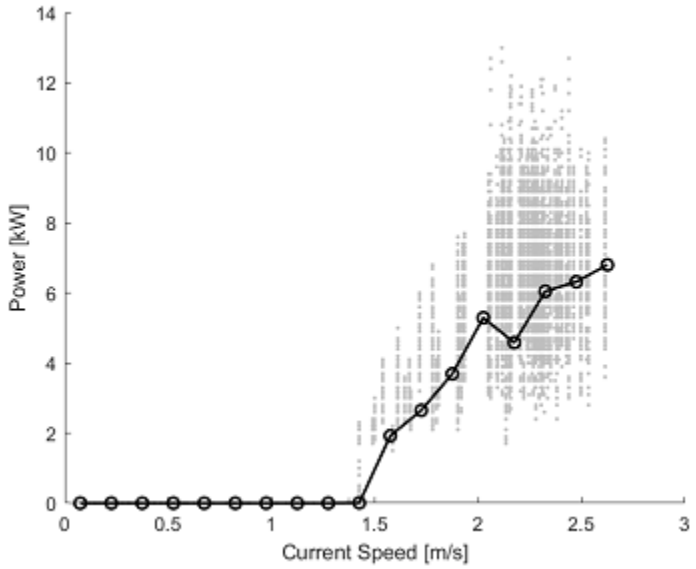

Figure 3.9: Power curve showing the raw data (gray) that was averaged to produce the black curve

The coefficient of power represents the overall efficiency of the device at extracting the energy theoretically available in the flow. The coefficient is defined as,

$$C_P = \frac{P_{actual}}{P_{available}} = \frac{P_{dumpload}}{0.5\rho A_{rotor} U^3} \tag{3.3}$$

The density of water, ρ, was taken to be $1024.6 kg/m^3$, which is the average value calculated from the CTD measurements at the site over the summer of 2017. The rotor area, A_{rotor}, is $5.44 m^2$ and U is the current speed. The power curve with the efficiency is plotted in Figure 3.10.

Based on the curve above the cut in speed for this turbine is 1.5 m/s and the peak efficiency is 23% which occurs at 2.025 m/s. The max sustained power was 6.8 kW in the 2.625 m/s current

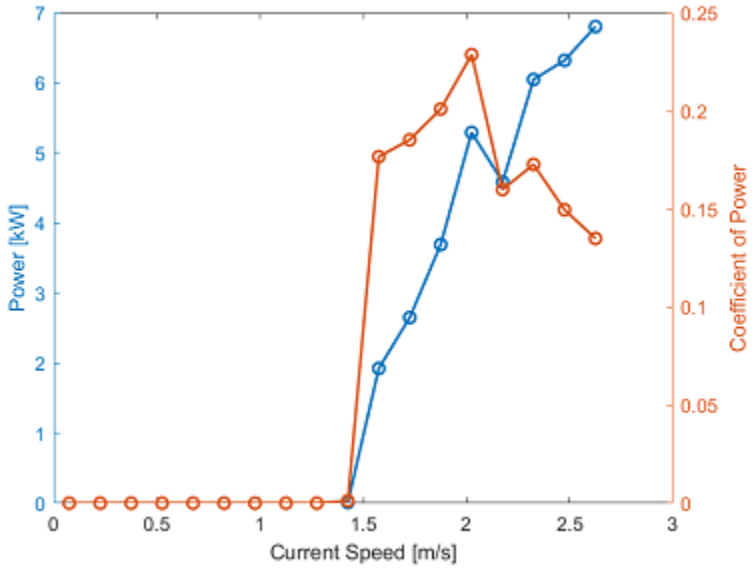

Figure 3.10: Power curve and the efficiency curve produced during the 3/20/19 off-grid test

bin. The max instantaneous power recorded was 13 kW and the max current recorded was 2.61 m/s, these did not occur at the same time.

The cut-in speed is higher than the value given by New Energy, which was 1.0 m/s. The difference is likely due to the new generator and power conversion equipment. The peak efficiency is seen near 2 m/s, which was the design point for the power electronics. A power factor correction system would modify the efficiency curve so that it would not drop off after 2 m/s as seen in Figure 3.10.

3.3 Energy Production Predictions

The annual energy production (AEP) is used to predict the amount of energy that a system could produce in one year. The AEP is calculated by summing up the power at each current speed weighted by the frequency that the current speed occurs. The power curve is a representation of how much power would be converted at each current speed and a histogram represents the probability of each current speed occurring based on the collected current data. These two tool are used to calculate,

$$AEP = H * \sum_{i=1}^{N_B} P_i * f_i \tag{3.4}$$

Where i is an index representing a bin of current speeds, P_i is the power at that current speed, f_i is the frequency of occurrence of that current speed, and H is the number of hours in a year.

Prior to the final design and fabrication of the tidal energy conversion system, initial predictions of the energy production were made. For the initial calculations a $6m^2$ cross-sectional area rotor and 0.7 m/s cut-in speed were used along with a theoretical power curve shown in Figure 3.11.

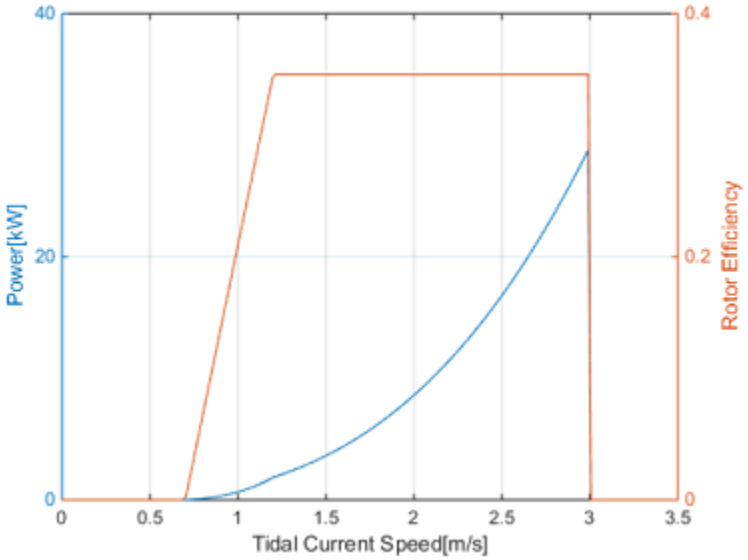

Figure 3.11: Theoretical power curve used for initial energy predictions [9]

The theoretical coefficient of power had a peak of 35%, which was assumed to be constant over the range of 1.2 m/s to 3 m/s. The ADCP current data collected during the HG-14 survey shown in Figure 3.12 was used for energy predictions. Using these assumptions and the HG-14 data, the annual energy production was predicted to be 10,249 kWh per year [9].

Figure 3.13 shows what percentage of the time a certain current speed was exceeded during the HG-14 survey. This type of plot can show how much of the time a turbine will be running. For example, with the theoretical cut-in speed of 0.7 m/s and the HG-14 currents a turbine would run 40.2% of the time.

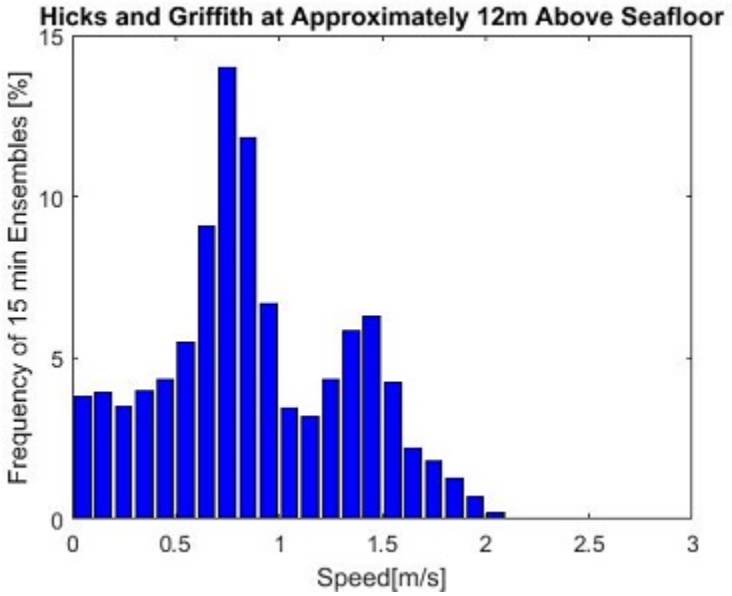

Figure 3.12: Histogram of the currents measured during the HG-14 ADCP survey with 0.1 m/s bins

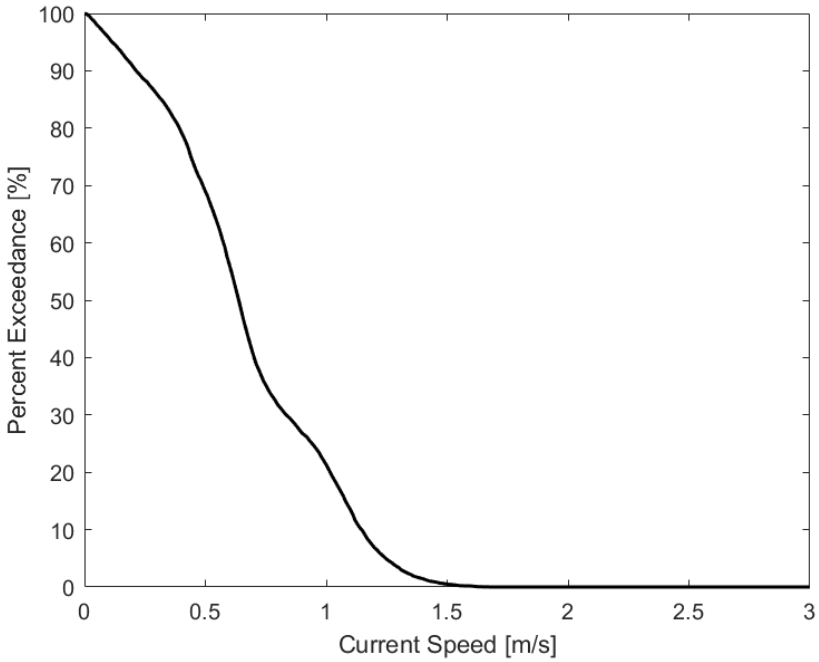

Figure 3.13: Percent exceedance of the current speed from the HG-14 survey

The initial prediction of AEP based on the HG-14 survey does not meet the specifications outlined in IEC TS 62600-201 [16]. The ADCP survey should be at least 90 days long and be conducted at the turbine location. The LB-17 survey does meet these requirements and combined with the power curve from the off-grid test of the installed turbine provides a more accurate estimation of the AEP. A histogram of the LB-17 ADCP survey using the combined current from both ADCP's is pictured in Figure 3.14.

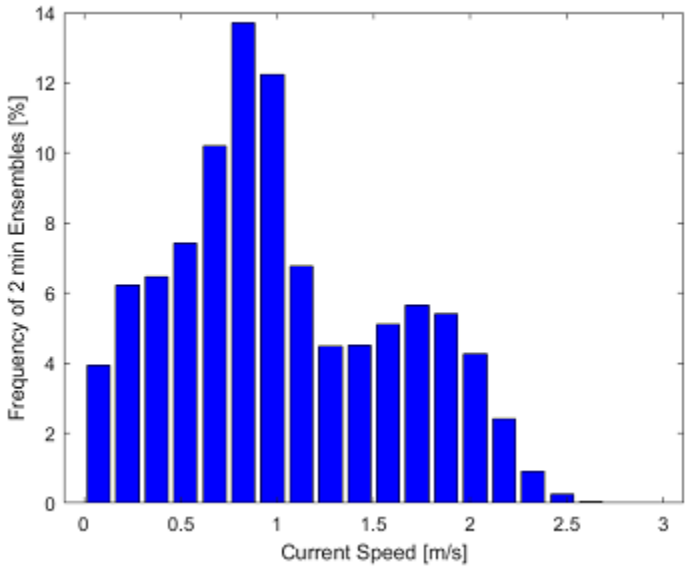

Figure 3.14: Histogram of the currents measured during the LB17 ADCP survey with 0.15 m/s bins

The AEP calculated using the off-grid test power curve and LB-17 survey was 7,528 kWh per year. This more accurate prediction is only 73 % of the original prediction of AEP.

The cut-in speed of 1.5 m/s from the off-grid test is over two times greater than the 0.7 m/s value used for the initial energy predictions.

Figure 3.15 shows that during the LB-17 survey the currents were greater than 1.5 m/s only 24.1 % of the time. This indicates that power would only be produced during that time based on the off-grid test with the installed turbine.

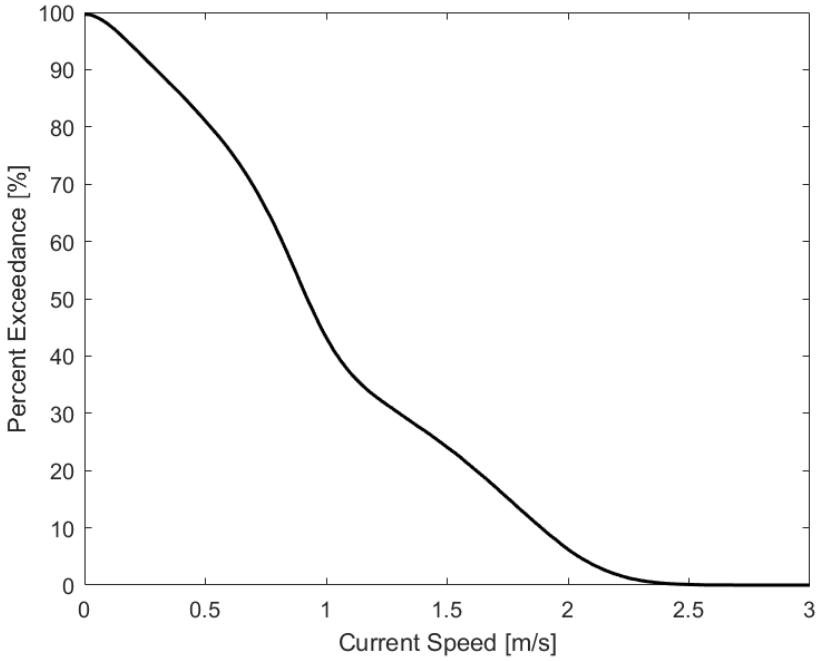

Figure 3.15: Percent exceedance of the current speed from the LB-17 survey

The peak efficiency seen in the off-grid test was 23%, lower than the 35% estimate used. Both the cut-in speed and efficiency contribute to the lower AEP predictions, although the mean kinetic power density was higher at the turbine deployment platform than at the HG-14 deployment site.

In order to improve the current resolution of the power curve, turbine testing should be conducted over multiple tidal cycles. A longer power and current data record would also lead to more confidence in the produced power curve.

CHAPTER 4

INSTRUMENTATION SYSTEMS

The instrumentation systems that are used for collecting data about the flow characteristics, water quality, environmental loads, and forces acting on the tidal energy conversion system. The full list of instrumentation specifically used for the tidal energy conversion system is provided in Table 4.1.

Model Name	Instrument Type	Parameters Measured
LinkQuest FlowQuest 1000 (x 2)	4-Beam Acoustic Doppler Current Profiler (ADCP)	Current Speed and Direction, Tidal Elevation
Nortek Signature 1000 (x 2)	5-Beam Acoustic Doppler Current Profiler (ADCP)	Current Speed and Direction, Tidal Elevation
Nortek Vector (x 2)	Acoustic Doppler Velocimeter (ADV)	Current Speed and Direction
Valeport Midas CTD + Multiparameter Profiler	Conductivity, Temperature, Depth (CTD) Sensor	Water Temperature, Salinity, Chlorophyll Level, Turbidity
Luxus Compact Camera (x 2)	Underwater Camera	Visual Information
Lite Enterprises Wildlife Mitigation Device System	Light Bars (x 2)	Wildlife Detection and Deterrence
Airmar 200WX WeatherStation Instrument (x 2)	Multiple Sensor Weather Instrument	Wind Speed and Direction, Air Temperature, Humidity, Barometric Pressure
Akamina AWP-24-3	Wave Height Gauge	Wave Height and Length
Spoondrift Spotter (x 3)	Wave Buoy	Wave Height, Length, and Direction
Yost Labs Watertight 3-Space Sensor	Inertial Measurement Unit (IMU)	Platform Motion
LCM Systems PTC-1 (x 2)	Low Profile Universal Load Cell	Turbine Thrust Force
Bridge Diagnostics, Inc (x 8)	Strain Gauge	Mooring Loads

Table 4.1: Instrumentation Associated with the Living Bridge Tidal Energy Conversion System

Data is collected from the instruments using a database system at the bridge and a mobile data acquisition system, these instrument integration systems will be described below. Most of the instruments are mounted with a universal instrument mounting system. This system is discussed below as well as additional mounting considerations specifically for the acoustic Doppler velocimeters (ADV's), including vortex shedding vibration mitigation and traversing system. The wildlife mitigation device system designed for this project by Lite Enterprises is still in development, so the information known about the system is documented below.

4.1 Instrument Integration

The baseline instrumentation connects to a database at the Memorial Bridge. Additional instrumentation not included in that system can be deployed with a mobile data acquisition system.

The instrument integration system is described by Figure 4.1.

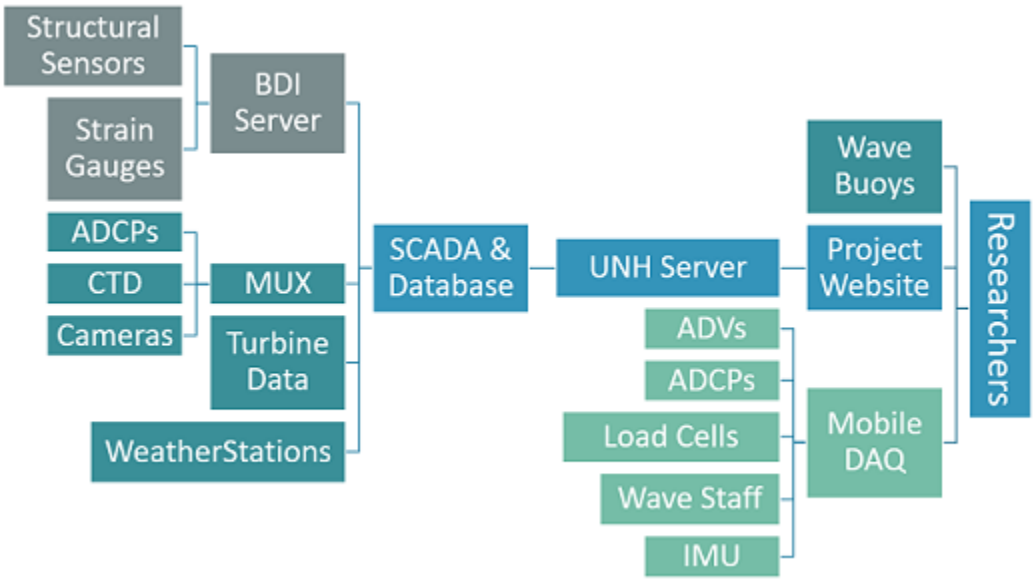

Figure 4.1: Flow Diagram Showing the Living Bridge Instrument Integration System

4.1.1 Bridge SCADA and Database System

The data from these instruments is combined with a multiplexer (MUX) and data and power is cabled up to a server room on the bridge.

The server includes a program developed by NorthEast Integration (NEI) that communicates directly with the sensors to collect all of the data and inputs it into a database. The data acquisition system is based on the GE Cimplicity software. Cimplicity allows the system to connect with and record data from the instruments and provide a graphical user interface (GUI). The GUI can be used to power the instruments, run their data collection scripts, and launch the associated manufacturer's software so that instrument settings can be changed. Cimplicity logs the data collected in a SQL database. Remote desktop is used for most of the communication with the server. A user's manual for the graphic user interface (GUI) and database was written by NEI and updated by researchers at UNH.

That database is then accessed by another server and database at UNH. After two years of using the origional database, the UNH database was redesigned to provide more user-friendly data files. [2] At the writing of this thesis the new database design has not yet been implemented. The project website is used to access the data in the database.

The `livingbridge.unh.edu` website accesses the UNH database for download of the data via the webpage. The database system also records data from the bridge structural health monitoring sensors, weather stations, and the turbine power electronics. The estuarine and weather data is accessible to the public while the bridge data requires permission from project leaders before access.

4.1.2 Mobile DAQ System

Additional instrumentation is for more temporary measurement campaigns and data is collected using a mobile data acquisition (DAQ) system or directly from the instrument. The mobile DAQ system was designed to allow for data collection when not connected to the bridge grid and server. This allows data to also be collected at locations other than the Memorial Bridge. The system also accommodates the additional instrumentation intended for temporary deployments. This system is based on the Modular Ocean Instrumentation System (MOIS) developed by the National

Renewable Energy Laboratory (NREL) and uses a National Instruments CompactRIO platform for data acquisition and control. [26] The requirements for the system were as follows:

1. Have reliable time that can be compared to time in the main database
2. Accommodate the wave staff, IMU, thrust load cells, ADV's, ADCP's, CTD, underwater cameras and other future instruments
3. Be able to be run autonomously for one tidal cycle, without personnel on platform, to meet this requirement it will need to:
   (a) Be water resistant
   (b) Have reliable power
   (c) Have enough data storage
4. Have data visible in real time or near real time

The time requirement was met by including a GPS in the system, allowing the data to be recorded with GPS timestamps. The instruments are accommodated by CompactRIO modules for analog, bridge, and serial signals and Ethernet switches. The CompactRIO and other components are housed in a National Electrical Manufacturers Association (NEMA) rated enclosure with bulkhead cable pass throughs to remain water resistant. A 12 V and 24 V supply are included to meet the power requirements. A relay board is used to regulate and monitor the power supplies. The system is run by a ruggedized field laptop, where real-time data can be viewed. A cellular modem allows for access to the internet for remote monitoring of the system. A diagram of the designed system is included in Appendix .

The development of the LabView code for the mobile DAQ system was started and initial testing of the system has taken place. [37] The second image in Appendix shows the components of the mobile DAQ that have been developed and tested to date. The current system can also be seen in Figure 4.2.

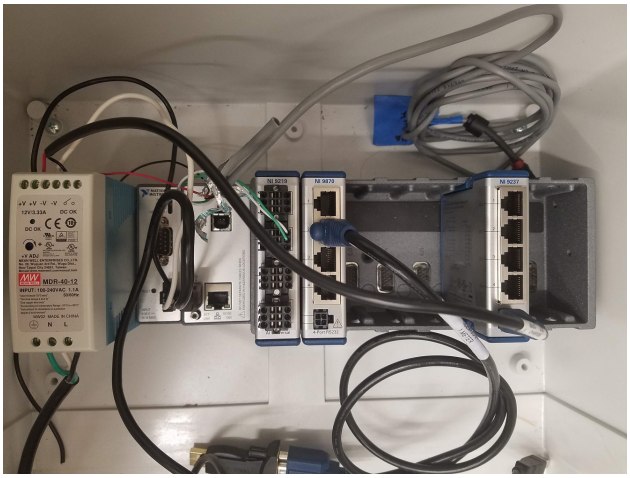

Figure 4.2: Picture of the assemble mobile DAQ system to date

LabView virtual instruments (VI's) have been developed for the wave staff and thrust load cells. The IMU VI is still in development. The wave gauge and load cell VI's use LabView Real-Time while the IMU uses the FPGA module for the CompactRIO. The wave staff and load cell VI's were tested in the lab before conducting a field test on the turbine deployment platform. The wave staff was installed on the universal instrument system as seen in Figure 4.3. The load cells are built into the turbine pitching mechanism to measure the thrust force on the rotor.

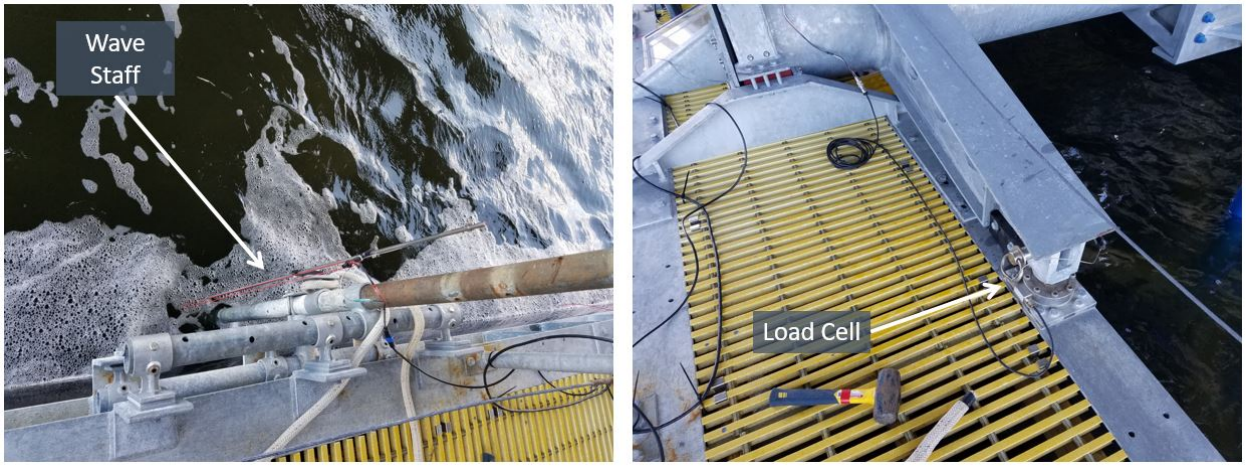

Figure 4.3: Wave staff (left) and load cell (right) during the mobile DAQ field test on the turbine deployment platform

The wave staff was tested with waves created by running the boat back and forth along the platform as seen in Figure 4.4. The load cells were tested by lowering the turbine and observing changes in the force output.

Figure 4.4: Waves created with the boat in order to test the wave staff and mobile DAQ system

The tests confirmed that the mobile DAQ system could be used for temporary deployments of the wave staff and load cells. To receive meaningful data from both instruments they need to calibrated correctly. The wave staff calibration procedure is well defined in the manual and can be done in the UNH Tow and Wave Tank. A procedure to calibrate the load cells so that force on the rotor could be determined from the output would need to be developed before acquiring thrust data. LabView VI's would need to be finished for the remaining instruments before the mobile DAQ system has the full capacity that it was designed for.

4.2 Instrument Mounts

4.2.1 Universal Instrument Mounting System

A universal instrument mounting system was designed in order to install a range of instrumentation on the turbine deployment platform. [4] The main goals of the instrument mounting system were to be resistant to the environment, easily operable by persons above the deck, flexible to allow for new instrumentation, and provide good instrument performance. The system was designed

out of 2 in, schedule 80, galvanized steel pipe and structural pipe fittings that are available off the shelf. For added security, the structural pipe fittings were modified to include through holes for 1/2 in bolts. The instruments are attached to the bottom of a vertical pipe with custom mounts for each instrument. The system is attached to angle iron tabs welded to the turbine deployment platform frame as seen in Figure 4.5. [4]

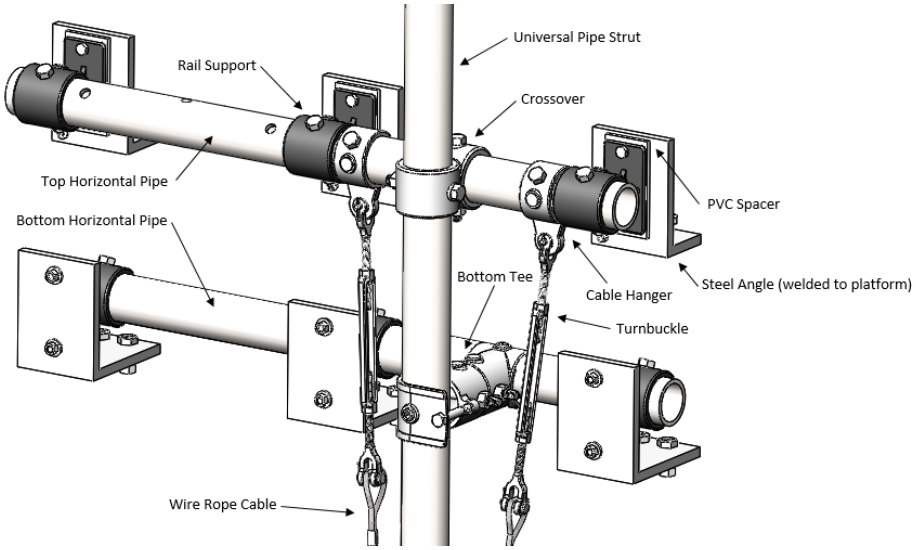

Figure 4.5: Diagram of the universal instrument mounting system, where the angles are welded to the turbine deployment platform and an instrument is attached to the bottom of the vertical pipe

The bottom tee can be removed so that the vertical pipe can rotate around the top pipe during instrument installation and removal. The universal instrument mounting system was originally designed for the baseline instrumentation but was also used to deploy the ADV's and a wave staff. Since the system was originally installed, many of the 1/2 in bolts have been replaced with pins to make installation and removal easier. Bolts should be used in the crossover between the vertical and top horizontal pipes to prevent vibration in the pipe.

4.2.2 ADV Mount Vortex Induced Vibration Mitigation

Mount vibration was encountered during field deployments of the ADV's on the turbine deployment platform. For the initial ADV deployment on 6/15/18, the goal was to get familiar with the operation and data collection of the instrument. The temporary mount was constructed out of

3/4 in electrical conduit clamped to a wood board. The probe was attached to the conduit with hose clamps as seen in Figure 4.6.

Figure 4.6: Temporary mount used for the first field deployment of an ADV on the turbine deployment platform on 6/15/18

The vibrations of the mount that contaminated the ADV data were due to vortex shedding. Vortex induced vibrations (VIV) are caused by vortices that shed alternately off of a cylindrical or spherical body. These vortices are formed by the velocity deficit resulting from the wake of the body as seen in Figure 4.7. [34]

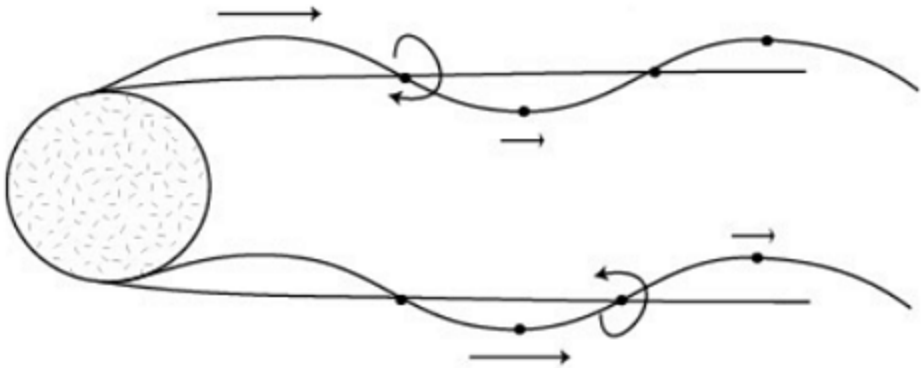

Figure 4.7: Depiction of the vortices behind a cylinder that cause VIV [34]

For a cylinder, the frequency of the vibrations is a function of the Strouhal number, S_t, the stream-wise velocity, U, and the diameter of the cylinder, d,

$$f_s = \frac{US_t}{d} \tag{4.1}$$

The Strouhal number is a function of the Reynolds number, which for a cylinder is defined as,

$$Re = \frac{Ud}{\nu} \tag{4.2}$$

Where ν is the kinematic viscosity of the fluid. Experiments have shown that Strouhal number varies with Reynolds number depending on the roughness of the cylinder as seen in Figure 4.8.

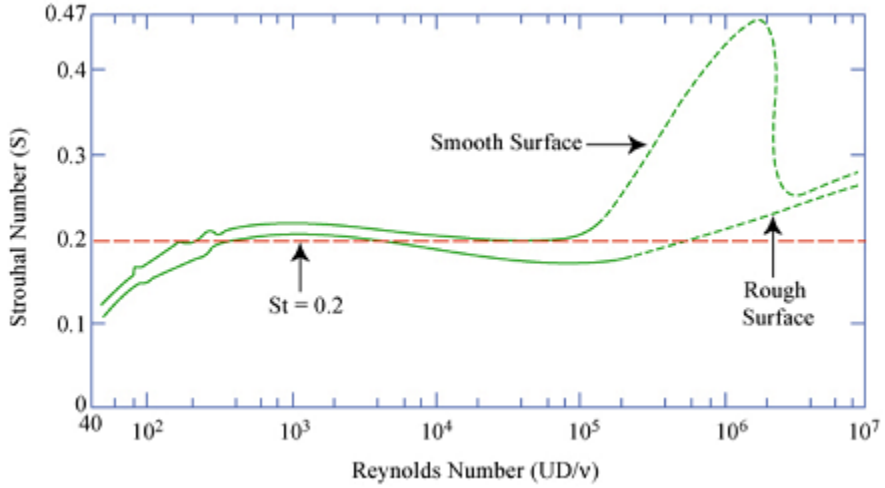

Figure 4.8: Reynolds number dependence of Strouhal number for rough and smooth cylinders [34]

In order to identify that the vibration in the original ADV mount was caused by VIV, the shedding frequency was calculated using Equation 4.1 and compared to the pre-multiplied spectral density of the velocity recorded by the ADV. The shedding frequency was calculated to be 17.16 Hz, based on a Reynolds number of 35000. Figure 4.9 shows the spectra of the stream-wise and cross-stream velocity. A more prominent peak is seen in the cross-stream spectra because the vibration due to the mean current occurs in this direction.

In order to reduce the effects of VIV on the ADV measurements, fairings were added. The diameter of the pipe was also increased to 2 in so that the mount was stiffer. Fairings are used

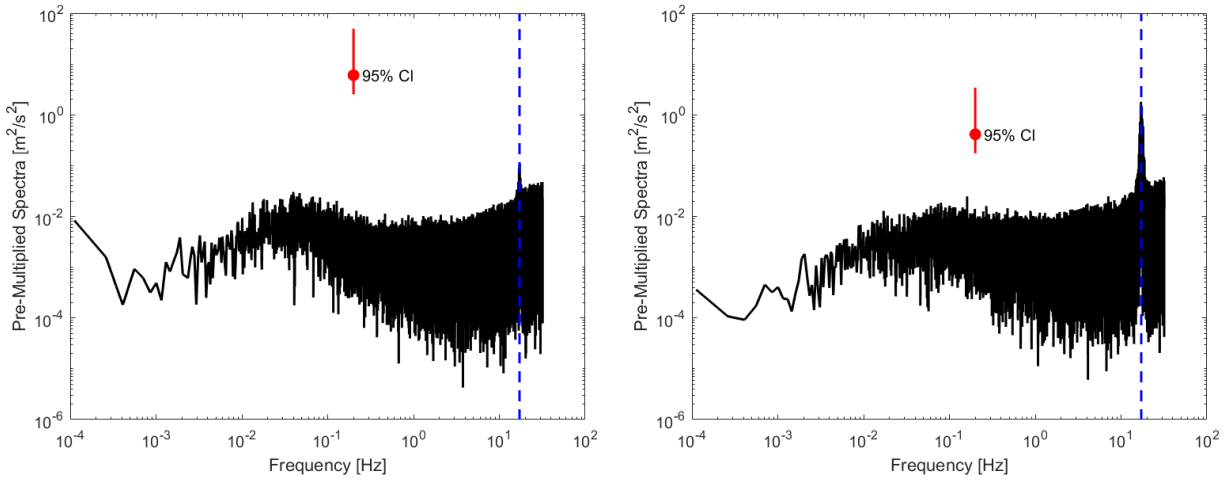

Figure 4.9: Pre-multiplied spectral density of the stream-wise (left) and cross-stream (right) velocity collected during the first field ADV deployment using the 3/4 in conduit mount (Reynolds number of 35000). The blue line indicates the calculated vortex shedding frequency of 17.16 Hz

to streamline structures in order to reduce drag. The streamlined shape obstructs the formation of vortices that cause VIV. Due to the asymmetric flow at the site, a fixed hydrofoil shape would create lift and greatly increase the forces applied to the mounting structure. The fairings need to be able to rotate a full 360 °in order to avoid these forces. The first iteration of the fairing design was formed by heating up and forming acrylic sheeting into a hydrofoil shape as seen in Figure 4.10.

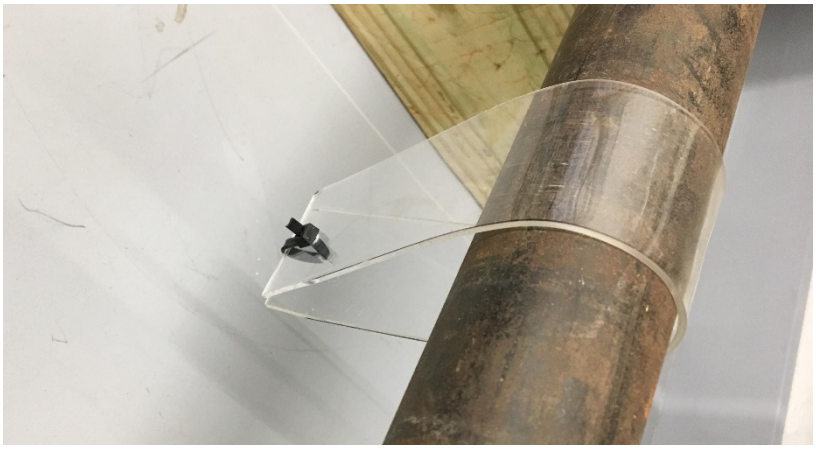

Figure 4.10: First fairing design created by forming acrylic sheeting

The fabrication of the acrylic fairings proved difficult and time consuming. The fairings often took on an odd shape or snapped during the forming process. For the second fairing iteration aluminum was chosen based on its flexibility. Aluminum dryer vents were used because they were already the correct size, requiring only bending and cutting for fabrication.

Multiple fairings of 1 ft lengths were used to allow for flow changes throughout the depth of the water. Initial deployments showed that the fairings would bunch up and separation between the fairing sections was necessary. The separating disks would need to clamp onto a 2 in steel pipe over the cable connecting the ADV probe and instrument body. The cable cannot be disconnected from either end, so the disk would need to fit over the probe head or come off completely. Hose donuts are available off the shelf and meet these requirements. Adjusta-flex hose donuts are made of flexible polyurethane and designed to lift sanitary hoses off of the floor. The hose donuts can open up and clamp onto a variety of hose and pipe diameters with two sets of bolts. Hose clamps around the edge of the hose donuts were also used to tighten the donut further around the pipe.

The aluminum fairings with the hose donuts were tested in the UNH Tow and Wave Tank as seen in Figure 4.11.

During the testing it was determined that the aluminum fairing edges were too sharp, making it difficult to safely deploy the instrument. The aluminum fairings were replaced with high density polyethylene (HDPE) sheeting. The HDPE is flexible and can be easily cut with scissors. Further testing of the fairings in the tow tank was conducted. The original 1/32 in thick HDPE was easily damaged and was replaced with 1/16 in thick HDPE sheeting. The final fairing design seen in Figure 4.12 was then used to deploy the ADV's on the turbine deployment platform during the 4/22/19 - 4/26/19 measurement campaign.

To investigate the effectiveness of the fairings in more detail, another test in the tow tank was done. The ADV was attached to a 2 in pipe with and without fairings and towed through the tank at 2 m/s. The tank was seeded with hollow glass spheres to ensure that enough acoustic scatters were present. The spectral density of both data sets was computed to examine the effect of the fairings. For the case without fairings the shedding frequency was calculated to be 6.66 Hz based

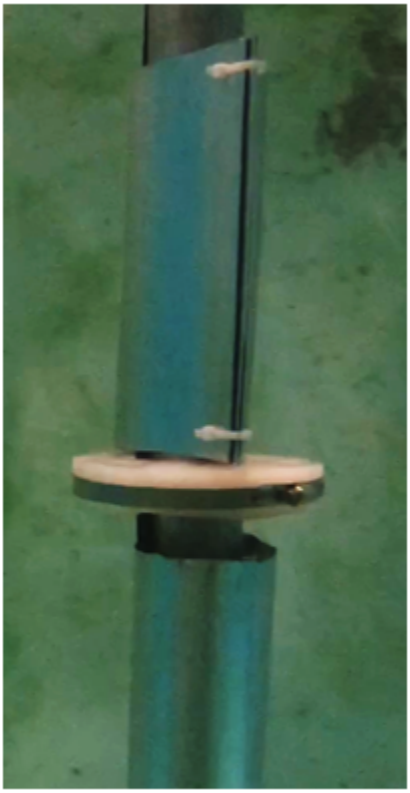

Figure 4.11: Second fairing design using aluminum dryer vents and hose donuts

Figure 4.12: Final fairing design using 1/16 in thick HDPE sheeting and hose donuts

on a Reynolds number of 103000. The test with the fairings had a calculated shedding frequency of 6.76 Hz based on a Reynolds number of 105000. Figure 4.13 shows that there is a peak at the shedding frequency for the test without fairings, but there is no longer a peak at the shedding frequency for the test with the fairings.

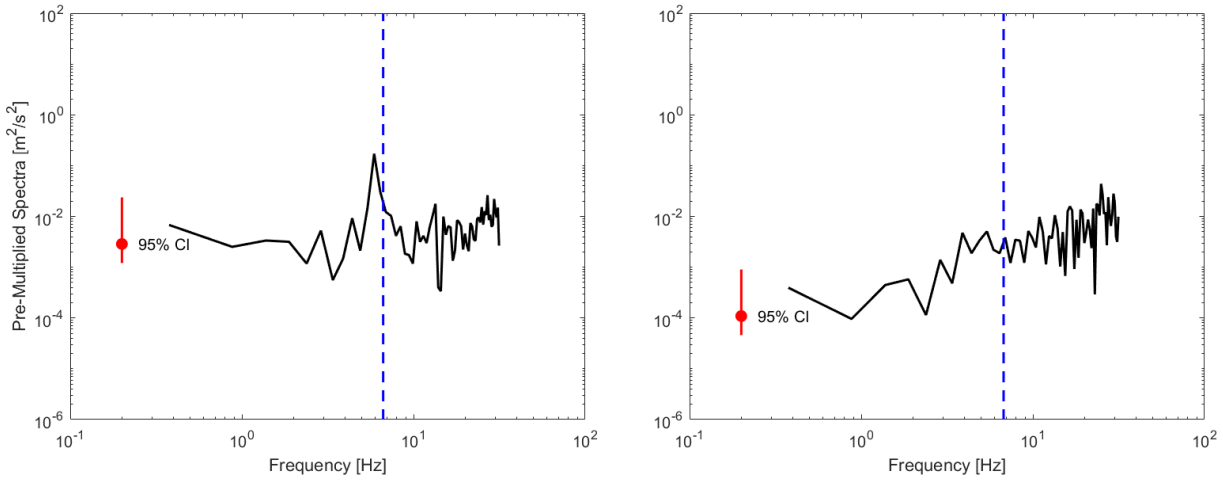

Figure 4.13: Pre-multiplied spectral density of the cross-stream velocity collected during the ADV test in the UNH Tow and Wave Tank without fairings (left) and with fairings (right). The blue line indicates the calculated vortex shedding frequencies of 6.66 Hz and 6.76 Hz, based on Reynolds numbers of 103000 and 105000 respectively

4.2.3 ADV Traverse

A traversing system was designed for taking measurements across the moon pool of the turbine deployment platform, where the instrument position can be changed in the horizontal and vertical directions. [3] The traversing system can in principle be used with any instrument, but the main instrument to be used was the ADV. The goal was to obtain a flow map of the turbine cross-section in the inflow and wake. The system pictured in Figure 4.14 has the ability to move the vertical pipe with the ADV horizontally and vertically. The horizontal traversing motion uses two hand-crank trailer winches and the vertical motion uses a sailboat winch.

The traversing system can be installed in the location indicated in Figure 4.15. There were mounting holes drilled in these locations so that the traverse can be secured with 1/2 in bolts.

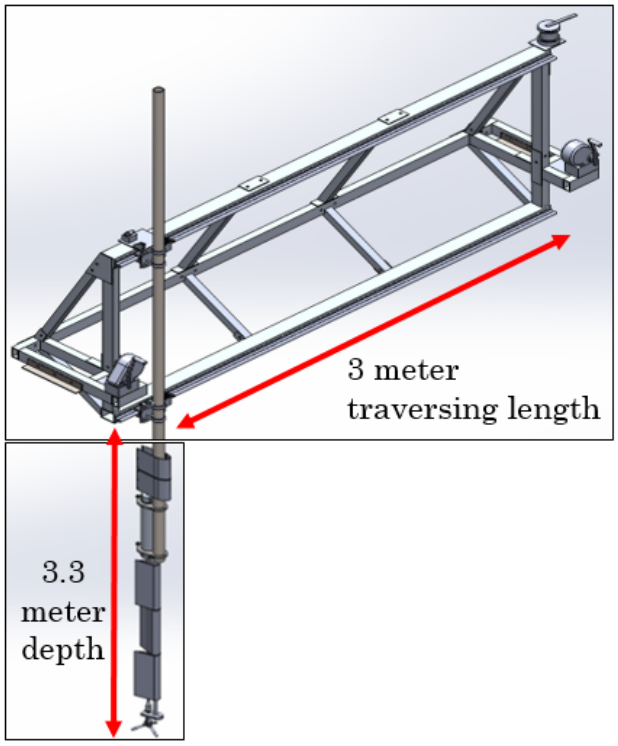

Figure 4.14: Model of the ADV traverse demonstrating the traversing directions

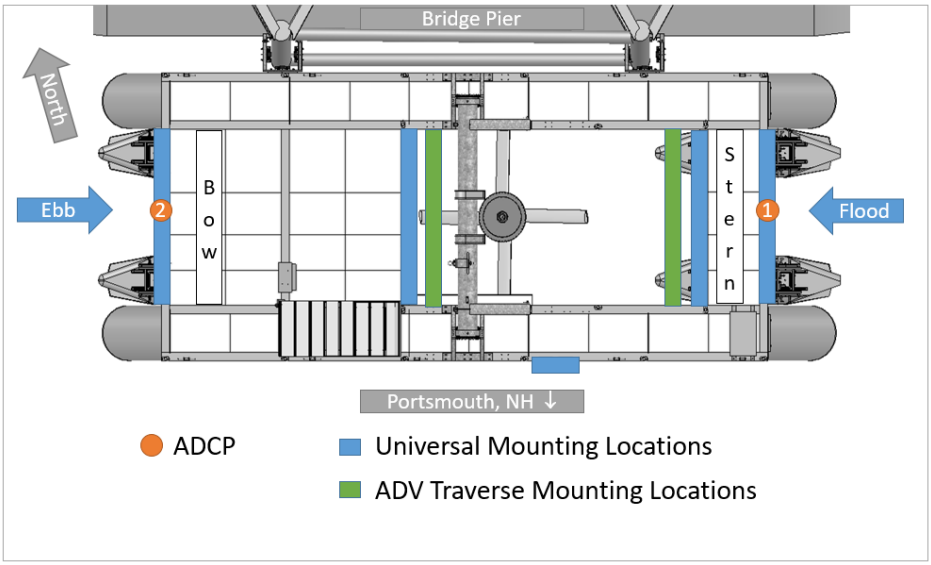

Figure 4.15: Locations on the turbine deployment platform where the ADV traverse can be installed

Two measurement campaigns were attempted with the ADV traversing system. The major challenges encountered were the long set up time and complicated experimental design.

The aluminum traverse frame consists of three 12 ft (3.6 m) sections and additional supports that were each designed to be under 100 lbs. For each measurement campaign the components must be brought out onto the boat and transported to the turbine deployment platform. The larger sections fit on the floor of the Galen J with approximately one foot to spare on either end. The sections must then be moved out of the boat onto the platform, up and over the railings, and positioned over the moon pool. The traverse frame can be seen installed in the moon pool in Figure 4.16.

Figure 4.16: ADV traverse installed in the moon pool of the turbine deployment platform

Due to the awkward shape of these sections, this process can be time consuming. The installation and operation procedures for the ADV traverse were designed for two people. From past experience three people are necessary in order for the process to be safe and take a reasonable

amount of time. In the past, the day before the experiment was dedicated to the frame installation and a day after the experiment was for the removal of the traverse frame. The previous experiments were conducted in October and December of 2018 and the cold weather played a factor, as most tasks took longer in the cold.

Each day that data was taken, the ADV would need to be installed on the traversing system. The ADV is mounted on a 10.5 ft pipe to reach the mid-turbine depth. This pipe needs to be held vertically so that the pipe fittings can be attached to the traversing system. This process proved difficult, and a good way to hold the pipe and line up the bolts was not found during the deployments. This process took up to three hours with two people.

Both experiments were designed so that a cross-stream profile of the inflow to the turbine location could be obtained. Measurements were taken at the bow end of the moon pool for the ebb tide and at the stern end of the moon pool for the flood tide. For the bow end of the moon pool, the turbine must be in the down location in order for the traverse frame to fit next to the spanning beam. The turbine was electrically braked and secured with ropes during the experiments at this location. The rotor was seen to drift over time, even with the electric brake, so it must be monitored so that it does not come in contact with the ADV mount. Due to the presence of the turbine, the ADV cannot be traversed the entire cross-stream distance, the traversing distance is limited to approximately 2 m.

The experiments were planned for a two hour window where the peak ebb or flood current were expected. With the long set up times and difficulty in installation, this window was missed completely during the first experiment. The second experiment allowed for extra time, but this lead to long exposure times during the cold December weather.

Three different traversing schemes were tried, sitting at each point for 5 min, sitting at each point for 1 min, and continually moving the ADV across at a steady pace. As was seen with the ADV data discussed in Section 2.2, the flow is changing rapidly. The mean current was changing over the duration of the traverses with 5 min and 1 min pauses. The second ADV was installed at the bow or stern, depending on the tide direction. This measurement was meant to act as a

reference for the traversing ADV. The instruments were not synchronized during this time, so the current speed changes seen by the fixed ADV could not be related to the moving ADV. This meant that it could not be determined whether the changes seen across the moon pool were attributed to temporal or spatial changes. For the continually moving ADV traverses, the mean was relatively constant. However, the movement of the ADV could not be removed because there was no means of measuring the speed of the traversing, although the movement was slow compared to the current speed.

The two traversing system experiment attempts informed the design of the final ADV experiments described in Section 2.2. It was determined that longer data sets were needed, based on the variability in the "snapshots" of the currents when data was collected. This also relaxed the need to schedule around the two hour tidal window and simplified logistics. It was also determined that synchronization was needed in order to achieve meaningful spatially variable measurements.

Based on the long set up time and difficult assembly involved in the traversing system, it was determined that it was not needed for taking day long data sets at coarse spatial resolution. Now that the tidal variation of the currents has been investigated in more detail, finer cross-stream measurements can be taken to add further information to the system. It is recommended that any future traversing experiments be conducted with at least three people and during warm weather. There should be a reference ADV that is synchronized to the traversing ADV. The traversing across the moon pool should be done in less than around 10 minutes so that the mean current is not changing too rapidly. A means for determining the location of the ADV needs to be used for any traversing experiments. The simplest form of this is documenting the times that the instrument is at each location.

4.3 Wildlife Mitigation Device System

The Wildlife Mitigation Device System (WMDS) developed by Lite Enterprises Inc. uses underwater cameras and light bars in order to detect and deter fish and other wildlife around the area surrounding the turbine [8]. The system was designed by Lite Enterprises specifically for the Liv-

ing Bridge Project, which is acting as a test bed for this new technology. Lite Enterprises has previous experience with deterring birds and bats from wind turbines, cell towers, and aquaculture farms. They developed the WMDS in order to expand to their technology to the marine energy sector.

The underwater cameras are part of the baseline instrumentation and are incorporated into the NEI data collection system and database. The images are sent to a control box developed by Lite Enterprises where images are analyzed to detect fish. When the system detects wildlife then the light bars flash and a flagged image is stored in the NEI database. Compatibility issues between the NEI system and the Lite Enterprises system resulted in the system being only fully operational for one week in the summer of 2017. The flagged images were analyzed in order to provide recommendations to Lite Enterprises for improvements to their system.

The flagged images were generated during the period from July 25, 2017 at 14:46:59 EST to July 26, 2017 at 11:46:14 EST. It is uncertain whether these photos represent all of the flagged photos from this time period but that is assumed to be the case. The images recorded during this time were taken every five seconds using Camera 1 which is located on the stern side of the moon pool facing upriver. During this time period ADCP 2 (located on the bow of the platform, upriver) was not recording due to a damaged pressure sensor, so any current speed data reported below is only from ADCP 1 (located on the stern, downriver).

The names of the saved files were used to determine how frequently files were flagged over this time period. Figure 4.17 shows the percentage of images flagged during a time bin where each bin is 10 minutes long. The current speed data for this period of time is included in Figure 4.17 to investigate any tidal dependence on the frequency of images flagged.

All of the flagged photos occurred during ebb tide, except the outliers. Outlying images flagged (beginning and end of time period) are of temporary, advected biofouling as shown in Figure 4.18.

No images were flagged at night. It is not clear whether this is related to the amount of light (even at night there is some lighting from the bridge, downtown Portsmouth, and the Naval Shipyard) or whether the images did not trigger the system. The majority of flagged images during ebb

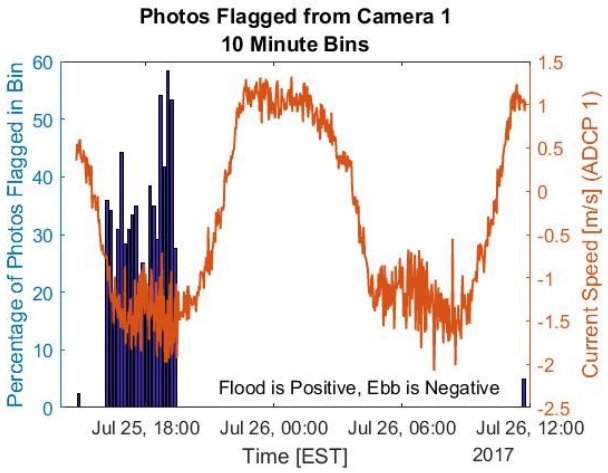

Figure 4.17: Frequency of photos flagged by the Wildlife Mitigation Device System compared to the current magnitude measured with an ADCP

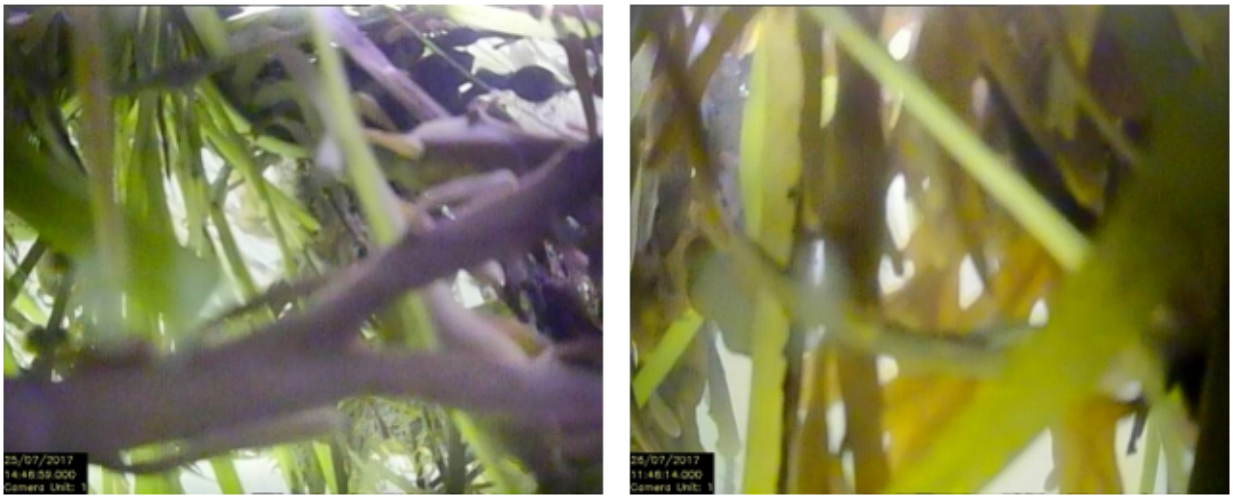

Figure 4.18: Outlying images flagged by the Wildlife Mitigation Device System of advected bio-fouling

tides show bubbles, however, the amount of bubbles (void fraction) varies greatly. Occasionally seaweed can be seen in the frame. In general, the color becomes more muted as it gets later in the evening as seen in Figure 4.19

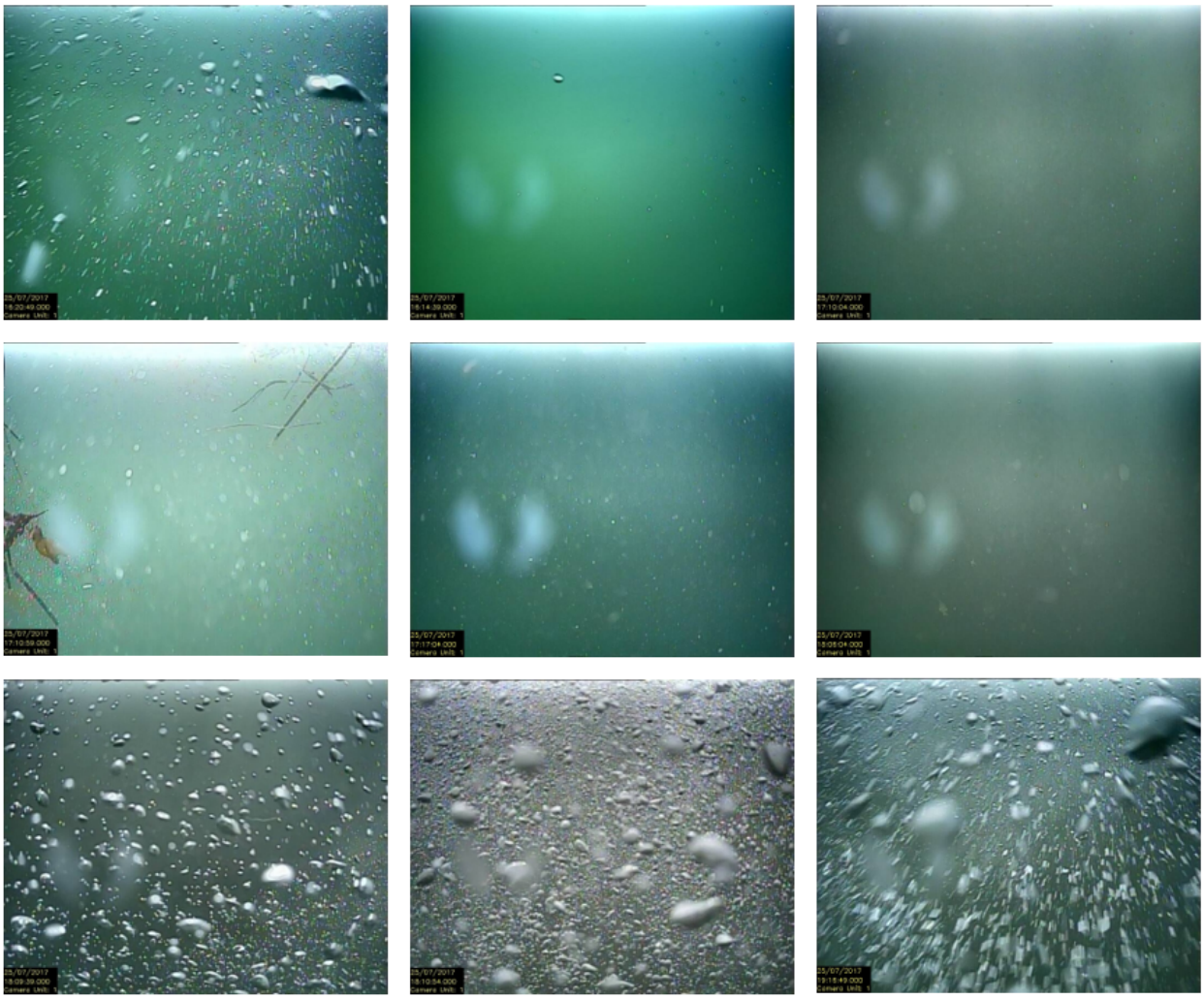

Figure 4.19: Images flagged by the Wildlife Mitigation Device System during the ebb tide in chronological order

Based on these images, recommendations about the process for determining the effectiveness of the system were made. In the present set of photos, only flagged images were stored. All of the images, flagged and unflagged, are needed in order to determine if the flagged images really show everything that is happening and evaluate how effectively the flagging algorithm is working. For this purpose, all images should be stored for a full tidal cycle (28.5 days). The horizontal visibility

distance, which is currently unknown, needs to be investigated during different times of day, of the year, and in the tidal cycle. This will give us a better idea of camera placement and give a better estimate of how far away from the camera objects are. The frame rate currently set to take one photo every five seconds should be changed to one photo per second.

Another consideration for increasing the frame rate is that it is under sampling if the goal is to capture images of objects or fish in motion. The maximum current velocity at the site are greater than 2.5 m/s; this means that non-actively swimming fish will move at the rate of 2.5 meters (8 ft) per second. The currently used frame rate of one photo every five seconds is too slow to capture objects moving in front of the camera, including fish.

The field of view is estimated to be defined by a 90 degree angle of view and a forward looking distance, d, as seen in Figure 4.20. If objects are moving in the plane of view they would travel a maximum distance of 2d across the frame. (If objects are moving towards or away from the camera, they would travel a distance of d towards or away from the camera.)

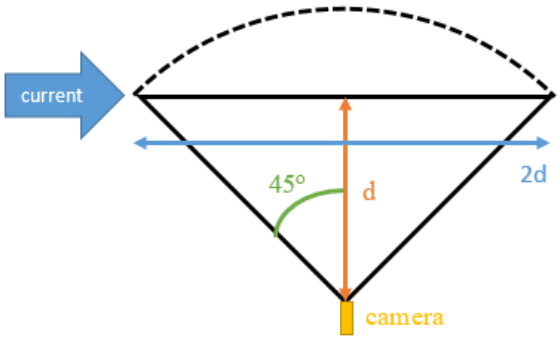

Figure 4.20: Images flagged by the Wildlife Mitigation Device System during the ebb tide in chronological order

The amount of time that an object is in the plane of view can be calculated using,

$$t = 2d/v \tag{4.3}$$

If d=3m and a fish is moving at v=4 m/s (2.5 m/s current + 1.5 m/s swimming) then the fish will be in the field of view for 1.5 seconds. If d=1m then that same fish would only be seen for 0.5

seconds. How far away a fish can be detected based on an interval between pictures is calculated by,

$$d = \frac{1}{2}tv \tag{4.4}$$

With the old frame rate of 1 image per 5 seconds (t=5 seconds) and v=4 m/s then objects can be detected at 10m away or farther. This distance may be farther than the cameras can see through turbid water. With the new frame rate of 1 image per 1 second (t=1 second) and v=4 m/s then objects can be detected 2m away from the camera. This seems like a reasonable distance for viewing objects in motions, objects closer than 2m would still be seen if the timing lined up with when a photo was taken. If closer images are necessary, the frame rate could be increased to 2 images per 1 second.

At the writing of this thesis these recommendations have not yet been implemented by Lite Enterprises, although they have been made aware of them.

CHAPTER 5

OPERATION AND MAINTENANCE OF THE TIDAL ENERGY CONVERSION SYSTEM

The turbine deployment platform was installed without a turbine in June of 2017. Since then, the turbine deployment platform, tidal energy conversion system, and instrumentation associated with the system have needed to be kept operational. This chapter describes some of these systems and the problems that have been encountered up to this point. The solutions that have been implemented and work that still needs to be done is also described here.

5.1 Turbine Installation and Issues

The turbine was installed on the turbine deployment platform in June of 2018, Figure 5.1.

Figure 5.1: Turbine installation in June of 2018 at the UNH Pier in Newcastle, NH

Representatives from New Energy Corporation assisted with the installation and the initial off-grid testing of the turbine. There were some initial problems related to the wiring and settings

of the system. After their departure, off-grid turbine testing continued while the UNH team got accustomed to the system and worked out some of the initial issues with New Energy remotely.

During the off-grid test on 8/6/18 damage to the generator occurred when the electric brake was applied while the turbine was free-wheeling. A ring of bolts that hold together two sections of a segmented housing were sheared. The ring of bolts indicated in Figure 5.2 on the lower housing were sheared and most of the upper bolt halves were recovered from the housing.

Figure 5.2: Stainless steel bolts sheared in the generator during turbine operation, the location of the bolts is indicated by the arrow in the picture of the turbine

The generator repair was conducted at the UNH pier from 10/1/18 to 10/4/18 with help from a representative from New Energy. The cables to the generator were disconnected and the turbine was lifted off of the platform with a crane. The blades were disassembled and the shaft removed from the generator. The lower and upper generator housings and bearings were removed for the shaft to be removed. The sheared bolts were removed. The lower housing was cleaned and

modified to accommodate new, stronger bolts. The turbine was assembled and lowered onto the platform. The generator wires were then reconnected in the junction box.

During the generator repair, the adapter bracket connecting the turbine to the turbine pitching mechanism was replaced. The original adapter bracket was under-designed and saw significant deflection and stresses while the turbine was in operation and there were concerns about the fatigue life of the bracket. The new bracket was designed to accommodate higher loads and has not had any issues since its installation.

Following the generator repair, the process for getting the system approved for grid connection was started. After the system was inspected and approved to be connected to the grid, the system was switched over to grid mode and grid-connected testing began. The first issue that arose was that the rectifier was displaying an "Over-Volt" error. The over voltage limit in the rectifier was originally set to 500 V, during testing this level was exceeded and the limit was increased to 750 V on 11/8/18. The rectifier is rated for 850 V, so the change was safe and resulted in the elimination of the "Over-Volt" error.

The inverter was then able to start up and it became apparent that the inverter and rectifier were not communicating with each other. This issue was resolved on 11/15/18 when the addresses of both pieces of equipment were corrected to the same value.

The next major issue was that the inverter was displaying an "ILeak-PRO04" alarm. It was determined that this error is caused by current leakage to ground from the system. The inverter is designed to only accept a floating DC signal, because of the current leakage a grounded DC signal is sent to the inverter. With assistance from electricians from NorthEast Integration (Portsmouth, NH), the current leakage threshold was lowered so that it could be determined if there were any other issues with the system. With the limit lowered a second alarm, "RelayChk", was displayed. Based on this error representatives from Ginlong determined that the inverter must be replaced. The original Ginlong inverter was replaced on 2/27/19 with a new inverter provided by Ginlong under warranty. On 3/1/19 the polarity of the new inverter was checked and then connected to the rest of the power electronics. With the turbine running the new inverter displayed the "ILeak-

PRO04" error. On 3/11/19 the ILeak Limit setting was raised to check for other errors. The same "ReleyChk Fault" error occurred with the new inverter as with the old inverter. At the writing of this thesis, the current leakage issue is still being investigated by UNH and NorthEast Integration.

5.2 Turbine Operation

The turbine can operate in either grid-tied or off-grid configurations. The process to operate the system is very similar for both configurations. The first step is to lower the turbine using the turbine pitching mechanism. The system is powered by a winch on the deck of the turbine deployment platform that attaches to the top of the strongback. When the turbine is in the up position the winch is reeled most of the way in. The winch is powered by a marine battery. This battery was originally stored on the platform continuously, but there were issues with keeping the battery charged. In order to ensure that the battery has a charge, the battery was stored at the UNH pier facility and only brought to the platform when deploying the turbine. The boat battery can also be used as an emergency power source. This procedure includes more hazards and should only be attempted by experienced personnel.

The winch is operated by a controller that can operate wirelessly or cabled to the winch. The cabled operation is much more reliable, so it is usually used. Both the main and backup winch controllers are typically kept in the emergency toolbox on the turbine deployment platform. For added safety, the strongback is usually attached to a hook on the platform frame by a lifting strap when leaving the turbine in the up position for long periods of time. This lifting strap and all of the railing cables surrounding the strongback and support arms need to be removed before deploying or removing the turbine. There are also a set of 1 in pins that hold the support arms to swivel blocks that need to be removed. If these pins are not removed and the winch is activated, damage to the turbine pitching mechanism will result. During winch operation, all personnel need to be aware of the operation and clear of the winch rope. The winch rope snapping could result in major injury to any personnel in the vicinity of the rope. Once the turbine is in the down position the pins should be installed.

During the winch operation, the turbine should be electrically braked. To apply the electric brake, the systems in the turbine interface panel must be powered on by opening all of the switches inside the panel. The turbine brake should automatically engage and the indicator light on the outside of the panel should light up. When the turbine is down, the pins are installed, and the railing cables re-installed, the turbine can be started. Both the grid and generator switches on the outside of the panel should be turned to the "On" position. The emergency brake can then be released and the blue reset button pressed. At the completion of this process the grid and generator lights should be on and the brake light off. If the current is strong enough, then the turbine will begin to spin up. The voltage outputted by the turbine will be displayed on the rectifier LED screen. This voltage will keep changing rapidly with the currents.

The difference between grid-tied and off-grid operation is where the power is sent from the rectifier. There is a switch on the outside of the turbine interface panel that indicates which configuration is being followed by the system. There are also settings related to the dumpload that must be changed with the rectifier's software. If the system is in off-grid mode the rectifier will send the power directly to the load bank. Heat will be dissipated by the load bank, which can be felt on the outside of the load bank during times of operation. If the system is in the grid-tied configuration, then the inverter will turn on once it has been provided at least 300 V. The inverter will go through a start up procedure before attempting to connect to the grid. At the writing of this thesis, the inverter has never been in full operation due to the problems described previously. Theoretically, it will start sending power to the grid if no errors are detected.

5.3 Boat Travel

The turbine deployment platform is not accessible from the bridge structure, so it is required to access the platform by boat. This was a safety request by the bridge owner, New Hampshire Department of Transportation, so that it would not be possible for people to access the bridge pier from the platform, which could be dangerous during lift operations. The majority of operations are conducted out of the Judd Gregg Marine Research Complex (UNH Pier) in Newcastle, NH.

The 22 ft, outboard-powered Galen J owned by UNH, is used for the majority of operations. Other small vessels normally docked at the Jackson Estuarian Lab (JEL) in Durham, NH can also be used. Transit to the Memorial Bridge takes approximately 15 minutes with the Galen J, depending on the tidal current direction and speed. The driver operating the vessel is in charge of docking and transit procedures. For docking to the platform, especially in high currents, it is important for all other team members on the vessel to listen to and act on the directions from the driver. The driver should identify which side of the vessel to dock on such that the vessel faces the oncoming tidal current. If it is expected that the current direction will change during the operation, a plan for switching the boat around should be made upon initial docking. The other team members on the boat will be in charge of making sure the fenders and dock lines are attached to the correct side of the boat. During docking, the driver or other team member will tie off the bow spring line first and then the stern line. Leaving the platform is completed in the opposite order, with the stern line being untied first and the bow spring line untied last.

5.4 Seasonal Hazards

5.4.1 Foul Weather Concerns

The tidal energy conversion system is designed to operate in all seasons, so foul weather operations are sometimes required. Weather hazards include strong winds, low air and water temperatures, precipitation, ice build up, and debris caused by melting. Foul weather gear including Grundens PVC coated jackets and bib pants, winter hats, thin gloves, large PVC coated gloves, and rubber gloves have been purchased for team members to wear during operations. There is also an 8ft x 8ft fold-able, insulated ice fishing hut that can be set up on the TDP deck during high winds and low temperatures. A tarp can be used to cover the deck and a propane heater can be used in the shelter for added warmth.

Figure 5.3: Cold weather shelter set up on the turbine deployment platform

5.4.2 Ice and Debris Damage

Several instruments were damaged during the late winter and early spring of 2019 due to debris and/or ice in the river. Both ADCP's were damaged and one of the ADV's was damaged in the first attempt of the measurement campaign described in Section 2.2.

On February 4, 2019 the mount attaching the ADCP at the stern to the platform was found detached as seen in Figure 5.4.

The two galvanized steel 2 in structural pipe fittings attaching the vertical pipe to the horizontal pipes were fractured. The tension cables were entirely holding the ADCP and mount to the platform. No problems were seen on the previous visit to the turbine deployment platform, so the damage could have happened anytime between 1/4/19 and 2/4/19. The ADCP bulkhead used to connect the cable to the instrument was damaged as seen in Figure 5.5.

The ADCP pressure housing was opened up to assess any internal damage. There was no noticeable water ingress or other issues. The bulkhead was replaced at UNH with a connector purchased from LinkQuest. The instrument has operated correctly since the new connector was installed.

Figure 5.4: Damage to the mount of the ADCP at the stern as found on 2/4/19

Figure 5.5: Damage to the ADCP bulkhead that was installed at the stern of the turbine deployment platform

The next day, February 5, 2019, one of the ADV's that had been installed the day before was also found damaged. The probe head was decapitated, leaving the instrument body and cable still attached to the mount as seen in Figure 5.6. During the impact the mounting pipe of the ADV was bent as seen in Figure 5.7.

Figure 5.6: Damage to the ADV probe head on 2/4/19

The data recovered from the ADV was used to pinpoint the time of damage to 8:30 pm on 2/4/19. The damage occurred during the ramp up of a flood tide when the current speed was approximately 0.8 m/s. A replacement probe head, cable, and internal electronics were purchased from Nortek. During the replacement at UNH, the electronic circuit board was damaged. The repair of the damage and final installation of the new probe head took place at the Nortek office in Boston, MA.

All other instruments were removed from the water after the ADV damage was discovered. Damage to the transducer housing on the other ADCP was found, as seen in Figure 5.8.

Figure 5.7: Bend in the mounting pipe (right) caused by the impact that caused damage to the ADV probe head on 2/4/19

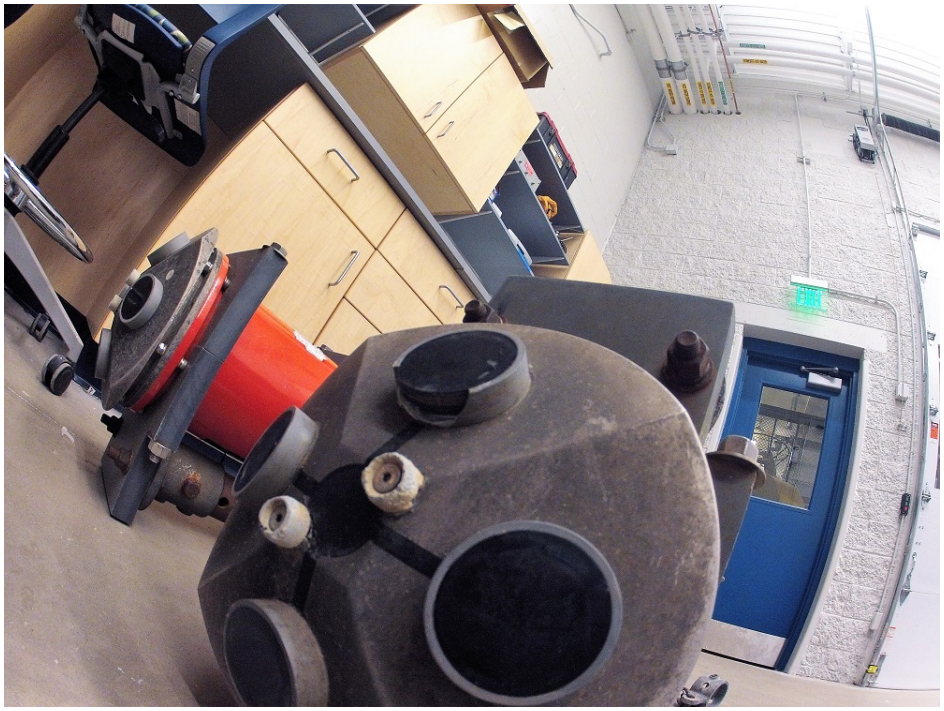

Figure 5.8: Damage to the ADCP transducer housing that was installed at the bow of the turbine deployment platform

LinkQuest reviewed images of the damage to the transducer housing and determined that the instrument will need to be repaired at their facility in San Diego, CA.

Debris has been seen in the river, for example on September 11, 2018 there was a log stuck on the platform and/or bridge pier as seen in Figure 5.9. The log had freed itself with the changing currents before it was possible to get out to the platform to remove it. No damage to the platform was observed after the event.

During the period of time in February when the instrument damages occurred there was a warm spell that caused melting and ice break up in the Great Bay and harbor areas. Ice chucks such as that in Figure 5.10 where seen around the platform. Other debris that might have been released during this melting was also observed during this time such as the log seen in Figure 5.11. Debris and ice of this nature is prevalent in the river during this time of year, so it is recommended that instruments be removed from the platform from mid-January until mid-April to avoid damage.

Figure 5.9: Log observed on September 11, 2018 stuck on the platform and bridge pier

Figure 5.10: Ice chunk observed impacting the turbine deployment platform in March 2019

Figure 5.11: Log observed in March 2019 near the Piscataqua River Bridge (I-95 Bridge), approximately 1 mile west of the Memorial Bridge

CHAPTER 6

CONCLUSIONS AND FUTURE WORK

The localized flow at the turbine deployment location was investigated in more detail with ADCP and ADV deployments. This data along with an as-built power curve from off-grid turbine testing was used to produce more accurate energy predictions. Knowledge was gained about the installation and integration of instrumentation on the turbine deployment platform. The turbine operation and issues that arose also lead to more knowledge of the system.

6.1 Flow Measurement Results

The ADCP current resource survey conducted over the summer of 2017 (LB-17) showed a higher mean kinetic power density than the previous two ADCP surveys (K-07 and HG-14) due to the faster currents seen at the Living Bridge deployment site. The changes in the flow conditions between the survey locations demonstrates the importance of taking localized flow measurements for tidal energy resource assessments. The Living Bridge ADCP's had a shorter ensemble length, but even with comparable ensemble lengths the Living Bridge deployment site still shows faster ebb tide currents than the previous ADCP surveys. The maximum current speed from the HG-14 survey was used for the design loads on the turbine deployment platform. This speed was surpassed during the LB-17 survey due to both the shorter ensemble interval and location difference. In order to obtain a more appropriate current speed for design loads, measurements closer to the deployment location should have been taken. The flow measurements for design loads would not need to be taken over a long period of time, but could be taken during an expected high tidal current speed time period.

To get a better idea of the flow characteristics directly around the turbine location, ADV measurements were taken at various locations on the turbine deployment platform. The ADV mea-

surements confirmed a change in the flood tide current direction that was also seen in the ADCP survey. This change in the flow direction away from the turbine deployment location will result in lower power production during the flood tide. Differences between the flow along the length of the platform were also seen. These differences in the current speed can be attributed to structural interactions with the bridge pier. The slower current seen at the stern during the ebb tide was also seen in the ADCP survey.

From the ADV data, the flow characteristics varied over the ebb and flood tides and from one tide to another. The turbulence intensity ranged from 0.109 to 0.281 and the time scales ranged from 10.2 seconds to 96.4 seconds. The average length scale for the ebb tides was 38.5 m and the average length scale for the flood tide was 50.9. As expected, these length scales are less than the width of the river and distances between the bridge piers. These long length scales are associated with "gusts" that appear to the turbine as periods of faster and slower current speed on the order of the time scales of the flow. These gusts will cause the turbine power output to fluctuate and effect the overall energy production of the system.

To build on the flow measurements taken with the ADCP's and ADV's described here measurements should be taken with the ADV traversing system. The preliminary traversing system experiments did not produce meaningful results due to the changing current conditions over the traversing time. Since those initial traversing experiments synchronization wires were installed in the ADV's, allowing for the traversing ADV to reference the stationary ADV. In order for this method to be effective the stationary ADV must be mounted close to the traversing ADV to decrease the time delay between the flow at the two sensors and the speed of the traversing ADV must be measured so that it can be removed from the signal. Any future measurement campaigns with the traversing system should also be planned carefully so that long time periods are allocated for set up and take down (at least 4 hours), at least three people are present for the installation and removal of the ADV mount, and the measurements are conducted during good weather where people can comfortably be out on the platform for up to 8 hours.

6.2 Turbine Testing Conclusions

The off-grid turbine testing produced a power curve that had a lower efficiency and higher cut-in speed than originally predicted and specified by the the manufacturer for the system. These differences resulted in a lower prediction of the annual energy production, even though the higher current speed observations from the LB-17 survey were used. Longer turbine testing should be done in order to add more confidence to the as-built power curve.

Additional testing of the system in off-grid mode should include 4-6 hours of operation during the ebb tide. Tests that include the cut-in and/ or cut-off speeds should be conducted whenever possible. At least one test should also be attempted on a flood tide that is predicted to be strong in order to confirm that the turbine does not spin up on the flood tide. The measurements from the rectifier and ADCP from the additional tests should be added to the data from the 4 hour test described here in order to refine the power curve and increase confidence in the results.

6.3 Instrumentation Systems Status

The baseline instrumentation data collection system is fully functioning, but a newly developed UNH database design should be implemented to make the data more easily accessible. The mobile DAQ system has been partially developed and tested on the turbine deployment platform. The LabView code for the additional instrumentation should be developed so that the entire system is functioning.

Some of the additional instrumentation was purchased so that design loads and their effect on the turbine deployment platform could be measured. The current design load was already investigated by deploying the ADCP's on the platform during the LB-17 survey, this resulted in a higher maximum current speed than was used for the design of the platform. The wind and wave conditions at the platform have not been studied and compared to the loads used for the design of the structure. The wave buoys should be used to determine the wave loads. Wave measurements during 1-2 months in the summer when there is high boat traffic should be taken as well as mea-

surements during storm events so that the maximum wave condition could be determined. The wave staff can also be deployed at the same time as the buoy in order to confirm that the measurements at the buoy represent the conditions at the turbine location. The wind measurements from both WeatherStations should be analyzed and compared to determine the appropriate wind loading conditions.

Over a shorter period of time (1 day to 1 week) the wave, wind, and current measurements should also be taken at the same time as measurements from the IMU, strain gauges on the vertical guide posts, and load cells in the turbine pitching mechanism. The loading conditions could then be related to the platform motion, mooring forces, and rotor thrust forces and compared to the reaction that was assumed during the design of the system. This test should be completed with the turbine out of the water, in the water but braked, and in the water and running to address all of the loading scenarios considered during the design.

Integration of the Wildlife Mitigation Device System with the bridge database should be completed and further testing of the system should be conducted. The fairings developed for the ADV mount proved to successfully mitigate vortex induced vibrations effects. The fairings and other improvements to ADV deployments on the turbine deployment platform can be used for deploying the ADV traversing system in the future.

6.4 Tidal Energy Conversion System Operation and Maintenance Lessons Learned

The turbine has produced power in off-grid mode after making repairs to the system. Some progress on resolving the issues with the turbine power electronics has been made but further work is needed in order to connect the system to the grid. The current leakage issue needs to be investigated in more detail, including testing to determine where the leakage to ground exists in the system. After the current leakage issue is resolved, it is likely that the inverter will need to be replaced as it was not designed to accept grounded DC power and was showing the "RelayChk" error when the current leakage limit was increased.

Once the tidal energy conversion system is fully operational in grid-tied mode then testing should be done before allowing the system to operate unattended. Short tests of 1-6 hours with someone constantly on the platform should be conducted first. If no issues arise then a longer, 12-24 hour test should be completed with frequent monitoring (checked on every hour and remote monitoring with the security cameras). Information from the rectifier should be logged either to the SD card or a laptop during these tests and an ADCP should collect current data. If the longer test is successful, then the system can be left unattended and run continuously with weekly trips to the platform and monitoring with the security cameras.

January and February of 2019 saw damage to both of the ADCP's and one of the ADV's. Based on this experience, the winter and spring time should be avoided for instrument deployments both due to the cold conditions and risk of ice and debris damaging instrumentation.

BIBLIOGRAPHY

[1] E. Bell, L. Hamilton, M. Wosnik, K. Baldwin, and T. Fu. *PFI:BIC: The Living Bridge: The Future of Smart, User-Centered Transportation Infrastructure (Award Number 1430260)*. National Science Foundation, 2014.

[2] C. Brown, R. Karp, M. Steinberg, and J. Velazquez. Living Bridge Database. *UNH CS 791 Senior Projects*, 2018.

[3] G. Caisse and K. Strohschneider. The Living Bridge Project: ADV Traversing System and Measurements. *UNH TECH 797 Ocean Projects*, 2018.

[4] K. Chancey, G. Ericsson, R. Tingley, and S. Torgesen. The Living Bridge Project: Environmental and Tidal Energy Resource Instrumentation. *UNH TECH 797 Ocean Projects*, 2017.

[5] D. B. Chelton. Physical Oceanographic and Atmospheric Data Analysis. 2015.

[6] T. H. Clark. A framework for classifying turbulence and its effects . In *European Wind Energy Association Resource Assessment 2015*, June 2015.

[7] E. Doherty. The Memorial "Living Bridge" Project: Designing and Implementing a National Science Foundation Smart Service System. *University of New Hampshire Master's Thesis*, 2016.

[8] D. Ducharme. *University of New Hampshire Living Bridge Overview*. Lite Enterprises, Inc., 2015.

[9] I. Gagnon. A Hydrokinetic Turbine Deployment System for Use at Bridges with the Memorial Bridge as a Case Study. *University of New Hampshire Master's Thesis*, 2018.

[10] I. Gagnon, M. Wosnik, T. Lippman, K. Baldwin, and E. S. Bell. Tidal Energy Conversion at an Estuarine Bridge: Resource Assessment, Turbine Sizing, and Energy Management System Analysis.

[11] W. K. George. Lectures in Turbulence for the 21st Century. 2013.

[12] M. Guerra and J. Thomson. Turbulence Measurements from Five-Beam Acoustic Doppler Current Profilers . *Journal of Atmospheric and Oceanic Technology*, 34:1267–1284, June 2017.

[13] M. Guerra and J. Thomson. Wake Measurements from a Hydrokinetic River Turbine . *Renewable Energy*, 139:483–495, August 2019.

[14] B. Gunawan, V. S. Neary, and J. Colby. Tidal Energy Site Resource Assessment in the East River Tidal Strait Near Roosevelt Island, New York, New York . *Renewable Energy*, 71:509–517, June 2014.

[15] H. Hicks and J. Griffith. Memorial Bridge Hydrokinetic Power Generation. *UNH TECH 797 Ocean Projects*, 2014.

[16] International Electrotechnical Commission. IEC TS 62600-201 Marine energy - Wave, tidal and other water current converters - Part 201: Tidal energy resource assessment and characterization. 2015.

[17] P. Jeffcoate, R. Starzmann, B. Elsaesser, S. Scholl, and S. Bischoff. Field Measurements of a Full Scale Tidal Turbine . *International Journal of Marine Energy*, 12:3–20, December 2015.

[18] P. Jeffcoate, T. Whittaker, C. Boake, and B. Elsaesser. Field Tests of Multiple 1/10 Scale Tidal Turbines in Steady Flows . *Renewable Energy*, 87:240–252, March 2016.

[19] J. Jimenez. The Largest Scales of Turbulent Wall Flows . *Center for Turbulence Research Annual Research Briefs*, pages 137–154, 1998.

[20] C. Kammerer. Tidal Currents in the Piscataqua River, NH, 2007.

[21] N. D. Kelley, R. M. Osgood, J. T. Bialasiewicz, and A. Jakubowski. Using Time-Frequency and Wavelet Analysis to Assess Turbulence/ Rotor Interactions . In *19th American Society of Mechanical Engineers (ASME) Wind Energy Symposium*, January 2000.

[22] K. C. Kim and R. J. Adrian. Very Large-Scale Motion in the Outer Layer . *Physics of Fluids*, 11(2):417–422, February 1999.

[23] M. Mashayekhizadeh. Developing three-dimensional multi-scale finite element model for in-plane service performance assessment of bridges. *Computer-Aided Civil and Infrastructure Engineering*, 34(5):385–401, 2018.

[24] K. McCaffrey, B. Fox-Kemper, P. E. Hamlington, and J. Thomson. Characterization of turbulence anisotropy, coherence, and intermittency at a prospective tidal energy site: Observational data analysis. *Renewable Energy*, 76:441–453, 2015.

[25] National Oceanic and Atmospheric Administration. NOAA Current Predictions: Help. online, https://tidesandcurrents.noaa.gov/noaacurrents/Help.

[26] E. Nelson. Modular Oceanographic Instrumentation System (MOIS) User Guide. Technical report, National Renewable Energy Laboratory (NREL), 2015.

[27] Nortek AS. *Vector: 3D Acoustic Velocimeter Brochure*.

[28] Nortek AS. *The Comprehensive Manual: AWAC | Aquadopp | Aquadopp Profiler | 2D Horizontal Profiler | Vector | Vectrino*, 2017.

[29] A. E. Perry, S. Henbest, and M. S. Chong. A Theoretical and Experimental Study of Wall Turbulence . *Journal of Fluid Mechanics*, 165:163–199, 1986.

[30] B. Polagye and J. Thomson. Tidal energy resource characterization: methodology and field study in Admiralty Inlet, Puget Sound, WA (USA). *Institution of Mechanical Engineers, Part A: Journal of Power and Energy*, 227(3):352âĂŞ367, 2012.

[31] M. Rowell, M. Wosnik, J. Barnes, and J. P. King. Experimental Evaluation of a Mixer-Ejector Marine Hydrokinetic Turbine at Two Open-Water Tidal Energy Test Sites in NH and MA . *Marine Technology Society Journal*, 47(4):67–79, July/August 2013.

[32] P. J. Rusello. *A Practical Primer for Pulse Coherent Instruments, Nortek Technical Note TN-027*. Nortek AS, 2009.

[33] G. I. Taylor. The spectrum of turbulence. *Proceedings of the Royal Society of London. Series A, Mathematical and Physical Sciences*, 164(919):476–490, 1938.

[34] A. H. Techet. *Design of Principles for Ocean Vehicles (13.42) Lecture: Vortex Induced Vibrations*. Massachusetts Institue of Technology Open Courseware, 2005.

[35] Teledyne RD Instruments. *Workhorse Sentinel: Self-Contained 1200,600,300 kHz ADCP Data Sheet*, 2009.

[36] Teledyne RD Instruments. *Acoustic Doppler Current Profiler Principles of Operation A Practical Primer*, 2011.

[37] T. Thompson and D. Wright. The Living Bridge: Turbine Deployment Platform Motion and Load Study. *UNH ME 756 Senior Projects*, 2019.

[38] J. Thomson, B. Polagye, V. Durgesh, and M. C. Richmond. Measurements of Turbulence at Two Tidal Energy Test Sites in Puget Sound, WA . *IEEE Journal of Oceanic Engineering*, 37(3):363–374, July 2012.

APPENDIX A

ADCP COMPASS CALIBRATION PROCEDURE

A.1 Preparation

Have at least two people on the floating platform (accessible by boat) and one person operating the software remotely by using Remote Desktop to access the server. (Server room not accessible from floating platform)

A.2 Field Procedure

1. Remove the ADCP such that the instrument is still in the mount and attached to the vertical steel pipe strut.
2. Place a bucket on top of a sheet of smooth material (such as aluminum). Greasing the sheet of material where the bucket will be placed or placing a cloth underneath the bucket may help to get a smoother rotation. Stand the ADCP in the mount on top of the bucket, with the mount edge 45 deg with respect to the edge of the bucket.
3. Communicate with the software operator to start the calibration.
4. Rotate the ADCP and the bucket around the instrument axis for at least two cycles being careful of the data cord. Keep the ADCP in the center of the bucket during this rotation. It should be rotated slowly, at maximum 3 deg/ 1 sec = 180 deg per minute. It is helpful to have one person timing the rotation and counting off for each 90 deg section.
5. Stop the rotation and untangle the data cable.
6. Repeat process if necessary.

A.3 Software Procedure

1. Use Remote Desktop to remotely access the bridge server.
2. Open the graphical user interface (GUI), "Living Bridge" icon on desktop.
3. Go to the "ADCP" tab and click "Stop Script" for whichever ADCP is currently being calibrated. (ADCP 1 is at stern, ADCP 2 is at bow)

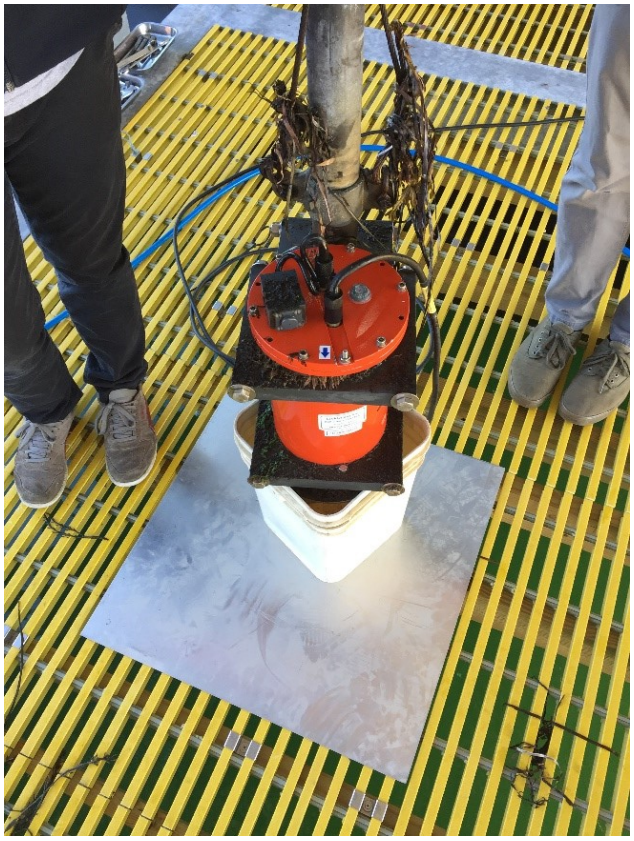

Figure A.1: ADCP set up for calibration on 9/29/17

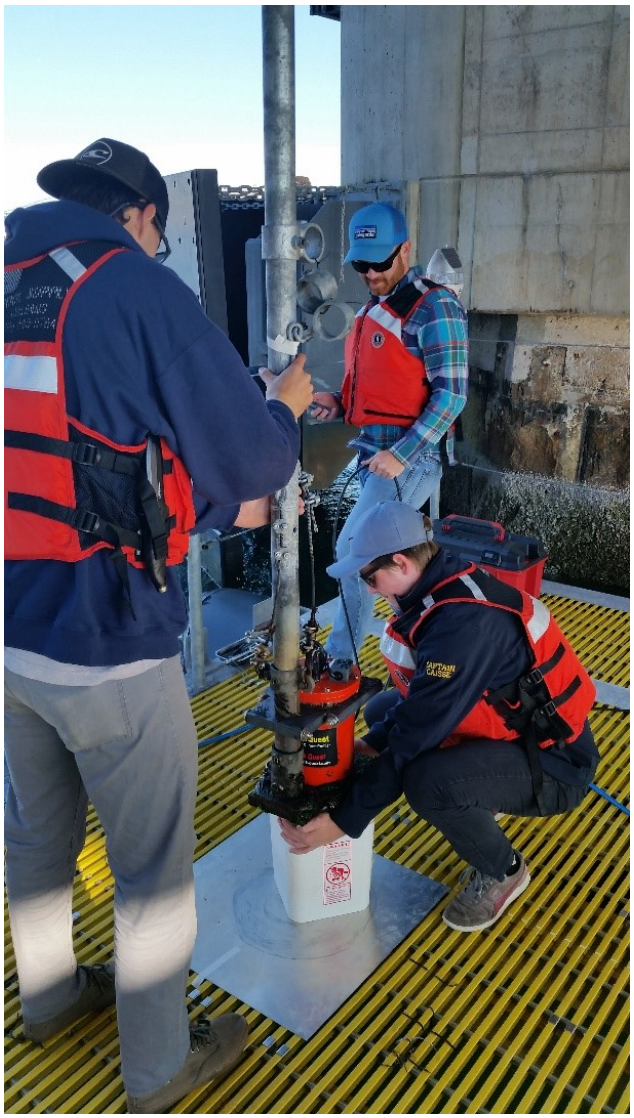

Figure A.2: ADCP rotation for calibration on 9/29/17

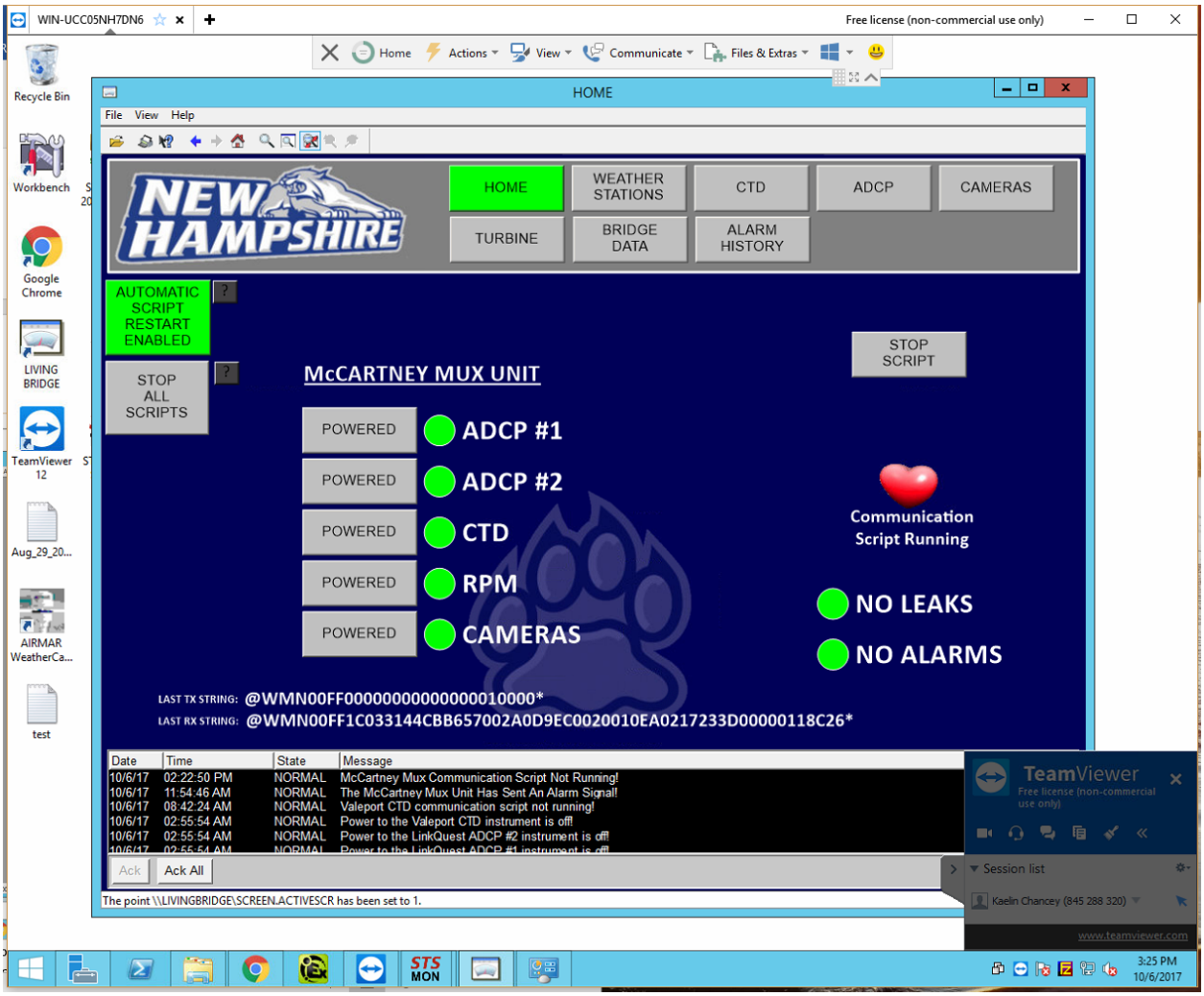

Figure A.3: Living Bridge GUI home page

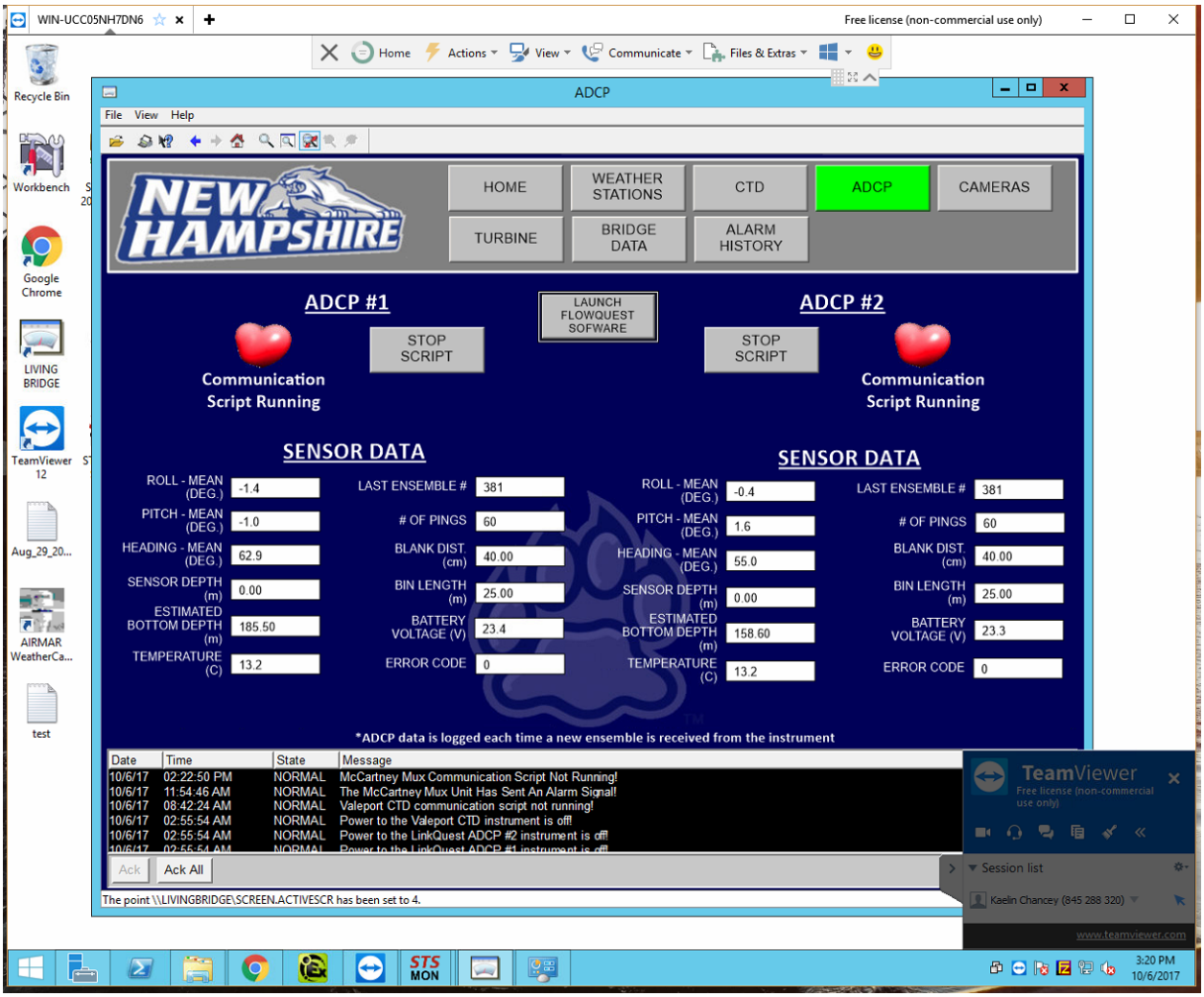

Figure A.4: Living Bridge GUI ADCP page

(a) Do not disable the "Automatic Script Restart" on the main page, this will cause the MUX script to stop running and problems to occur with the ADCP as a result. The calibration will still work even if the ADCP script starts again in the background.

4. Open the FlowQuest software by clicking "Launch Flowquest Software".

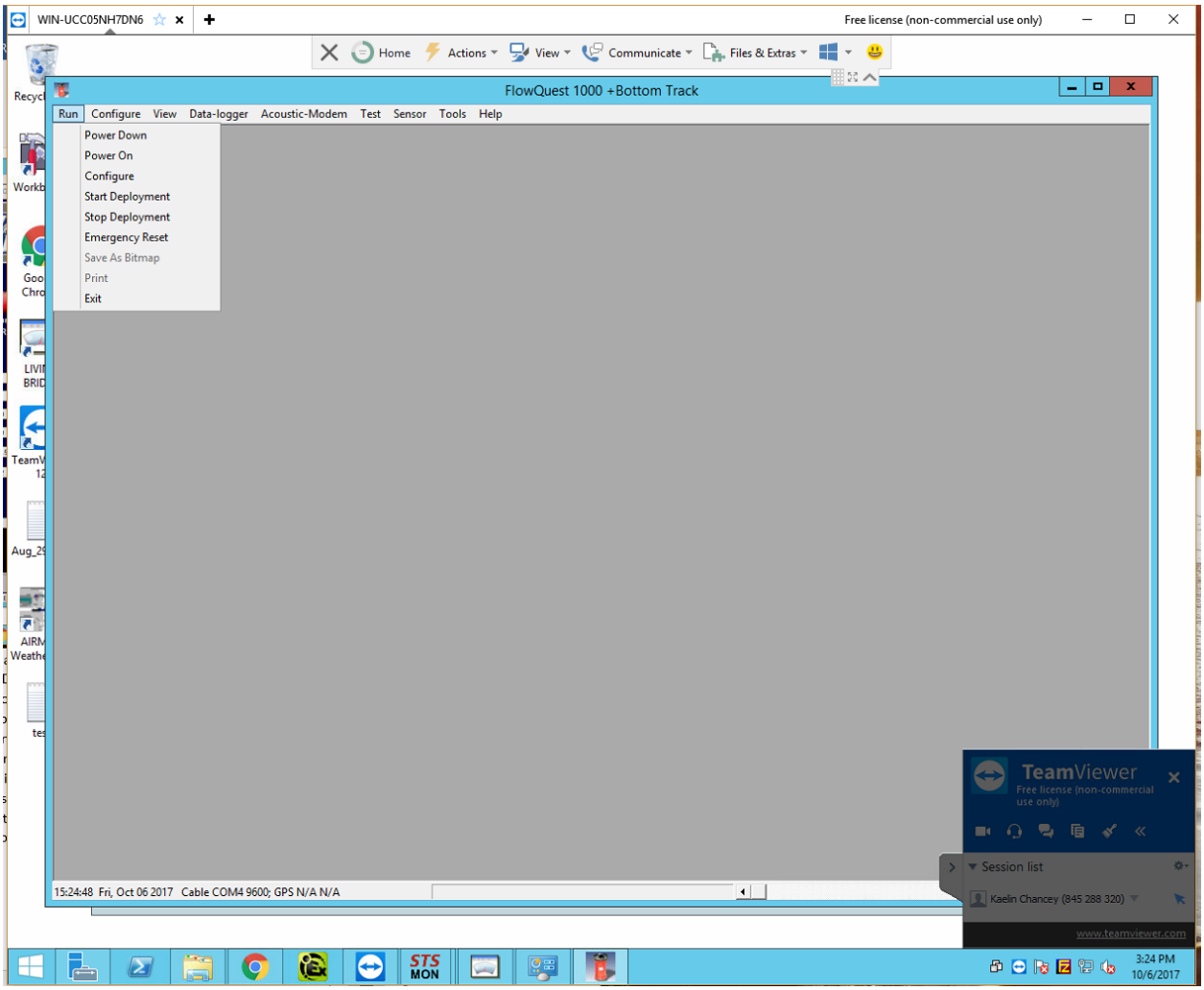

Figure A.5: LinkQuest FlowQuest software run menu

5. Chose which ADCP to connect to by selecting "Configure" > "Serial Port" and entering the COMM Port number that matches the ADCP which you stopped the script for. (ADCP 1 is COMM 4, ADCP 2 is COMM 5)

6. Enter the ADCP into "Configuration Mode". The software is reluctant to exit deployment and enter configuration, so it is best to use the terminal emulator as described in Appendix B or follow this procedure:

   (a) Run > Configure (Repeat 3x, if unsuccessful, skip)

(b) Run > Stop Deployment (Repeat 3x, if unsuccessful, skip)

(c) Run > Emergency Reset

(d) Run > Power On

(e) Run > Exit

(f) Make sure ADCP script is running, if not, restart script.

(g) Stop ADCP script

(h) Launch FlowQuest software

(i) Restart this procedure until ADCP enters "Configuration Mode", this will be indicated at the bottom of the screen.

7. Start the compass calibration software procedure by selecting Sensor > Compass > Calibrate

8. When the field researchers are ready to begin, click "Start". As the ADCP is rotated a circle or ellipse will begin to form on the screen.

9. When the two rotations are complete "Stop" the calibration. If the calibration is good save the calibration data to the device.

   (a) The calibration can also be good but then fail to save to the instrument. If this occurs, you must perform an emergency reset of the system and start another calibration.

10. If the calibration was not successful it could be for the following reasons:

    (a) "Not enough rotations": This error could be a result of not rotating the instrument for two full rotations or if the rotation was done too slowly so that points began being deleted from the beginning of the calibration, making it impossible to close the second rotation loop.

    (b) "Bad calibration due to magnetic interference or not in flat plane": This error could be from not rotating the ADCP around its axis the entire time. If this occurs it will be obvious that the two rotations do not align, as shown in Figure A.8.

11. When the calibration is done exit the FlowQuest Software (Run > Exit) and start the ADCP script if it is not running.

12. Before exiting the graphical user interface ensure that no alarms are displayed at the bottom of the window. Exit the graphical user interface and Remote Desktop.

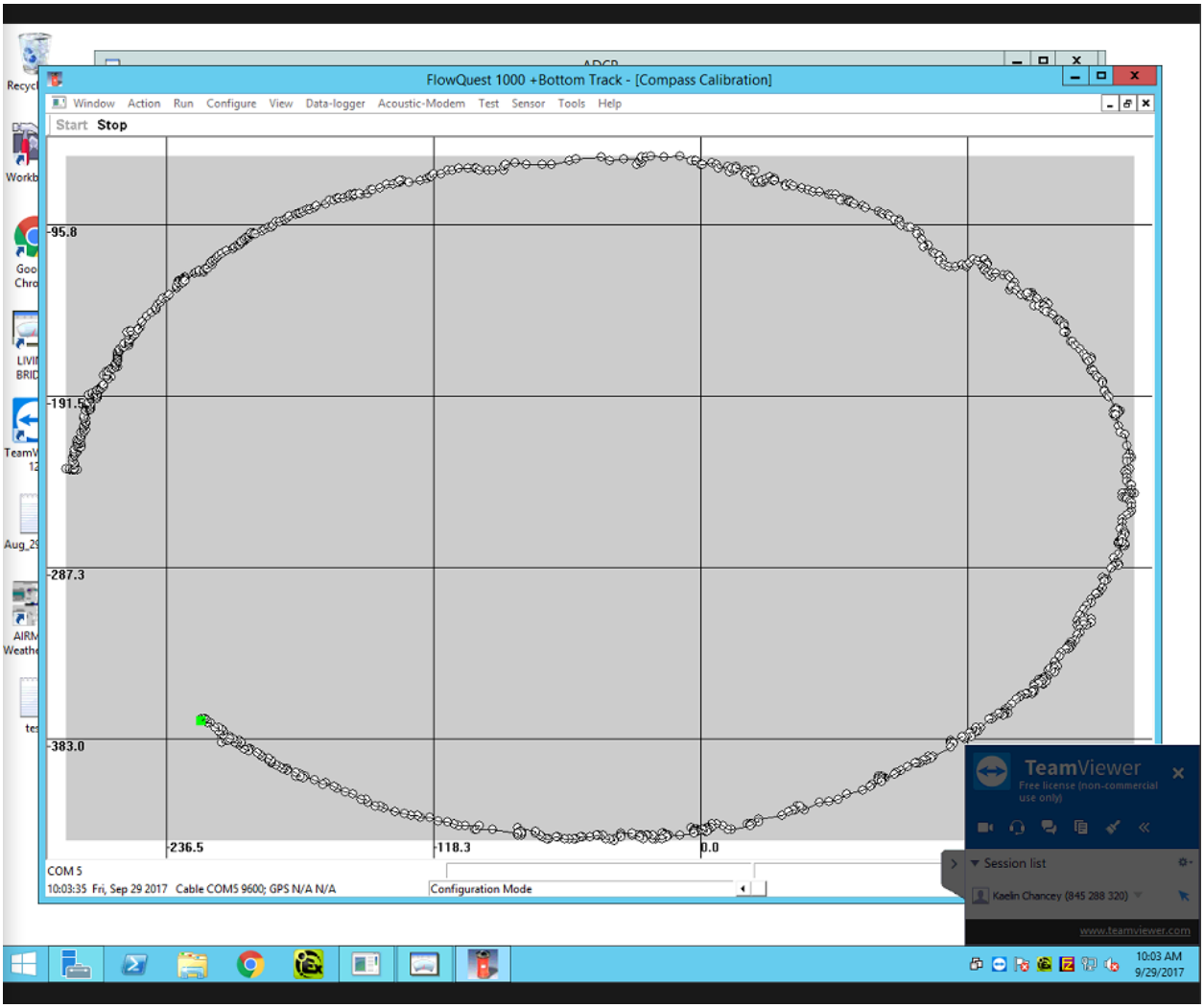

Figure A.6: Ellipse formed during compass calibration

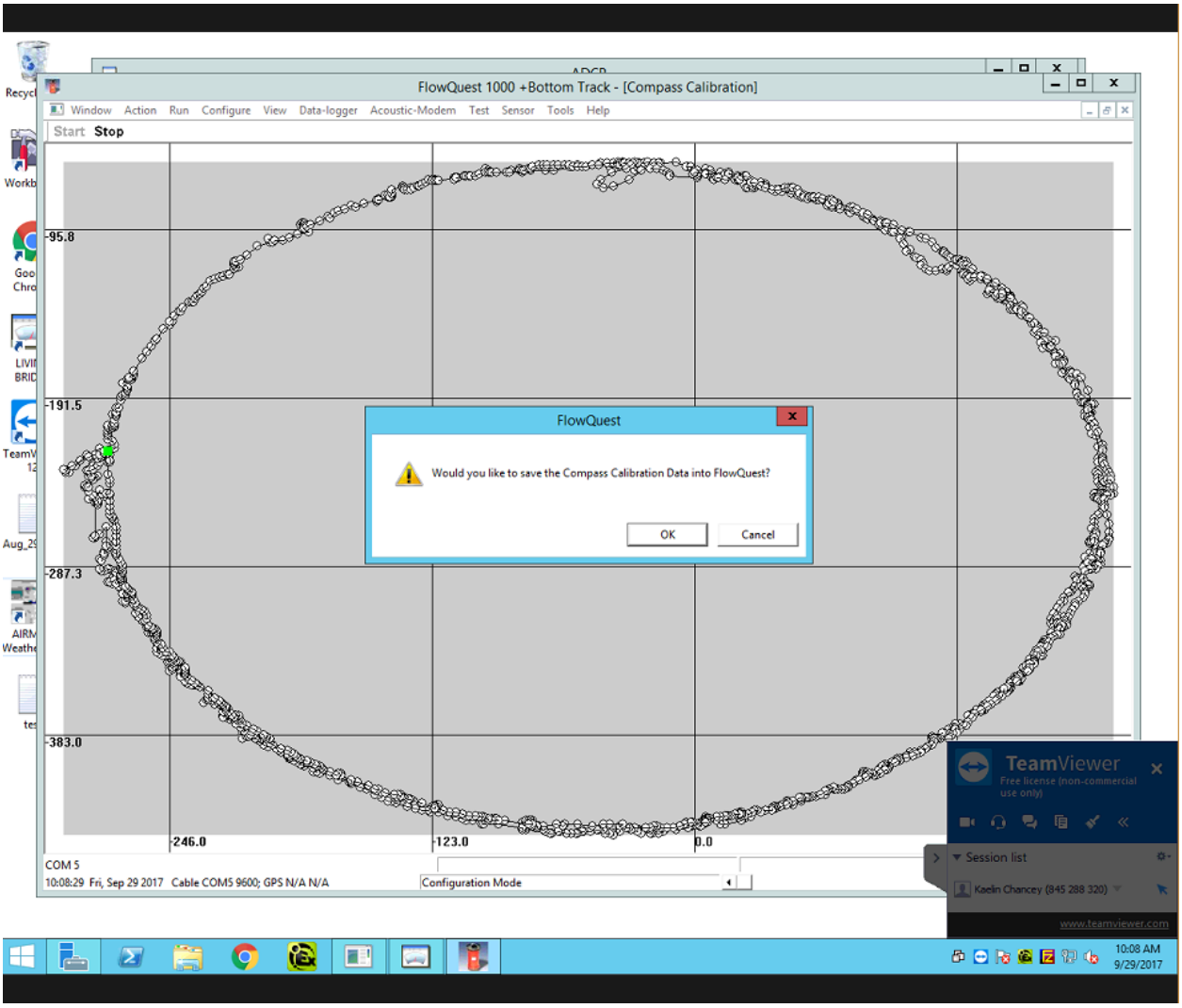

Figure A.7: Successfully completed compass calibration

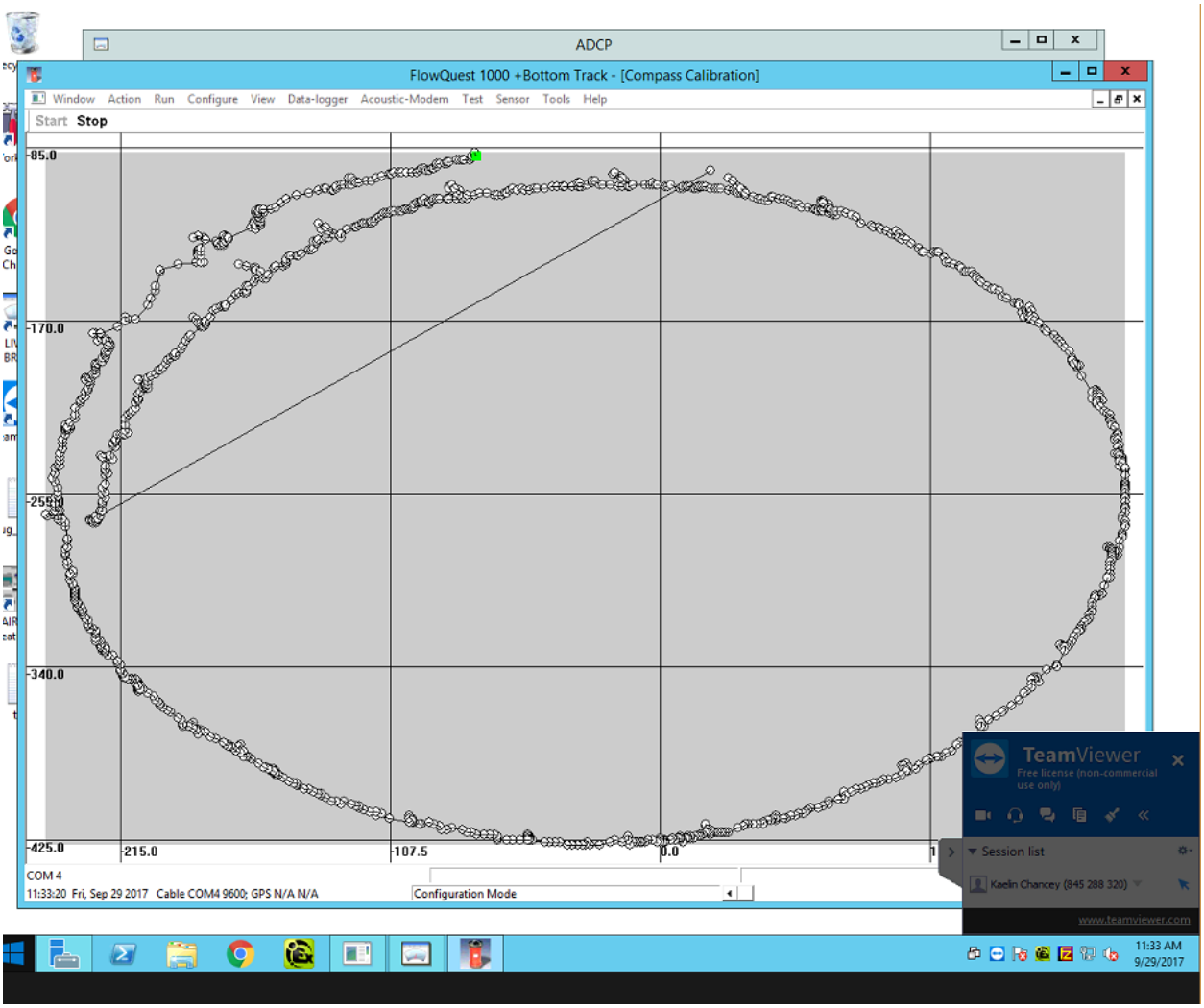

Figure A.8: Two ellipses not aligned suggesting that the ADCP was not successfully rotated about it's axis

APPENDIX B

TERMINAL COMMUNICATION WITH LINKQUEST FLOWQUEST ADCP'S

A terminal emulator program can be used to communicate directly with the LinkQuest FlowQuest 1000 ADCP's. A document describing those commands was provided by LinkQuest after agreeing that the information contained would not spread outside of UNH. These instructions describe generally how to communicate with a terminal emulator and what commands are useful but it does not provide the syntax of the commands or responses.

The FlowQuest software provided with the ADCP's does not always connect to the instruments and often stops responding and closes. The terminal commands are a way of bypassing this software but they do not provide all of the functionality found in the software. The best use of the terminal emulator is to initially connect to the ADCP so that it can connect to the software more readily. This also works for connecting to the Living Bridge SCADA system.

The terminal emulator Tera Term was used to communicate with the ADCP's but any other terminal emulator program would also work.

B.1 Bridge Server - Connect an ADCP to the FlowQuest Software using the Terminal Emulator

1. Connect to the Bridge Server using Remote Desktop
2. Open the Living Bridge GUI
3. On the Living Bridge GUI, Stop the ADCP script
4. Open Tera Term
5. On Tera Term, File > New Connection > Serial > Select COM port (ADCP 1: COM4, ADCP 2: COM5)
6. On Tera Term, Set Up > Serial Port > Select Baud Rate (usually 9600, try others if not correct)
7. On Tera Term, Set Up > Terminal > Confirm that Local Echo is checked and that Transmit is set to CR + LF
8. Enter the "Stop DSP" command into the terminal window
9. Enter the "Stop Data Logger" command

10. Repeat steps 8 and 9 until a response is received from both commands, the ADCP is then in Configuration Mode
11. On Tera Term, File > Disconnect
12. Open FlowQuest software
13. On FlowQuest software, Configure > Serial Port > Select COM port and baud rate
14. On FlowQuest software, File > Configure. If the action is successful, then the ADCP is connected to the software and settings can be changed. Repeat this step if the action fails. Make sure that the ADCP has not reconnected to the Living Bridge GUI. If it still fails, follow steps 4-14 again.

B.2 Bridge Server - Connect an ADCP to the Living Bridge GUI using the Terminal Emulator

1. Connect to the Bridge Server using Remote Desktop
2. Open the Living Bridge GUI
3. Stop the ADCP script
4. Open Tera Term
5. On Tera Term, File > New Connection > Serial > Select COM port (ADCP 1: COM4, ADCP 2: COM5)
6. On Tera Term, Set Up > Serial Port > Select Baud Rate (usually 9600, try others if not correct)
7. On Tera Term, Set Up > Terminal > Confirm that Local Echo is checked and that Transmit is set to CR + LF
8. Enter the "Stop DSP" command into the terminal window
9. Enter the "Stop Data Logger" command
10. Repeat steps 8 and 9 until a response is received from both commands, the ADCP is then in Configuration Mode
11. On Tera Term, File > Disconnect
12. On the Living Bridge GUI, Start the ADCP script
13. Use the instructions described in the NEI Living Bridge Data Acquisition User's Manual in order to determine that the ADCP is recording (both header and velocity tables)

B.3 Lab Bench Testing of the ADCP using the Terminal Emulator

1. Connect the ADCP test cable to an external power supply, between 22 and 26 VDC, up to 5 A
2. Connect an RS232 to USB converter to the test cable and the computer
3. Check the COM port using the device manager
4. Open Tera Term
5. On Tera Term, File > New Connection > Serial > Select COM port
6. On Tera Term, Set Up > Serial Port > Select Baud Rate (usually 9600, try others if not correct)
7. On Tera Term, Set Up > Terminal > Confirm that Local Echo is checked and that Transmit is set to CR + LF
8. Plug the test cable into the ADCP, a response should appear in the terminal window
9. Enter the "Stop DSP" command into the terminal window
10. Enter the "Stop Data Logger" command
11. Repeat steps 9 and 10 until a response is received from both commands, the ADCP is then in Configuration Mode
12. To put the unit into Deployment Mode, enter the commands for "Start Data Logger" and "Start DSP", responses should appear from both commands
13. To stop the deployment, enter the "Stop Data Logger" and "Stop DSP" commands, repeat until you receive responses from both commands

B.4 Additional Notes

1. "Start DSP" and "Get Parameters" output ASCII strings that at this point cannot be deciphered
2. No response has been received from "Get Baud Rate", "Power On", or "Power Off"

APPENDIX C

MOBILE DAQ DIAGRAMS

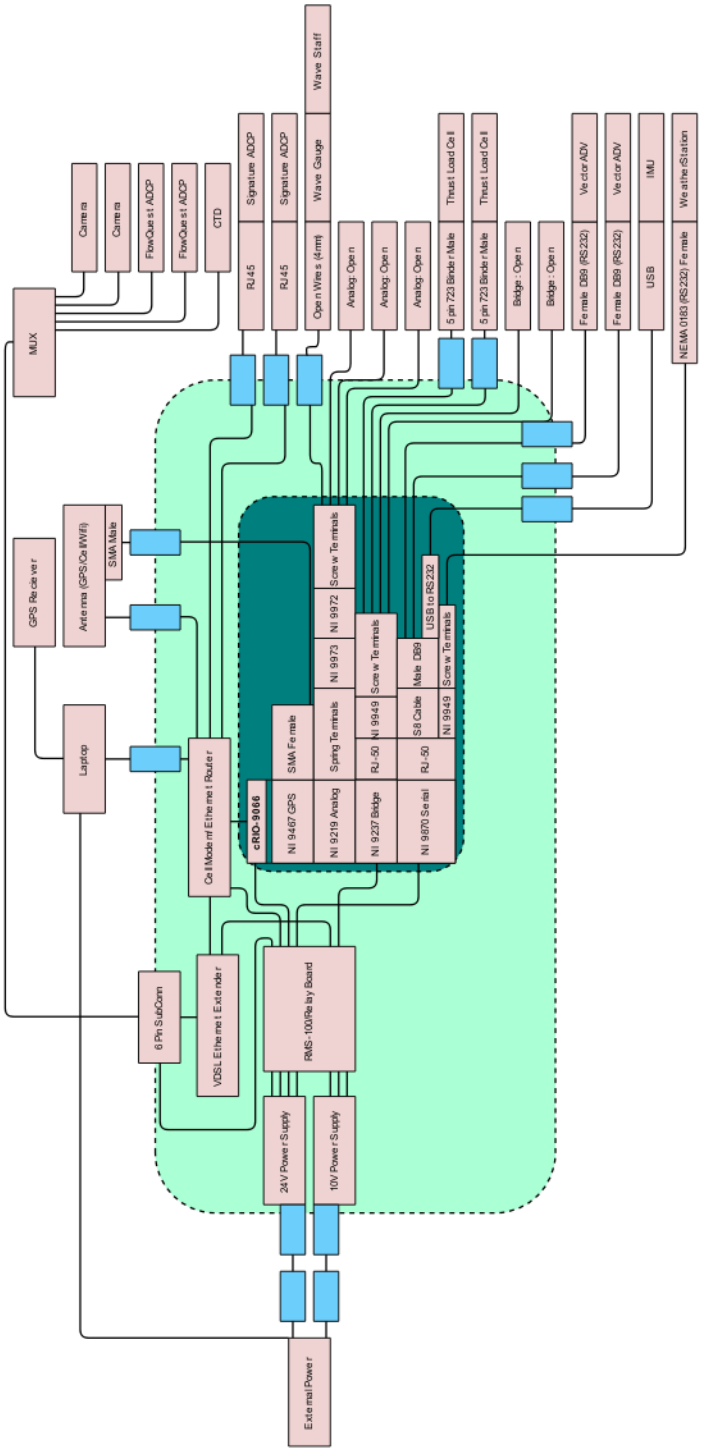

Figure C.1: Diagram of the designed mobile DAQ system

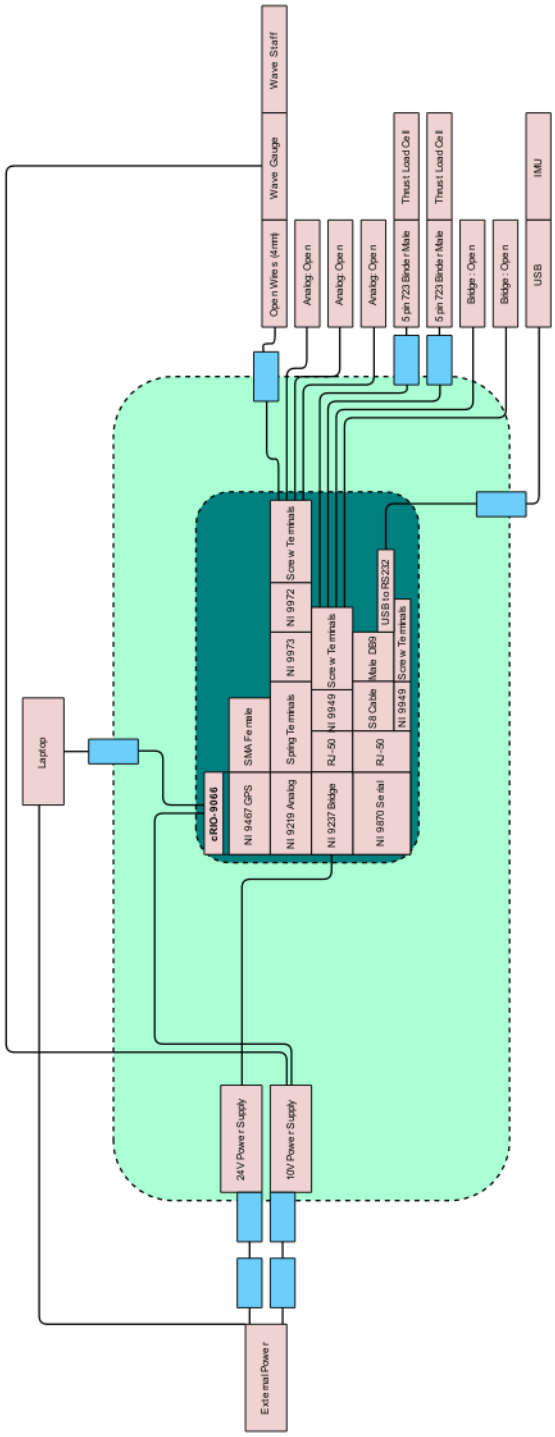

Figure C.2: Diagram of the parts of the mobile DAQ system that have been developed and tested